ISTANBUL TECHNICAL UNIVERSITY * GRADUATE SCHOOL OF SCIENCE ENGINEERING AND TECHNOLOGY

MULTI-SCALE MODELING AND INVESTIGATION OF ACTIVATION MECHANISMS OF G PROTEIN-COUPLED RECEPTORS

Ph.D. THESIS

Ramin EKHTEIARI SALMAS
(509092227)

Department of Chemistry

Chemistry Programme

Thesis Advisor : Professor Dr. Mine YURTSEVER

Co-advisor : Associate Professor Dr. Serdar DURDAĞI

JANUARY 2015

İSTANBUL TEKNİK ÜNİVERSİTESİ * FEN BİLİMLERİ ENSTİTÜSÜ

G-PROTEİN KENETLİ RESEPTÖRLERİN AKTİVASYON MEKANİZMALARININ ÇOK BOYUTLU MODELLEME YÖNTEMLERİ İLE İNCELENMESİ

DOKTORA TEZİ

Ramin EKHTEIARI SALMAS
(509092227)

Kimya Anabilim Dalı

Kimya Programı

Tez Danışmanı: Prof. Dr. Mine YURTSEVER

Eş Danışmanı : Doç.Dr. Serdar DURDAĞI

OCAK 2015

Ramin EKHTEIAIR SALMAS, a **Ph.D.** student of ITU **INSTITUTE OF SCIENCE AND TECHNOLOGY** student ID **509092227**, successfully defended the thesis entitled "**MULTI-SCALE MODELING AND INVESTIGATION OF ACTIVATION MECHANISMS OF G PROTEIN-COUPLED RECEPTORS**", which he prepared after fulfilling the requirements specified in the associated legislations, before the jury whose signatures are below.

Thesis Advisor:	**Professor Dr. Mine YURTSEVER**..... Istanbul Technical University
Co-advisor:	**Associate Professor Dr. Serdar DURDAĞI**…..... Bahcesehir University
Jury Members:	
	Professor Dr. Pemra DORUKER TURGUT..... Bogazici University
	Professor Dr. Özlem KESKIN ..... Koc University
	Associate Professor Dr. Fethiye Aylin SUNGUR …..... Istanbul Technical University
	Associate Professor Dr. Nurcan TÜZÜN..... Istanbul Technical University
	Assistant Professor Dr. Bülent BALTA …..... Istanbul Technical University

Date of Submission : 8 December 2014

Date of Defense : 23 January 2015

To my Mother,

FOREWORD

First and foremost, I wish to thank to the respectful members of chemistry department of Istanbul Technical University and biophysics department of Bahcesehir University for giving me the opportunity to study on my Ph.D. thesis. I would specially like to thank and tell my regards to my advisors Prof. Mine Yurtsever and Assoc. Prof. Serdar Durdagi who were great mentors and spent their valuable time on my thesis, guided me throughout my study and shared their knowledge with me. I want to thank to my parents for their moral support. Finlay, I would also like to remember my father I lost during my Ph.D.

January 2015 Ramin Ekhteiari Salmas

TABLE OF CONTENTS

Page

FOREWORD.....**ix**
TABLE OF CONTENTS.....**xi**
ABBREVIATIONS.....**xv**
LIST OF TABLES.....**xvii**
LIST OF FIGURES.....**xix**
SUMMARY.....**xxv**
ÖZET.....**xxix**
1. INTRODUCTION.....**1**
1.1 Purpose of Thesis.....1
1.2 Scientific Aim of the Thesis.....2
1.3 Innovation Potential.....2
1.4 Scientific Excellence and Originality of The Thesis.....3
1.5 Current State of Science and Technology.....4
1.5.1 Protein-ligand binding.....6
1.6 Motivation.....7
2. THEORETICAL BACKGROUND.....**9**
2.1 Molecular Dynamics (MD) Simulations.....9
2.1.1 Historical background.....11
2.1.2 Statistical mechanics.....11
2.1.3 Introduction to statistical mechanics.....11
2.1.3.1 Ensembles.....11
2.2 MD Trajectory Analysis.....12
2.2.1 Root-Mean-Square Deviation (RMSD).....12
2.2.2 Root-Mean-Square Fluctuation (RMSF).....13
2.3 Molecular Docking.....13
2.3.1 Theory.....13
2.3.1.1 Search algorithm.....13
2.3.1.2 Scoring functions.....13
2.3.1.3 Different types of interactions.....13
2.3.2 Molecular docking protocols.....14
2.4 Principal Component Analysis (PCA).....14
2.4.1 Applying PCA on MD simulations.....14
2.5 In-silico Mutation Study.....15
2.6 Ramachandran Plot.....15
3. COMPUTATIONAL DETAILS.....**17**
3.1 Homology Models for GPCRs-Ligand Data Base.....17
3.2 Molecular Docking and MD Simulations.....17
3.3 3D-QSAR Studies.....18
4. D2R STRUCTURE ON THE BASE OF ACTIVE AND INACTIVE

TEMPLATES.....21
4.1 Introduction.....21
4.2 Methodology.....23
4.2.1 Homology modeling.....23
4.2.2 Normal Mode Analysis (NMA).....24
4.2.3 Ligands data set.....24
4.2.4 Molecular docking.....25
4.2.5 Re-docking of crystallographically resolved ligands.....25
4.2.6 3D-QSAR.....25
4.3 Results and Discussions.....26
4.3.1 Model validations and preparation for subsequent ligand docking.....29
4.3.2 Normal Mode Analyses (NMA).....31
4.3.3 Signaling pathway of D2R.....34
4.3.4 Validation of the accuracy and performance of Glide and IFD docking..35
4.3.5 Molecular docking and binding energy calculation.....37
4.3.6 Distance analysis.....46
4.3.7 Computational alanine scanning mutagenesis.....47
4.3.8 3D-QSAR modeling.....48
4.4 Conclusion.....54
5. INHIBITORY TREATMENT OF CHEMOKINE RECEPTOR 5 (CCR5)....57
5.1 Introduction.....57
5.2 Materials and Methods.....58
5.2.1 Hybrid computational services.....58
5.2.2 The modeling of apo and holo proteins.....59
5.2.3 Classical molecular dynamics (cMD) simulations protocol.....60
5.2.4 Minimization and constrained equilibration.....61
5.2.5 Calculations of non-bonding interaction energies.....61
5.2.6 Principal Component Analysis (PCA).....61
5.2.7 Applying PCA on MD simulations.....62
5.2.8 Graphical facilities.....62
5.3 Results and Discussions.....62
5.3.1 MD equilibration.....63
5.3.2 Fusion facilitates influence on CCR5 conformer.....63
5.3.3 Non-bonded interactions.....65
5.3.4 Root Mean Square Fluctuation (RMSF) Calculations.....71
5.3.5 Clustering analysis.....72
5.3.6 Dynamic cross-correlations.....74
5.3.7 Principal Component Analysis (PCA).....75
5.3.8 Conformational clustering respect to main PCs.....76
5.4 Conclusion.....78
6. INHIBITORY TREATMENT OF DOPAMINE D2 RECEPTOR.....79
6.1 Introduction.....79
6.2 Methods.....81
6.2.1 Homology modeling.....81
6.2.2 Ligand preparation.....81
6.2.3 Induced Fit Docking (IFD).....82
6.2.4 Embedding of predicted model in membrane bilayer.....82
6.2.5 Molecular dynamic (MD) simulations.....82

6.2.6 Minimization and constrained equilibration....83
6.3 Results and Discussions....83
6.3.1 Homology modeling....83
6.3.2 Molecular docking of known drugs at the derived D2R model....85
6.3.3 Molecular dynamics (MD) simulations....86
6.3.4 Protein and ligands flexibility analysis....86
6.3.5 Hydrogen bond analysis....92
6.3.6 Non-bonding energy calculation....93
6.3.6.1 Risperidone....94
6.3.6.2 Ziprasidone....96
6.3.6.3 Aripiprazole....97
6.3.6.4 Clozapine....98
6.3.6.5 Olanzapine....98
6.3.6.6 Quetiapine....99
6.3.7 Binding energy comparison of six standard drugs....99
6.3.8 Shift of the TM5 from IC site during simulations....100
6.3.9 His393 dihedral angle....101
6.4 Conclusion....104
7. MECHANISM OF LIGAND-BINDING IN κ-OPIOID RECEPTOR....107
7.1 Introduction....107
7.2 Methods....109
7.2.1 Molecular dynamics Simulations....109
7.3 Results and Discussions....113
7.3.1 MD simulations in water....114
7.3.1.1 Conformational properties of holo and apo κ-OR forms....114
7.3.1.2 Hydrogen bond interactions....117
7.3.2 MD simulations in DPPC lipid bilayer....120
7.4 Conclusion....123
8. SUGGESTIONS FOR FUTURE WORK....125
REFERENCES....127
CURRICULUM VITAE....145

ABBREVIATIONS

CCR5 :C-C Chemokine receptor type 5

DPPC :1,2-dipalmitoyl-sn-glycero-3-phosphocholine

MD :Molecular dynamics

GPCRs :G protein coupled receptors

EC :Extracellular loop

IC :Intracellular loop

GPU :Graphics process unit

TM :Trans membrane

PCA :Principal component analysis

HIV :Human immunodeficiency virus

AIDS :Acquired immunodeficiency syndrome

D2R :Dopamine d2 receptor

QM :Quantum mechanics

MM :Molecular mechanics

NMA :Normal mode analysis

IFD :Induced fit docking

RMSD :Root mean square deviation

RMSF :Root mean square fluctuation

3D-QSAR :Three dimensional quantitative structure activity relationships

LIST OF TABLES

Page

Table 4.1 : Calculated binding energy (from IFD, kcal/mol) of known binder in to D2R. Experimental Ki (Exp. Ki, nM) (1) with respective references are also shown.....38
Table 4.2 : Ligand protein interaction of D2R antagonists docked with IFD.....41
Table 4.3 : The change in relative binding energies for several alanine mutants relative to the D2R (Inactive) wild type binding energies.....48
Table 4.4 : Statistical parameter values for the top 3D-QSAR model AHPRR and derived scores for the generated model.....54
Table 6.1 : Binding enthalpy energy and IFD score of D2R model with atypical anti-psychotic drugs and also their experimental binding affinity values...100
Table 6.2 : Hydrogen bond occupancies (%) between amino acid residues from different TMs.....102

LIST OF FIGURES

Page

Figure 2.1 : The Ramachandran plot.....16
Figure 4.1 : 2D chemical structures of marketed schizophrenia drugs (for clarity non-polar hydrogen atoms are not shown at the Figure).....23
Figure 4.2 : Flowchart of homology modeling evaluation.....24
Figure 4.3 : Sequence alignments for (a) inactive and (b) active templates and D2R. The yellow highlighted parts indicate ECL2 domains.....27
Figure 4.4 : (left) Superimposition of the second extracellular loops (ECL2) of D2R (blue) and the template (PDB ID: 3D4S) (purple) produced by the structural modeling. (right) Presentation of Asn186 and Ile184 residues at ECL2 of homology model that point into the binding-site.....27
Figure 4.5 : Ramachandran plots of the (a) active (b) inactive β2-adrenergic receptor-based DRD2 models generated with PROCHECK.....29
Figure 4.6 : Side (left) and top (right) views of superimposition of refined active (red) and inactive (green) state D2R model structures.....30
Figure 4.7 : Representation of the superimposition of binding sites of (top) X-ray crystal structures and (bottom) model-structures for the active (carbon atoms are shown with red) and inactive (carbon atoms are shown green) states). Hydrogen atoms are not shown.....31
Figure 4.8 : The flexibility graphs for each residue index are shown using normal mode analyses (NMA) of D2R homology models for active and inactive states. The rectangular boxes and blanks represent alpha helices and loops, respectively.....32
Figure 4.10 : Correlation maps for D2R homology models. Black boxes and blank represent alpha helices and loop domain, respectively. The color measure indicates from dark red (positive correlation) to dark blue (negative correlation).....33
Figure 4.11 : Identification of signaling pathway on active D2R model. The main residues and domains were highlighted on model.....35
Figure 4.12 : The validation of accuracy and performance of Glide/SP, XP and IFD docking protocols for inactive state (PDB ID: 3D4S). The docked timolol (brown) and co-crystallized structure of timolol (blue) showed a root mean square deviation of (a) Glide/SP-0.69 Å, (b) Glide/XP-1.07Å, (c) Glide/IFD (SP) (re-docking with SP)-0.53Å, (d) Glide/IFD (XP) (re-docking with XP)-0.74 Å.....36
Figure 4.13 : The validation of accuracy and performance of Glide/SP, Glide/XP and Glide/IFD docking for active conformer (3SN6). The docked BI-167107 (brown) and BI-167107 at the crystal structure (blue) demonstrated a root mean square deviation of (a) Glide/SP-1.79 Å, (b) Glide/XP-1.44Å, (c) Glide/IFD (SP) (re-docking with SP)-1.09Å, (d) Glide/IFD (XP) (re-

docking with XP)-0.50 Å.....37
Figure 4.14 : Calculated IFD scores with their standard deviations for docked ligands against active and inactive modes.....39
Figure 4.15 : Top-docking pose of Ziprasidone at D2R active model. Binding interactions of ECL2 residues (Ile184 and Asn186) and Ser193 (TM5), Asp114 (TM3) are shown. Dashed lines indicate salt bridge and HB interactions.....42
Figure 4.16 : The docking poses of Aripiprazole antagonist with D2R in inactive (left) and active (right) state models.....43
Figure 4.17 : Schematic 2D plots of protein-ligand interactions created for IFD: (a) Risperidone docked into the inactive receptor and (b) Risperidone docked into the active form of the D2R. Hydrogen atoms are omitted for clearance.....44
Figure 4.18 : Schematic view of the comparison of binding modes of (a) Aripiprazole, (b) Clozapine, (c) Quetiapine, (d) Risperidone, (e) Ziprasidone, (f) Olanzapine in the homology models for active (carbon atoms are shown in red) and inactive (carbon atoms are shown in green) conformers of D2Rs. Amino acid residues that formed hydrogen bonds with ligands have been also shown at the figure.....45
Figure 4.19 : Representation of the superposition of binding site of active (red) and inactive Dopamine D2 receptor interactions with Risperidone. (For clarity, non-polar hydrogen atoms on ligands were not shown and only residues that provide H-bond and π-π stacking interactions with ligands are shown).....46
Figure 4.20 : Distance calculation on active sites of both D2R models.....47
Figure 4.21 : Chemical structures of used ligands in 3D-QSAR study.....49
Figure 4.22 : Correlation between experimental and predicted activity value of contracted 3D-QSAR model.....53
Figure 4.23 : Alignment of generated pharmacophore model with used reference, active and inactive compounds.....54
Figure 5.1 : Chemical structure of maraviroc used as co-crystallized ligand in holo system.....59
Figure 5.2 : Simulated systems which is consist of embedded CCR5 chemokine (CCR5 is represented as a green cartoon) complex into lipid bilayer (DPPC, shown with stick representation), waters (shown as quick surface) and counter ions (K+/Cl-, shown with blue and pink balls, respectively).....60
Figure 5.3 : The Root mean squared deviations (RMSD) of Cα atoms of comparative apo and holo forms in the course of 0.3 μs MD simulations (left). The RMSD of heavy atoms of the maraviroc during MD simulations (right). 61
Figure 5.4 : Distance analysis between Val131 (cytoplasmic side of TM4) and Leu222 (cytoplasmic side of TM5). Superimposition of representative structure from MD (red) with crystal structure (green).....65
Figure 5.5 : Non-covalent bond interactions between the amino acid residues at the binding pocket with the inhibitor (left). In order to identify individual amino acid residues participate in interaction with each segment of the ligand, the 2D chemical structure of maroviroc was inserted into the

profile. The occupancy in percentage of each residue participating in H-bonding with the inhibitor (right).....66
Figure 5.6 : Representative complex from 30000 derived frames after MD simulations has been shown. 2D and 3D ligand interaction diagrams show key interactions at the binding site.....67
Figure 5.7 : H-bond occupancy of second extracellular loops (EC2) amino acids residues in percentage. A comparative analysis is performed for two states.....68
Figure 5.8 : Superimposition of representative apo and holo forms. Upper panel shows extra-cellular side and lower panel display 7TM active cavity...69
Figure 5.9 : Distance plot shows the distance evolution between Val131 (TM5) and Leu222(TM6) amino acid residues respect to MD time.....70
Figure 5.10 : RMSF values of Cα atoms versus residue numbers during 0.3 μs MD simulations. Fluctuation of each TM and loop domains are indicated and compared between the ligand bound- and ligand-free CCR5 chemokine. 71
Figure 5.11 : RMSD evolution of EC2 amino acid residues with the base of Cα atoms for apo and holo systems.....72
Figure 5.12 : Clustering analysis of the maraviroc conformation into the CCR5 chemokine receptor cavity during MD simulations. A color code is inserted (red: initial, blue: final frames).....73
Figure 5.13 : Histograms over Cα atoms RMSD values (Å).....73
Figure 5.14 : Cα-residue dynamics cross correlation map for the ligand-free and ligand-bound CCR5. The color measure operates pink (-1 to -0.75) to white (-0.25 to 0.25) to cyan (0.75-1). Negative amounts (pink) show that Ca atoms displace in opposite way, called anti correlated motions, but positive amounts (cyan) display correlated motions happening at the one way.....74
Figure 5.15 : Clustering profiles of average-linkage algorithm on different subspace dimensions projected by first three PCs. Clustering was performed on the overall (except first 20 ns) MD trajectory frames. Percentage of increasing eigenvector participation to the overall CCR5 motion by the apo and holo state.....75
Figure 5.16 : Domains, directions and degrees of motions respected to the first three PCs were illustrated. The main motion are indicated by broadened tubes (color was changed with the course of time step). First and second columns display the apo and holo state of CCR5, respectively.....76
Figure 6.1 : Amino acid sequence alignment of D2R and D3R. TM and loop domains are indicated by tube and line, respectively. Similar residues from template and target are highlighted with the same colors. The ICL3 part was removed from template and it was artificially modeled, this loop domain is not effective to TM domains.....84
Figure 6.2 : Z-score plot of predicted D2R model.....84
Figure 6.3 : Ramachandran plot of D2R model.....85
Figure 6.4 : 3D chemical structure of used ligand in this work.....85
Figure 6.5 : Cα RMSD evolution of TM domains for all apo and holo systems respect to MD times. Each complex and apo form are shown by various colors. Apo system revealed the lowest conformer stability.....87

Figure 6.6 : RMSD plot of active side residues.....87
Figure 6.7 : Average RMSF values for individual amino acids (only Cα atoms are considered) during MD simulations. Helical and loop domains of D2R models are indicated by tube and line, respectively. The ECL3 domain is broken.....89
Figure 6.8 : RMSF plot of individual amino acids with the base of side chains.....89
Figure 6.9 : Cα radius of gyration values for overal apo and holo systems.....90
Figure 6.10 : Heavy atom RMSD evolutions of D2R inhibitors along MD simulations.....90
Figure 6.11 : Clustering analysis of D2R inhibitors during MD simulation into the 7TM binding cavity. MD color scale is initiated from dark red (corresponds to docking pose) to dark blue, 100 ns in length. Each panel clearly shows the evolution of ligand position respect to the MD time. The positions are clustered (threshold of >2 Å was applied) and popular conformers are considered.....92
Figure 6.12 : H-bond occupancy analysis of ligand-protein interactions (left), For each ligand-bound system occupancy (%) of H-bonds between ligand and receptor are estimated using 10000 MD trajectory frames. Evolution of the H-bond forming and breaking between active residues and inhibitor during MD simulation for each complex (right).....93
Figure 6.13 : Non-bonding interaction analysis for all systems. Active ligand binding residues were selected and their average interaction energy values in six complexes with inhibitors were estimated during MD simulations. To make clear, energy values of Asp114 are excluded from column plot and represented as text.....94
Figure 6.14 : 2D representative structures of D2R inhibitors into binding cavity. H-bond (salt bridges), hydrophobic, polar and π−π stacking interactions are shown by their symbols (as displayed in legend). Phe390, Trp389, His393 and Trp386 residues have participated in π−π stacking interactions. Asp114 is a constrained residue which establishes strong polar interactions with protonated nitrogen of inhibitors.....95
Figure 6.15 : Representative 3D pose of D2R inhibitors in 7TM cavity. Ligand positions of six representative complexes are displayed, and also their ligand-protein interactions (main residues are included) are indicated. TM numbers are displayed on each helical part (TM1-7) and colorized on the base of their positions. H-bonds are shown by black dash line, Asp114 is constrained in all complexes.....97
Figure 6.16 : Conformational deviations of TM5 in different systems. Representative conformer of all apo and holo receptor are superimposed and TMs5 are focused for the better analysis. Dark red helical is responsible for apo form and the other colors display holo conformers. TM5 of aripiprazole-bound revealed a higher displacement from apo form, the other holo conformer have approximately shared the same deviations in the position TMs5.....101
Figure 6.17 : Conformational analysis of critical amino acid residues in ligand binding pocket. Representative positions of amino acid residues which participated in ligand-binding pocket are superimposed and their deviations and displacements from each other are illustrated.....103

Fugue 6.18 : Dihedral angle analysis (atoms: C-Cα-Cβ-Cγ) of His393 during MD simulation for each complex.....104
Figure 7.1 : (a) Chemical structures of JDTic and SalA. (b) Antagonist JDTic (green) bound to human κ-OR (yellow); the complex is merged into a DPPC lipid bilayer (blue) surrounded by water molecules (red). JDTic into the binding site of κ-OR, as depicted by (c) the crystal structure, and (d) the representative structure after 100 ns of MD simulation. Residues that are implicated in κ-OR selectivity of JDTic are shown in blue, residues participating in hydrogen bond interactions with JDTic (after the MD calculation) are shown in red, and Asp138 is shown in yellow.....108
Figure 7.2 : (a) Top: RMSD for Cα atoms of κ-OR residues in JDTic-bound form (red), SalA-bound form (blue), and unbound (apo) form (black). Bottom: RMSD for all atoms of JDTic (red) and SalA (blue) in κ-OR complexes; (b) RMSD for Cα atoms of κ-OR residues participating in hydrogen bonds with JDTic (Asp138, Tyr139, Glu209) and with SalA (Gln115, Leu212, His291); (c) Cα atomic fluctuations of κ-OR residues in its ligand-bound and apo forms; (d) Representative structures of the two dominant JDTic conformations into κ-OR (in water), after clustering analysis. Percentages denote the population of each cluster. 112
Figure 7.3 : (a) Representative structures of the three dominant JDTic conformations in water, after clustering analysis. Percentages denote the population of each cluster; (b) Comparison of free JDTic (Cluster 2, black) with the JDTic κ-OR−bound structures from Figure 7.2d; (c) Comparison between the three free (blue) and the two bound (red) JDTic structures; (d) Angle variation (left) defines changes in JDTic's shape in water and in κ-OR (right).....113
Figure 7.4 : (a) Distances between Cα atoms of selected κ-OR residues (black) that define the shape of the binding site. The seven transmembrane domains are in different colors; (b) Distance between the binding site−covering loop Glu209 (Cα) and His291 (Cα); (c) Distance calculations estimate the size of the binding site in JDTic-bound, SalA-bound, and apo forms of κ-OR.....116
Figure 7.5 : Main hydrogen bond interactions versus time in JDTic−κ-OR and SalA−κ-OR complexes. The numbering on the charts (left) corresponds to the hydrogen bonds shown on the cartoons (right). Chart bars denote the time evolution of HBs and vary in the frequency of HB appearance. 118
Figure 7.6 : (a) Superimposition of representative structures of receptor−JDTic in water (shown in green ribbons) with receptor−JDTic in lipid bilayer (shown in purple ribbons). RMSD = 2.9 Å; (b) Superimposition of representative structures of receptor−SalA in water (shown in green ribbons) with receptor−SalA in lipid bilayer (shown in purple ribbons). RMSD = 3.2 Å; Superimpositions of ligands (c, JDTic), (d, SalA), and active sites of representative structures.....120
Figure 7.7 : DPPC membrane simulations: (a) All-atom, and (b) Cα RMSD of κOR residues; (c) RMSD of residues that participate in hydrogen bonds with ligands; (d) all-atom RMSD for ligands; (e) Cα RMS Fluctuations for

JDTic and SalA complex residues (residue numbering started with 1 in this figure); (f) RMSD of each frame with respect to the average structure.....121
Figure 7.8 : Ligand interaction diagrams of κ-OR−JDTic (top) and of κ-OR−SalA (bottom) in water (left) and in membrane (right).....122

MULTI-SCALE MODELING AND INVESTIGATION OF ACTIVATION MECHANISMS OF G PROTEIN-COUPLED RECEPTORS

SUMMARY

G-Protein Coupled Receptors (GPCRs) constitute the largest class of membrane proteins involved in signal transduction across the biological membranes. They are essential targets for cell signaling and are of great commercial interest to the pharmaceutical industry. They make up ~50% of clinically marketed drugs and ~25% of top-selling drugs targeting this receptor family. Recent advances made in molecular biology and computational chemistry open new avenues in designing novel therapeutic compounds. Molecular biology has provided the crystal structures of several GPCRs in active and inactive states, which can be used as accurate templates in modeling studies. Computational chemistry offers a range of simulation, multi-scale modeling and virtual screening tools for definition and analysis of protein-ligand, protein-protein interactions. Development of new techniques on statistical methods and free energy simulations helps to predict novel optimal ligands.

In this thesis, our aim is to use all these advances by developing an integrated approach for better understanding of activation mechanisms of GPCRs, which will help to rationalize the ligand screening process and facilitate design of new therapeutic compounds for these targets. Defining the activation mechanisms and atomistic determinants of ligand binding to GPCR targets would allow greater safety in human life.

The thesis includes four chapters in which various binding interaction mechanisms based on solved and unsolved GPCR crystal structures are studied in detail. Specifically, activation mechanisms of Dopamine D2, Chemokine receptor type 5 and κ-opioid type GPCRs are elucidated using different *in-silico* approaches as explained below:

Chapter 1 : Dopamine D2 receptor (D2R) plays a crucial role in nervous systems. Its dysfunction leads to the Schizophrenia and Parkinson's diseases. Since the crystal structure of this receptor was not solved yet, it becomes difficult to discover novel, potent and highly selective anti-psychotic drugs. Homology model structures of the dopamine D2 receptor (D2R) were generated starting from the active and inactive states of β2-adrenergic crystal structure templates. To the best of our knowledge, the active conformation of D2R was modeled for the first time in this study. The homology models are built and refined using MODELLER and ROSETTA programs. Top-ranked models have been validated with ligand docking simulations and *in-silico* Alanine scanning mutagenesis studies. The derived extra-

cellular loop region (ECL2) of the protein models are directed towards the binding site cavity which is often involved in ligand binding. The signaling pathway were investigated using normal mode analysis (NMA). Pair residue correlation analysis indicated distinct differences in correlation matrix between active and inactive systems. The binding sites of protein models were refined using induced fit docking to enable the side-chain refinement during ligand docking simulations. The derived models were then tested using molecular modeling techniques on several marketed drugs for schizophrenia. Alanine-scanning mutagenesis study was performed to determine critical amino acid residues in active cavity. We believe that these new D2R receptor models are very useful for better understanding of action mechanisms of drugs to be targeted to the binding sites of D2Rs and they contribute significantly to drug design studies involving G-protein coupled receptors (GPCRs) in the future. In addition 3D-QSAR study was performed using fifty-two approved D2R inhibitors to suggest the common pharmacophores. Our generated D2R pharmacophore model includes AHPRR hypothesis which indicated the role of hydrophobic and polar active site in D2R-ligand interaction.

Chapter 2 : In the this section, structure of the D2R is modeled based on a recently crystallized structure of the Dopamine D3 receptor (D3R). These receptors share a high amino acid sequence homology (> 70%). Several marketed anti-psychotic drugs are then screened at the binding pocket of the generated model. In order to better understand the effect of weak and tight bounded standard drugs on the binding cavity of the receptor, long molecular dynamics (MD) simulations have been performed. Binding energy calculations in molecular level for individual complexes using 0.7 μs MD simulations, in total, assisted mechanistical elucidation of D2R inhibitory treatment. Trajectory analysis of MD simulations showed that, class-I and class-II D2R antagonists exhibit different binding interaction behaviors at the active site of the target.

Chapter 3 : Chemokine receptor 5 (CCR5) belongs to GPCR membrane protein family. CCR5 was included in the treatment of human immunodeficiency virus (HIV) infection. HIV uses CCR5 protein as a co-receptor to get in and infect human cells. Tan et al. (Science, 2013) crystallized CCR5-bound complex with an approved antiretroviral drug (maroviroc) in 2013. During the CCR5 X-ray crystal studies, in order to stabilize the structure, amino acids (Cys224, Arg225, Asn226 and Glu227) at the third intra-cellular loop (IC3) were replaced by rubredoxin molecule. In the current study, we aimed to understand the effect of inserted rubredoxin to the structural properties of TM domains of the target protein. Thus, a homology modeling study is performed by excluding the rubredoxin. Conformational analysis study was then performed during very long (micro-second time-scale) MD simulations. In the light of the current study, a high resolution CCR5 model which does not include fused partner (rubredoxin molecule) was suggested. The derived model structure revealed a distinctive deviation in the cytoplasmic domain of the fifth trans-membrane domain (TM5) as well as third intra-cellular loop (IC3) in the absence of rubredoxin. Thus, it was shown that the existence of the fused partner effects the overall topology of the protein structure. In order to characterize the inhibitory mechanism and conformational space of CCR5 in the presence of the maraviroc drug and to shed light into the functioning of the inhibitor which prevents the binding of envelope glycoprotein gp120 to the co-receptor, 0.6 μs MD simulations, in total, in the *apo* and *holo* forms of the protein were carried out. Our

results revealed that Thr171, Glu172 and Lys173 residues in the extra-cellular loop (EC2) played a critical role in activating gp120 co-receptor. The Trp86, Tyr108, Tyr251, and Glu283 residues were the key-amino acids in the CCR5 binding pocket. The derived results along with a through principle component analysis (PCA) and MD trajectory analyses highlighted important structural and dynamical differences at *apo* and *holo* forms of the target, which are quite striking, and they suggest a greater future role for simulations in deciphering complex patterns of mechanisms of action of the inhibitor.

Chapter 4 : Opioid G protein–coupled receptors (GPCRs) have been implicated in modulating pain, addiction, psychotomimesis, mood and memory, among other functions. We have employed the recently reported crystal structure of the human κ-opioid receptor (κ-OR) and performed MD to elucidate the binding mechanism in complexes with antagonist JDTic and agonist SalA. The two systems were modeled in water and in DPPC lipid bilayers, in order to investigate the effect of the membrane upon conformational dynamics. MD calculations for the complexes in water showed that each ligand was stabilized inside the binding site of the receptor through hydrogen bond interactions that involved residues Asp138 (with JDTic), and Gln115, His291, Leu212 (with SalA). The static description offered by the crystal structure was overcome to reveal a structural rearrangement of the binding pocket, which facilitated additional interactions between JDTic and Glu209/Tyr139. The role of Glu209 was emphasized, since it belongs to an extracellular loop that covers the binding site of the receptor and is crucial for ligand entrapment. The above interactions were retained in membrane complexes (SalA forms additional hydrogen bonds with Tyr139/312), except the Tyr139 interaction, which is abolished in JDTic complex. For the first time, we report that JDTic alternates between a “V-shape” (stabilized via a water-mediated intramolecular interaction) and a more extended conformation, a feature that offers enough suppleness for effective binding. This study provides previously unattainable information on the dynamics of human κ-OR, and insight on the rational design of drugs with improved pharmacological properties.

G-PROTEİN KENETLİ RESEPTÖRLERİN AKTİVASYON MEKANİZMALARININ ÇOK BOYUTLU MODELLEME YÖNTEMLERİ İLE İNCELENMESİ

ÖZET

G-Protein kenetli reseptörler (GPCR) biyolojik membranlardaki sinyal iletiminde önemli bir rol oynayan membran proteinlerinin büyük bir bölümünü oluştururlar. Ticari olarak satılmakta olan ilaçların yaklaşık % 50'sinin hedef yapılarıdır. Son yıllarda moleküler biyoloji ve hesaplamalı kimya alanındaki gelişmeler yeni ilaçların daha iyi tasarımına yeni yollar açmaktadır. Moleküler biyoloji alanında GPCR'ların aktif ya da aktif olmayan haldeki kristal yapılarının bulunması, modelleme çalışmalarının daha güvenilir başlangıç yapılarıyla başlatılabilmesine olanak sağlamaktadır. Hesaplamalı kimya alanındaki yeni yöntemler ve bilgisayar teknolojisindeki hızlı ilerlemeler protein-protein ve protein-ilaç etkileşimlerinin kuantum mekanik ve istatistik mekanik olarak moleküler düzeyde çok boyutlu olarak incelenmesinde ve istenilen özellikteki ilaçların önerilmesinde önemli bir rol oynamaktadır.

Bu tezde, yukarıda bahsedilen gelişmelerin ve yeni yöntemlerin ışığı altında GPCR'ların etkime mekanizmaları aydınlatılmaya çalışılarak, GPCR'ları hedef alan, yan etkileri en aza indirilmiş ya da yok edilmiş yeni ilaçların önerilmesi hedeflenmiştir. İlaç- protein etkileşimlerinin ve etkime mekanizmalarının hassas olarak ve pek çok yöntemin bir arada kullanıldığı bir yaklaşımla incelendiği bu çalışma farklı bölümlerden oluşmuşmaktadır. Özellikle GPCR ailesinden 3 farklı proteinle (Dopamin D2, Kemokin tip 5 ve κ-opioid) bilgisayar ortamında yapılan çalışmalar 5 ayrı bölümde detaylı olarak incelenmiştir:

Dopamin D2 reseptörleri (D2R) vücudumuzdaki sinir sisteminde kritik bir rol oynar. Bu reseptörlerin fonksiyonlarında meydana gelebilecek herhangi bir bozukluk, şizofreni ve Parkinson gibi ciddi nörolojik hastalıkların meydana gelmesine sebep olabilmektedir. D2 reseptörünün kristal yapısı tam olarak aydınlatılamadığından, yüksek derecede seçici, güçlü ve yeni antipsikotik ilaçların tasarımını ve geliştirilmesini oldukça zorlaşmaktadır. Bu çalışmada D2 reseptöre ait model yapılar, β2-adrenerjik proteininin aktif ve inaktif kristal yapılarından yararlanarak oluşturulmuştur. Bildiğimiz kadarıyla D2R’nin aktif konformasyonu ilk defa bu çalışmada modellenmiştir. Homoloji modelleri, MODELLER ve ROSETTA paket programları vasıtasıyla oluşturulmuş ve gerekli olan iyileştirmeler yine bu programlar aracılığı ile gerçekleştirilmiştir. Oluşturulan en iyi modeller, ligand-docking simulasyonları ve in-silico alanin taramalı mutagenez çalışmalarına tabi tutulmuş ve bunların validasyonları yapılmıştır. Protein modellerinin hücre dışında

kalan bölgeleri (extracellular loop, ECL2) ligant (ilaç) bağlanmasında görev alan bağlanma merkezine doğru yönlendirilmiştir. Sinyal iletim yolu normal mod analizi (NMA) ile belirlenmiştir. Çift kalıntı (pair residue) analizi; aktif ve inaktif sistemlerin korelasyon matrisleri arasında belirgin farklar olduğunu göstermiştir. Protein modellerinin bağlanma bölgeleri, ligant-docking simulasyonları sırasında yan zincirle olan etkileşimleri daha iyi detaylandırmak için indüklenmiş uyumlu docking (induced-fit docking) yöntemiyle iyileştirilmiştir. Daha sonra oluşturulan modeller moleküler modelleme yöntemleriyle günümüzde şizofreni hastalığının tedavisi için kullanılan bazı ilaçlar üzerinde test edilmiştir. Alanin-taramalı mutagenez ve moleküler docking çalışmaları test edilen bu ilaçlarla ilgili benzer sonuçlar vermiştir. Oluşturulan yeni D2 reseptör modelleri test edilerek, ilaçların etki mekanizmalarının anlaşılmasında kullanılabilecek doğru model oldukları ve ileride GPCR içeren ilaç tasarım çalışmalarında da çok faydalı olacakları sonucuna ulaşılmıştır. Yapılan çalışmalara ek olarak ortak bir farmakofor önermek için 52 adet D2R inhibitörü üç boyutlu kantitatif yapı-aktivite ilişkisi (3D-QSAR) çalışmasına tabi tutulmuştur. Oluşturduğumuz D2R farmakoforu, D2R-ligant etkileşiminde hidrofobik ve polar aktif bölgenin rolünü ifade eden AHPRR hipotezinin doğruluğunu ortaya koymaktadır. Kemokin reseptör 5 (CCR5) , insan bağışıklık yetmezlik virüsünün (HIV) hücre içine girmek için bağlandığı ve böylece AIDS hastalığına yol açtığı GPCR ailesinden bir proteindir. 2013 yılında Tan et al. tarafından (Science, 2013) CCR5 proteininin bir antiviral ilaca (maroviroc) bağlı bulunduğu bir kristal elde edilmiştir. CCR5 yapısının X-ray kristal çalışmaları sırasında, yapıyı stabilize etmek için üçüncü hücre iç bölgedeki (intarcellular loop, IC3) bazı amino asitler (Cys224, Arg225, Asn226 ve Glu227) rubredoxin molekülü ile değiştirilmiştir. Bu çalışmada amaç, eklenen rubredoxin molekülünün, hedef proteindeki transmembran (TM) bölgelerinin yapısal özelliklerine etkisinin incelenmesidir. Bu amaçla, rubredoxin içermeyen yapı üzerine bir homoloji modelleme çalışması yapılmıştır. Uzun süreli (μs mertebesinde) moleküler dinamik (MD) simulasyonları gerçekleştirilerek konformasyonel analizler yapılmıştır. Bu çalışma ile, rubredoxin molekülü içermeyen yüksek çözünürlüklü bir CCR5 modeli ortaya konulmuştur. Elde edilen modelde, rubredoxin yokluğunda beşinci transmembranın (TM5) ve IC3 'ün sitoplazmik bölgesinde belirgin farklılıklar görülmektedir. Buna göre, rubredoxin molekülünün varlığında, protein yapısının bütün topolojisinin etkilendiği gösterilmiştir. Bu çalışmada, CCR5'in maraviroc ilacı varlığındaki inhibisyon mekanizmasını ve konformasyonel değişimlerini karakterize etmek, bunun yanında kılıf glikoproteinin gp120 koreseptöre bağlanmasını engelleyen inhibitörün fonksiyonunu aydınlatmak için proteinin apo ve holo halinde ayrı ayrı 0.3 μs MD simulasyonları yapılmıştır. CCR5 bağlanma bölgesindeki Trp86, Tyr108, Tyr251, ve Glu283 kalıntılarının en önemli amino asitler olduğu bulunmuştur. Temel bileşen analizi (Principal Component Analysis, PCA) ve MD analizleri ile elde edilen sonuçlar, hedef proteinin apo ve holo formlarındaki önemli yapısal ve dinamik farklılıkları ortaya koymuştur. Bu çarpıcı sonuçlar, gelecekte inhibitörlerin etki mekanizmalarının deşifre edilmesi için yapılacak simulasyon çalışmaları açısından önemli bir role sahiptir. Üçüncü bölümde D2R yapısı, kristali yakın zamanda elde edilmiş olan Dopamin D3 reseptörü (D3R) baz alınarak modellenmiştir. Bu reseptörlerin amino asit sekansları yüksek benzerlik (> 70%) taşımaktadır. Elde edilen yapının bağlanma bölgesinde, piyasada bulunan çeşitli antipsikotik ilaçlar taranmıştır. Reseptörün bağlanma bölgesine zayıf ve güçlü bağlanma özelliği

gösteren ilaçların etkisini daha iyi anlamak için uzun süreli moleküler dinamik (MD) simulasyonları yapılmıştır. 0.7 μs MD simulasyonları kullanılarak her kompleks için moleküler düzeyde bağlanma enerjisi hesaplamaları yapılmış ve D2R inhibisyon mekanizmasının aydınlatılmasına çalışılmıştır. MD simulasyonlarının analizleri, tip-I ve tip-II D2R antagonistlerinin, hedefin aktif bölgesinde farklı bağlanma davranışları gösterdiğini ortaya koymuştur. Opiod G-protein reseptörleri, ağrı modülasyonu, bağımlılık, psikotomimesis, ruhsal durum ve hafıza ve bunlardan başka çeşitli bazı fonsiyonlar ile de ilişiği olan reseptörlerdir. Yakın zamanda kristal yapısı çözülen insan κ-opioid reseptörünün (κ-OR), antagonist JDTic ve agonist SalA ile olan komplekslerinin bağlanma mekanizmalarını aydınlatmak amacıyla moleküler dinamik (MD) simulasyonlar gerçekleştirilmiştir. Konformasyon üzerine membran etkisini araştırmak amacıyla, iki sistem de su ve DPPC lipid çift tabakası içerisinde modellenmiştir. Su ortamında gerçekleştirilen MD hesaplamaları, ligantların Asp 138 (JDTic ile) ve Gln115, His291, Leu212 (SalA ile) kalıntıları ile hidrojen bağı etkileşimleri kurarak reseptörün bağlanma bölgesinde kararlı olduklarını göstermiştir. Kristal yapıdan gelen bilgi, bağlanma bölgesinde yeni bir yapısal düzenlenme olduğunun ortaya çıkarılışı ile geliştirilmiştir ve bu düzenlenmenin JDTic ve Glu209/Tyr139 arasında ilave etkileşimlere olanak tanıdığı gösterilmiştir. Reseptörün bağlanma bölgesinde bulunan ECL'e ait olması ve ligant yakalamada kritik bir öneme sahip olması sebebi ile Glu209 amino asite özellikle vurgu yapılmıştır. Yukarıda bahsedilen etkileşimler, membran komplekslerinde de korunmakla beraber bunlara ilave olarak SalA ile Tyr139/312 arasında hidrojen bağları gözlenmiştir. JDTic ile Tyr139 arasındaki etkileşim kaybolmuştur. İlk defa olarak, JDTic'in deneysel olarak da önerilen v-şekli bu çalışmada gözlenmiştir. Ligant su ortamında moleküler arası etkileşimler yoluyla kararlı konformasyonlar arasında gidip gelmekte olup etkin bir bağlanma için yeterli esnekliğine sahip olduğu gözlenmiştir. Bu çalışmayla insan κ-OR reseptörünün dinamiği üzerine daha önce elde edilememiş bilgiler elde edilmiştir. Sonuçlarımızın geliştirilmiş farmakolojik özelliklere sahip ilaçların gerçekçi tasarımına ışık tutacağına inanıyoruz.

1. INTRODUCTION

1.1 Purpose of Thesis

Mutations of receptors, enzymes and ion channels may result in protein mis-folding. This can result in dysfunction of proteins and thus leads to disease. Finding compounds that target specific G protein-coupled receptors (GPCRs), which are involved in such diseases, is therefore a primary concern for the pharmaceutical industry [1]. Pharmaceutical companies are currently going through a depressive phase. The number of new drugs reaching the market is at an all time low while the cost of developing a new drug has escalated to billions of dollars. The classical high-throughput screening methods which were widely adapted by the pharmaceutical industry in the 1990s have proven to be very costly and have had limited success in finding new drug leads. Increased vigilance against potential side effects of new drugs has also had an adverse effect in drug discovery. The additional screening required has further increased the costs and slowed down the rate of discovery. The industry appears to be affected from an innovation deficit and it needs, new, more rational approaches to drug design. Recent advances made in molecular biology and computational chemistry opens new avenues in designing novel therapeutic compounds. Molecular biology has provided the crystal structures of several GPCRs in active and inactive states, which can be used as accurate templates in modeling studies. Computational chemistry offers a range of simulation, multi-scale modeling and virtual screening tools for definition and analysis of protein-ligand, protein-protein interactions. Development of new techniques on statistical methods and free energy simulations helps to predict novel optimal ligands. In this work, our aim is to use all these advances by developing a multi scale modeling approach to drug discovery, which will help to rationalize the ligand screening process and facilitate design of new therapeutic compounds. The overall goal of the bilateral research work is the investigation of activation mechanisms and development and assessment of drug candidate structures for GPCRs, which are the major drug targets in the

pharmaceutical industry (With more than 800 members in the human genome, GPCRs represents the largest class of membrane proteins involved in signal transduction across the biological membranes. They are essential targets for cell signaling and are of great commercial interest to the pharmaceutical industry, with ~50% of clinically marketed drugs and ~25% of top-selling drugs targeting this receptor family) [1].

1.2 Scientific Aim of the Thesis

Recent advancements in hard and software development nowadays enable to do simulations that were not feasible until a few years ago. The elucidation of the activation process of inactive to active conformational transitions of GPCRs is of fundamental to the understanding of ligand binding modes. Using long MD simulations provided us to elucidate conformational changes of proteins upon binding to agonist/antagonist compounds. Since only 1% of GPCR structures were solved, so the majority of homology modeling methods is appeared in any ligand-protein interactions, structural virtual screening docking and conformational analysis of proteins.

1.3 Innovation Potential

We focused on GPCRs in this study because they offer the widest class of drug targets. Better understanding of activation mechanisms of these targets will help therapeutic solutions of many genetic and acquired diseases. Therapeutic interventions in these diseases require finding ligands that bind to specific sites on the corresponding GPCR and modulate its function so as to ameliorate the disease condition.

Beyond the generation of new therapeutical approaches to treat frequently occurring diseases with new drug candidates, the main conceptual innovation in the thesis is the integrated approach to drug discovery that combines molecular docking, coarse-grained MD simulations, 3D quantitative structure-activity relationships (QSAR) studies and de novo drug design under a single umbrella. Each method has its own strengths and weaknesses, and when used alone, is not likely to yield very useful

results. However, when these methods are combined with positive feedback loops, they enhance each other so that one is much more likely to obtain successful drug leads. In more detail, the conceptual and methodological innovations in the work are:

- We used the crystal structures and homology models of GPCRs (dopamine D2, chemokine receptor type 5 and Opioid receptors) and embed them in their native lipid bilayer, which allowed accurate molecular representation of the receptor sites in docking and MD simulations.
- We tested the energetically favored states and docking results using the more accurate MD simulations, and choose the best docking program and parameterization as input in QSAR studies. This enhanced the quality of the QSAR results and thereby increase the probability of successful prediction of high-affinity ligands for GPCRs.
- We combined the QSAR studies with De Novo drug design using an iterative process. This helped to extend the ligand data base beyond the known compounds, and lead to prediction and design of novel compounds with better binding properties such as higher affinities and better specificity for the target GPCR. The simulation tools developed before are generic can be applied to other membrane proteins. As the membrane proteins are the main targets for therapeutic treatments, these tools had widespread use in the design and development of novel drugs.

1.4 Scientific Excellence and Originality of The Thesis

47 novel three-dimensional structures of ligand-bound GPCRs (which show 19 distinct GPCRs) have been solved in the last five years. Out of 47 ligand-bound GPCRs, 36 were co-crystalized with antagonists and rest were co-crystalized with agonists [1]. Recently new crystal structures of ligand-bound GPCRs (β2-adrenergic receptor) have been determined. (In one, the receptor was stabilized in an active state with a potent agonist, and other structure is crystallized with inverse-agonist bound to the β2-adrenergic receptor [2],[3],[4]. At the same year (2011) agonist-bound active state of another GPCR (A2A adenosine receptor) is crystallized [5]. These has opened a broad avenue of experimental and computational studies that aim to obtain a better understanding of the structure-function relations in GPCRs. On the

computational side, rapid developments in high performance computing and computational methodologies have enabled accurate molecular-level simulations of biomolecules and their interactions with ligands. This is particularly important for the design of drugs targeting GPCRs because computational studies can help to relate the functional data on binding of specific drugs to the molecular structure of an GPCR. The work aims to develop an integrated approach to drug discovery by multiscale modeling, which resulted in design of novel ligands for GPCRs with better binding properties. To the best of our knowledge, the proposed integrated approach to *in-silico* drug design has not been implemented elsewhere yet. While the aim of the study is to investigate activation mechanism of GPCRs and design novel therapeutic ligands targeting GPCRs. Because the majority (>50%) of the drug targets are membrane proteins, the potential for their application is enormous. Recently, many studies using different combined *in-silico* approaches (docking, MD simulation, homology modeling, 3D-QSAR) on the base of GPCRs have been carried out [6]-[10].

1.5 Current State of Science and Technology

G-protein coupled receptors are the target of intense scientific research in the medical and pharmaceutical fields. Given their large number and widespread distribution and roles in cell physiology and the regulation, GPCRs have physiologically very important roles in clinical medicine. A number of monogenic diseases linked to GPCRs have been determined. Genetic disorders identified in GPCRs can influence receptor GPCRs have a hydrophobic exterior, which makes them insoluble in water and thus hard to crystallize for X-ray diffraction. NMR spectroscopy provides an alternative method but it is limited to determining the structures of small peptides or protein segments. GPCRs are located in the plasma membrane and transduce signals through their interactions with ligands from extracellular (EC) side or from intracellular (IC) G proteins. All GPCRs share a common α-helical seven transmembrane (TM) domains. The role of computational chemistry in structure-function relationships for GPCRs has been reviewed by Li et al. [11] and is not repeated here. Recently, Bruno et al. [12] recently have the shown the influence of the membrane composition on the conformation of the amphiatic helix [11] from MD

simulations [12]. Thus special attention has to be paid to a suitable membrane-model in which the receptor is to be embedded. GPCRs bind tri-heteromeric G-protein complexes that include α, β and γ subunits. Upon ligand binding, the Gα protein becomes uncoupled from the Gβγ proteins, allowing it to initiate cellular signaling cascades. G protein mediated signaling starts with an agonist binding molecule to EC side of GPCR that leads to activation of target protein. GPCR is also a guanine nucleotide exchange factor that induces the exchange of guanosine disphosphate (GDP)/guanosine triphosphate (GTP) associated with Gα subunit. Because of the conformational changes at activated GPCR, it promotes exchange of GTP for GDP on the Gα domain which leads to dissociation of Gβγ dimer from Gα subunit. Activated G proteins in this way constitute an amplified representation of the activated GPCR. Activated Gα and Gβγ subunits bind to various effectors, thus switch them either on or off in different systems. The intrinsic GTPase activity of Gα comes into play, that leads to conversion of bound GTP into GDP and hence the inactivation of G proteins cascade [11]. Spectroscopic techniques on purified protein preparations helped to understand the structural differences and structural changes during the receptor activation. These observations suggest essential conformational differences between active and inactive states [13]. Most of the structural and simulation studies so far have relied on the crystal structure of bovine rhodopsin by Palczewski et al. [14]. The rhodopsin structure provided a great deal of information about how GPCRs looked like and revealed for the first time how a GPCR functions at the atomic level. Rhodopsin, however, crystallized in the inactive state. Only recently, protein crystal structures of GPCRs in their ligand-bound active state have become available. This opens a completely new area of research: Investigation of drug binding selectivity and sensitivity to the receptor’s conformation and the conformation transition associated with drug binding. This will be entry point for the project and has the potential to generate new patentable drug-like molecules. GPCRs are activated by a diversity of agonists which differ with respect to chemical class, physical properties and size. It was hypothesized that binding of any agonist induced the active state conformation that activated a single G-protein type to initiate an intracellular signal. It is now discovered that GPCR signalling is much more complex than this. Individual GPCRs can activate multiple types of G-protein and signaling

can be G-protein independent, such as β-arrestin-dependent GPCR activation of MAPK (Azzi et al. [15]). Thus in this research, we used available active and inactive forms of GPCR structures and investigate computationally the activation mechanisms of GPCRs. In order to do this, we created atomistic models of homology models of several families of GPCRs and ligand/receptor interactions were studied using these targets. Furthermore, receptor-based models were matched with ligand-based models to be assured the correct representation of atomistic details at the binding cavity. Binding of a ligand to an GPCR EC sides can stabilize the protein in an active or inactive form. Thus, finding such ligands that bind with high affinity at these different states may lead to therapeutic interventions that modulate the function of a receptor as desired. Jojart et al. [16] for example, have shown that the binding of agonist and antagonist molecules to the human histamine receptor H4 are associated with large conformational changes [16]. The availability of new protein X-ray structures from GPCRs and the realm of computer simulations in this area have not been exploited yet [17]. Its prospects, however, have been recognized and are reviewed in [18]. Since not all crystal structures of proteins from GPCR family are available, drug/receptor interactions for these targets are to be investigated using homology models of proteins of interest that are derived using available crystal structure from same family.

1.5.1 Protein-ligand binding

Accurate prediction of protein-ligand interactions is a major problem in molecular biology and pharmacology [19]. Various experimental techniques are employed for this purpose, e.g., structures of ligand-bound complexes are data mined from X-ray crystallography and NMR, binding energies from rate constants, and specific pairs of residues involved in binding from site-directed mutagenesis studies. While experiments can provide a fairly complete description of a protein-ligand complex, such experiments usually require a great deal of effort and cannot be performed routinely. Similar information on bound complexes may be obtained more easily using molecular modeling techniques such as molecular docking and MD simulations, which have become feasible during the last decade thanks to the rapid growth in computational power [20]. This is a very important consideration in drug

discovery process because one has to screen large numbers of ligand candidates to find the most potent one for a given target receptor.

1.6 Motivation

Parallel to the significant progress made in understanding of molecular mechanism, structure, and function of GPCRs, a growing number of discoveries have linked genetic mutations in these proteins with various diseases. Because GPCR targets play fundamental roles in the regulation of membrane excitability, abnormalities in their structure disrupt the normal functioning of neurons, smooth muscle and cardiac cells, leading to many genetic and acquired diseases such as neurodegenerative, cardiovascular and renal diseases [20]. Therefore, finding therapeutic compounds that target GPCRs that are involved in such diseases is crucial. The classical high-throughput screening methods have proven to be very costly and have had limited success in finding new drug leads. The industry appears to be suffering from innovation costs and would benefit from new, more rational approaches to drug design which exploit the recent advances made in molecular and structural biology and computational chemistry. Computational chemistry provides a range of simulation tools for description of protein-ligand binding, statistical methods for analysis of the binding data that help to predict the optimal ligands, and molecular modeling tools that enable construction of novel ligands. The study aimed to exploit all these advances by developing a multiscale modeling approach to drug discovery, which helped to rationalize the ligand screening process and facilitate design of new compounds with optimum binding properties. Thus, defining the activation mechanisms and atomistic determinants of ligand binding to GPCR targets would allow greater safety in the human life. There are two main hypotheses for the conformational change of GPCRs in response to agonist binding: (i) Conformational selection and (ii) ligand induction. According to the conformational selection model, there are two states of the GPCRs: Active (R*) and inactive (R). Agonists preferentially binds to the receptor in the active state R* and increase the lifetime of active state. The ligand induction hypothesis suggests that transition between the active and inactive states is very rare in the absence of an agonist. Binding of agonist to state R may induce the transition to state R* [13]. Binding of a ligand to an active

site of an GPCR can stabilize the protein in an active or inactive state. Finding such ligands that bind with high affinity could lead to therapeutic interventions that modulate the function of a receptor as desired. The aim of this inter-disciplinary project is, thus, to investigate the molecular mechanisms and energetics of ligand binding to GPCRs using computational methods and exploit these results in the design of new drugs. More specifically: Using the known crystal structures for GPCRs as templates (active and inactive states), develop homology models for a range of target structures from GPCR family. Construct a ligand database for interested target from GPCR family using the potent molecules reported in the literature and computationally designed novel molecules. Evaluate the binding scores for these ligands at the binding pockets of target receptor using *in-silico* docking methods, and perform MD simulations for the best receptor-ligand complexes to examine their stability, study the interactions involved in the binding, and calculate the free energy of binding to test the docking results. Use the measured and predicted binding affinities from docking calculations and MD simulations to perform three-dimensional quantitative structure-activity relationships (3D-QSAR) studies. Use the statistical results derived from 3D-QSAR models as input in de-novo drug design studies to propose novel bioactive compounds with high affinities for specific GPCR and assess their free energies of binding. Perform multi-scale simulations to elucidate the inactive to active transformation of GPCRs.

2. THEORETICAL BACKGROUND

2.1 Molecular Dynamics (MD) Simulations

One of the important approach in *in-silico* study of biological systems is the method of MD simulation. This protocol is performed on the base of time dependent treatment of a atomic system. MD simulations provide rich information on the base stability and conformational changes of protein and nucleic acids. These approaches are now mostly used to elucidate the conformation, mobility and thermodynamics of large biological systems. In addition MD methods are used in crystallography and NMR tools to increase the quality of structure. MD simulations are so useful in elucidation of ligand-protein complexes in order to develop novel drugs.

MD simulation is provided on the base of Newton's second law or the equation of motion, F=ma. Integration of equation of motion will reveal accelerations, velocities and positions.

Newton's second law is defined by:

$$F_i = m_i a_i \qquad \textbf{(2.1)}$$

where F, m and a are the force, mass and acceleration, respectively.

The force can be described as the gradient of the potential energy,

$$F_i = -\nabla_i V \qquad \textbf{(2.2)}$$

These two equation are combined, and the result is ;

$$\frac{-dV}{dr_i} = m_i \frac{d^2 r_i}{dt^2} \qquad \textbf{(2.3)}$$

where V is the potential energy,

A simple application in MD:

Newton's second law:

$$F = ma = m\frac{dv}{dt} = m\frac{d^2 x}{dt^2} \qquad \textbf{(2.4)}$$

acceleration is defined as:

$$a = \frac{dv}{dt} \tag{2.5}$$

obtaining the velocity by integration:

$$v = at + v_0 \tag{2.6}$$

$$v = \frac{dx}{dt} \tag{2.7}$$

again integration,

$$x = vt + x_0 \tag{2.8}$$

combining the equation (2.6) with the equation (2.8) gives the equation (2.9), this equation offers value of x at time t as a function of initial potion (X_0), initial velocity (V_0) and acceleration.

$$x = a t^2 + v_0 t + x_0 \tag{2.9}$$

Acceleration value is obtained from derivative of energy (E) with respect to position. (r).

$$a = -\frac{1}{m}\frac{dE}{dr} \tag{2.10}$$

Initial velocity of the system is calculated by Maxwell-Boltzmann or Gaussian distribution (11 and 12).

$$P = \sum_{i=1}^{N} m_i v_i = 0 \tag{2.11}$$

$$P(v_{ix}) = \left(\frac{m_i}{2\pi k_B T}\right)^{\frac{1}{2}} \exp\left[-\frac{1}{2}\frac{m_i v_{ix}^2}{k_B T}\right] \tag{2.12}$$

The temperature is obtained using equation (2.13).

$$T = \frac{1}{(3N)}\sum_{i=1}^{N}\frac{|p_i|}{2m_i} \tag{2.13}$$

Potential energy of the system is defined as bellow;

(Lennard-Jones potential (also referred to as the L-J potential, 12-6 potential), coulomb , bonds, angles, and dihedral energy),

$$V(r_1 \ldots r_n) = \sum_{ij} \epsilon\left[\left(\frac{\sigma_{ij}}{r_{ij}}\right)^{12} - \left(\frac{\sigma_{ij}}{r_{ij}}\right)^{6}\right] + \sum_{ij}\frac{1}{4\pi\epsilon_0}\frac{q_i q_j}{r_{ij}^2} + \sum_{dihedral} K_\phi[1 + \cos(n\phi - \delta)]$$
$$+ \sum_{bonds}\frac{1}{2}K_d(d - d_0) + \sum_{angles}\frac{1}{2}K_0(\theta - \theta_0) \tag{2.14}$$

2.1.1 Historical background

Molecular dynamics approach has first presented by Alder and Wainwright in the late 1950's [21],[22] to investigate the hard spheres. The second main improvement was in 1964 by Rahman [23] employed the MD simulation method using force field. The initial molecular dynamics simulation of protein was applied by Mc Cammon and et al. [24] on bovine pancreatic trypsin inhibitor.

2.1.2 Statistical mechanics

MD simulation create data on the base of macroscopic stage, including coordinates, velocities. Microscopic information should be converted to macroscopic data such as energy, temperature, pressure and etc using statistical mechanics. Statistical mechanics is the base of investigation of bio-systems using MD approaches. In this part we introduce a summary of important topics [25],[26].

2.1.3 Introduction to statistical mechanics

MD simulations try to calculate the macroscopic properties for example binding free energy between drug and receptor, conformational changing of protein upon ligand binding or examine the mechanism of enzyme inhibition [25],[26]. MD simulations connect macroscopic properties to microscopic information using statistical mechanics which provides the rigorous mathematical expressions. MD simulation can proved thermodynamics properties and time dependent kinetic informations for system.

2.1.3.1 Ensembles

Newton's equations of motion provided us to employ the constant energy for a system. In order to keep constant temperature and pressure of systems during MD simulation different ensembles should be used. There are three kinds of ensembles, including microcanonical ensemble (NVE), canonical ensemble (NVT) and Isothermal–isobaric ensemble (NPT).

The constant-energy, constant-volume ensemble (NVE) is known as microcanonical ensemble. In statistical mechanics NVE is used for the systems with a specific total energy. This system is isolated in the sense that system can't exchange particle or energy from environment, so the energy is the same as initial energy at starting time.

During MD simulation, volume, shape of system, energy and number of particles are kept constant in all possible states.

In statistical mechanics, NVT is known as canonical ensemble that system is in all possible properties share an equilibrated temperature. The system is isolated in the scene that number of particles, volume, and temperature are constant along MD simulation. In simple form, canonical ensemble was defined as probability P:

$$P = e^{\frac{A-E}{kT}} \quad \textbf{(2.14)}$$

where E is the total energy of system, and k is Boltzmann's constant. The number A is corresponded to Helmholtz free energy. The P and A will change if different N, V and T are imported.

NPT is the isothermal–isobaric ensemble which is used in MD simulation. Pressure is kept constant during MD simulation.

The partition function is written as sum of the partition function of canonical ensemble, Z (N, V, T).

$$\Delta(N,P,T) = \int Z(N,V,T)\exp(-\beta PV)CdV \quad \textbf{(2.15)}$$

where $\beta = \frac{1}{k_B T}$ (k_B is the Boltzmann constant) and V is the volume of the system.

2.2 MD Trajectory Analysis

2.2.1 Root-Mean-Square Deviation (RMSD)

RMSD is one of the mostly used MD trajectory analysis. RMSD of all trajectory frames from initial conformer were calculated using followed formula:

$$RMSD = \sqrt{\frac{1}{N}\sum_{i=1}^{N}\delta_i^2} \quad \textbf{(2.16)}$$

where δ is the distance between N pairs of equivalent atoms,

Given two sets of n points (v and w), the RMSD is described as follows:

$$RMSD(v,w) = \sqrt{\frac{1}{n}\sum_{i=1}^{n}\left\|v_i - w_i\right\|^2} \quad \textbf{(2.17)}$$

where n is the number of atoms. V_i is defined as the coordinates of protein V atom I. Here, the RMSD is used to calculate a comparison between the structures of two protein (v and w) folds.

2.2.2 Root-Mean-Square Fluctuation (RMSF)

RMSF is mostly used for flexibility analysis of protein (all atoms or only backbone atoms), which is identified by equation 2.18;

$$RMSF = \sqrt{\frac{1}{T}\sum_{t_j=1}^{T}\left(x_i(t_j) - \widetilde{x}_i\right)^2} \qquad \textbf{(2.18)}$$

where T is the simulation time, x_i is the coordination of particle in time t_j.

2.3 Molecular Docking

2.3.1 Theory

Molecular docking is divided into two parts.

2.3.1.1 Search algorithm

These algorithms consider all possible conformers (position and orientation) of complex. Search algorithm includes different types as follow;

- Molecular dynamics
- Monte Carlo methods
- Genetic algorithms
- Fragment-based methods
- Point complementary methods
- Distance geometry methods
- Systematic searched

2.3.1.2 Scoring functions

This step includes mathematical calculation on the base of docked positions. The energy of established non-covalent interactions between small molecule and protein are predicted and then converted to the numerical values like docking scores.

2.3.1.3 Different types of interactions

- **Electrostatic forces :** Forces between two charged atoms like as charge-charge, charge-dipole and dipole-dipole interactions.
- **Electrodynamics forces :** Van der Walls force is included in this class forces.
- **Steric forces :** Steric forces occur when two atoms of different molecules come closer to or overlap each other and it may leads to change of free energy of system.

- **Solvent-related forces :** Included any forces between the solvent and the protein or ligand such as, Hydrogen bond, hydrophobic interaction.

2.3.2 Molecular docking protocols

In the thesis molecular docking simulations were performed with the Glide Induced Fit Docking (IFD) [27] to conduct flexible docking. The IFD scoring algorithm applies reasonable hydrophobic, hydrogen-bonding interactions and penalizes steric clashes. The IFD protocol is a multi-step processing that includes of (i) an initial Glide docking of ligands during which the van der Waals radius of both the ligand and the receptor are scaled to 0.5 (ii) Prime refinement and minimization of the side-chains for each complex and residues within a 5.0 Å cut-off of each ligand pose. (iii) Then it uses Glide for re-docking of each pose. For all methods, the docking site was defined as an outer box of (28 × 28 × 28) $Å^3$, and an inner box of (10 ×10 ×10) $Å^3$ centered on essential amino acids at the binding site region.

2.4 Principal Component Analysis (PCA)

PCA is a popular statistical data-processing analysis for the decreasing of large-dimensional observations sets onto collective data. In other words, PCA is a process of determining models in data, and describing the data as to focus on their likenesses and distinctions.

2.4.1 Applying PCA on MD simulations

A standard MD trajectory involves the coordinates of overall atoms stored during the simulation. For a system of N atoms, the input data set for PCA can be a statistical data matrix and each column of the matrix indicates Cartesian coordinate for a particular atom at every frame. Before starting the PCA, each frame should be aligned respect to the initial frame because not the displacement and rotations of the structure but the fluctuation of the atoms are considered.

Mathematically obtaining PCs for MD trajectories includes two important stages:

i) generation of the covariance matrix (C),

$$C_{ij} = < \left(x_i - < x_i > \right) \left(x_j - < x_j > \right) > \qquad \textbf{(2.19)}$$

ii) the next stage is diagonalization of the 3N×3N covariance matrix C that can be calculated by eigenvalue decomposition (EVD) as

$$C = V\Lambda V^T \quad \textbf{(2.20)}$$

where Λ describes the diagonal matrix containing the eigenvalues and V describes a matrix including eigenvectors. The eigenvalues display the mean squared displacements (MSD) of atoms (C_α atoms in this study) throughout the used eigenvector.

2.5 *In-silico* Mutation Study

In order to examine the critical amino acid residues in the active site of receptors (ligand binding domain) and their roles in the stability of inhibitors, *in-silico* mutation approaches was performed. For this aim, all amino acid residues within a 4 Å distance from ligand were considered. According to the number of amino acid residues in active site, several complexes were constructed and for individual complexes only one of the considered amino acid residues was manually mutated to Alanine amino acid residue. Constructed systems were then submitted in docking simulations by known ligands. Glide/IFD Docking protocols were employed for estimation of ligand-protein binding energies (docking scores). All of the predicted binding energies values of mutated systems were compared with wild types.

2.6 Ramachandran Plot

A Ramachandran plot [28] identifies the information on all the dihedral angles Φ and Ψ of a proteins. Ramachandran profile is divided into there domains, favorite (red), allowed (yellow) and disallowed (white) areas as shown in Figure 2.1. This plot is a useful validation approach for predicted protein models on the base of homology modeling as we employed in this study.

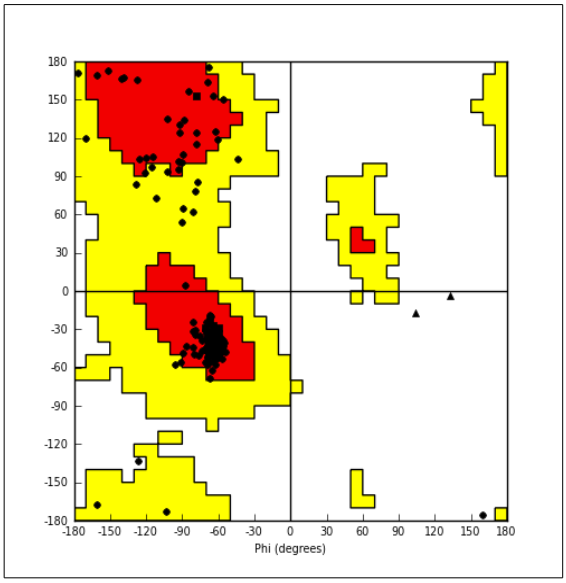


Figure 2.1 : The Ramachandran plot.

3. COMPUTATIONAL DETAILS

We used the simulation methods described below to study the interactions of existing and De Novo designed ligands with GPCRs with the aim of finding novel drug leads. Because of their well-known links with diseases, we focused on dopamine and chemokine and opioid receptors.

3.1 Homology Models for GPCRs-Ligand Data Base

Homology modeling is necessary in the majority of cases where the crystal structure of a GPCR is not known but a high-resolution structure of a homologues protein is available. Because of the high degree of sequence similarity among the GPCRs, construction of a homology model is relatively straightforward. We used the crystal structures (active and inactive forms) of β2 adrenergic receptor for modeling the D2R receptor. Initially we constructed a ligand database for GPCRs from synthesized molecules reported in the literature. As explained below, this database was enriched in later stages of the project by addition of computationally designed novel ligands.

3.2 Molecular Docking and MD Simulations

For docking studies, it is essential to use a realistic receptor system. To this end, the GPCR models were embedded in a well-chosen lipid bilayer, including the critical water molecules at the ligand-binding pockets. Molecular docking studies of ligands and the receptor models gave clues about the ligand binding pockets in the studied GPCR. The amino acid residues of the binding pockets found were compared with the reported studies, and flexible docking using various thresholds and filtering criteria were performed using these binding pockets. From the derived binding poses of ligands, a database was constructed and a cluster analysis was performed based on torsional angle values of rotatable bonds of the ligand. Cluster analysis provided a set of different binding poses as families. From each family, the best docked

complexes were used as input in MD simulations. MD simulations used a similar system as in docking but the system was fully hydrated with several layers of water to complete the simulation box. The ligands selected from the docking studies were placed in the predicted binding positions. The resulting system was equilibrated in long MD simulations, slowly relaxing the restraints on the protein-ligand complex. The trajectory data was analyzed to ensure the stability of the ligand in the binding site. Subsequently, we performed a conformational analysis of the ligand at the binding site and contrast it with that in bulk solution to see if binding is accompanied with any conformational changes. A similar analysis were carried out for the protein contrasting the apo and ligand-bound states, again seeking conformational changes associated with ligand binding. Finally, we used the data to study the interactions between the protein and ligand. Accuracy of the scoring functions and the predicted ranking of ligands is a major issue in molecular docking studies. The docking program and parametrization that yield the most successful ranking when compared to MD results were adapted in subsequent ligand searches for other GPCR families. Specificity of a ligand for a given receptor is a major issue in drug discovery. We performed additional free energy calculations for the ligands selected for all GPCR families so that their binding affinities are determined for all targets. This data helped to assess the potential side effects of a ligand due to unwarranted action on other receptor sites.

3.3 3D-QSAR Studies

We performed 3D-QSAR studies to derive indirect binding information from the correlation between the biological activity of a training set of molecules and their 3D structures. The 3D QSAR study was carried out with the PHASE program of the Schrödinger molecular modeling package. Pharmacophore sites were derived for the different conformations. PHASE uses the most active compounds (high affinity) in the training set to build the pharmacophores. To define a common pharmacophore or hypothesis, PHASE employs an analysis of k-point pharmacophores derived from the conformational sets of active compounds and then identifies all spatial arrangements with pharmacophore features that are shared by those molecules. Thus, a common pharmacophore must match a minimum required number of active ligands (m).

Pharmacophores from different conformations of all m active ligands in the training set was analyzed, and those conformations with identical sets of k point pharmacophore sites that were similarly spatially arranged was clustered and scored determine the critical residues involved in binding. The initial data set was constructed using the molecules reported in the literature and their measured affinities. This data set was be divided into training and test sets. The training set was be used to derive QSAR models and the test set was used to test the stability of constructed models as true unknowns. The wide variation of biological activity and subtle structural variations were taken into consideration throughout the construction of the training and test sets. A conformational search method was be performed with the Monte Carlo Multiple Minimum (MCMM) method (with the ‘enhanced’ torsion sampling option) to derive representative conformers for each ligand in the training and test sets. Subsequently, the importance of steric and electrostatic characteristics were revealed by aligning structurally similar analogues using pharmacophoric features as structural superimposition guides. The predictive ability of the constructed model was be examined using test set compounds, and stability of the constructed model was be tested by partial least square (PLS) statistical analysis.

4. D2R STRUCTURE ON THE BASE OF ACTIVE AND INACTIVE TEMPLATES

4.1 Introduction

G-protein coupled receptors (GPCRs) belong to the largest membrane protein family and are of great importance in a large number of biochemical processes at the cell membrane [29]. They play a significant role in cell signaling processes in response to hormones and neurotransmitters [30]. Human GPCRs are important targets of clinically used drugs [31]. The ligand binding to a GPCR activates or inhibits its target to different extents. According to the activating efficiencies of the ligands, they are named as full or partial agonists, neutral antagonists and inverse agonists [32], [33]. There are around 390 GPCRs encoded in the human genome (excluding olfactory receptors) which were divided into 4 classes [34]. Nineteen of these GPCRs have crystal structures for the inactive state. Active state structures were only available for the β2-adrenergic receptor (β2AR) [35], the adenosine 2A receptor (A2AR) [5],[36], the muscarinic M2 receptor (M2R) [37] and rhodopsin (RHO) [14], [38].

In this study, we focused on the dopamine receptors due to their vital role in cellular signaling in the human nervous system [39],[40]. In the dopamine family, there are 5 receptors identified. Based on their pharmacological similarities identified in brain tissues [41]-[43], they are classified as D1-like dopamine receptors which include D1, D5 dopamine receptors and D2-like dopamine receptors which include D2, D3, D4 dopamine receptors. The dysfunction of the dopaminergic neurotransmitter receptor system has been implicated in a variety of neurological and neuropsychiatric disorders, such as schizophrenia, Parkinson’s disease, and drug addiction since many antipsychotic drugs are dopamine receptor antagonists. In particular, antagonism of the D2-like dopamine receptors has been related to the therapeutic effect of these drugs [41]. Antagonists of the Dopamine D2 receptor (D2R) are studied intensively for being potential drugs against the psychomotor diseases [44]. However, these

antagonists stimulate the prolactin release and they cause severe side effects including induction of acute extra-pyramidal symptoms (EPS), tardive dyskinesia, and problems of galactorrhea [45].

Schizophrenia is a severe illness affecting approximately 1% of the human population. Atypical antipsychotic drugs, such as clozapine, olanzapine, risperidone, quetiapine, ziprasidone are the most widely used marketed drugs for the treatment of schizophrenia, although their mechanisms of actions are still unclear [46].

In this study, we attempt to predict and validate 3D models of unsolved human D2R target structure with the base of active and inactive templates. Recently, Chien and et al succeed to crystallize X-ray structure of dopamine D3 receptor (D3R) (PDB ID: 3PBL) [47] with a high homology degree to D2R amino acid sequence in an inactive conformer. But because of our subjective, D3R crystal structure was not employed as a template in present work. The potential of current insight is using of two active and inactive conformers as templates with the same homology sequence to clearly understand the influence of conformation transition to 7TMs active cavity. For this aim flex receptor docking was performed on generated models. Marketed anti-psychotic drugs were employed as D2R antagonist ligands for docking approach. Alanine-scanning mutagenesis is also used for the prediction of the catalytic or functional role of critical residues. In addition, in order to identify the signaling transcription pathway of D2R activation, we apply normal mode analysis (NMA) on our predicted active and inactive models. Employing full active conformer of β2-adrenergic receptor (β2AR) aids us to shed light on the critical amino acids or secondary structural elements in signaling transmitting providing by D2R. Pair residue amino acids correlation method which was examined by Karplus and et al. [48] used for this strategy.

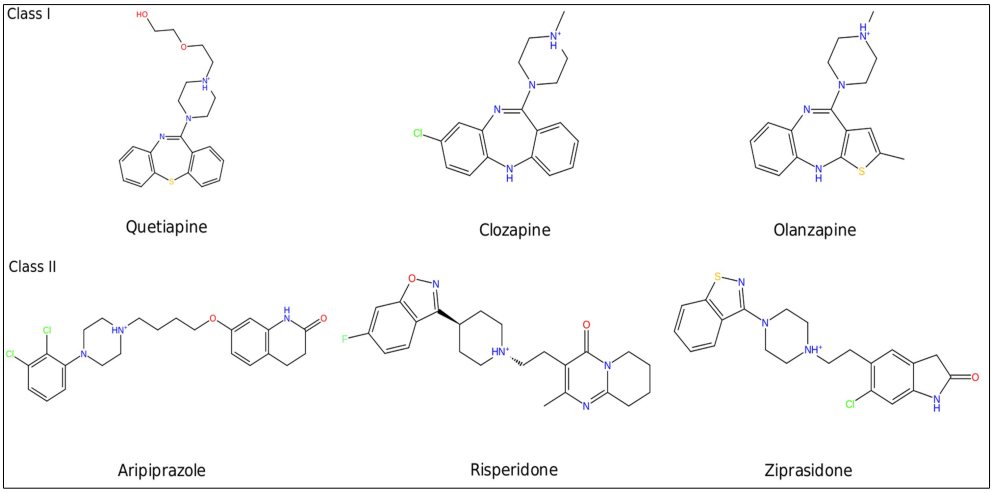


Figure 4.1 : 2D chemical structures of marketed schizophrenia drugs (for clarity non-polar hydrogen atoms are not shown at the Figure).

4.2 Methodology

4.2.1 Homology modeling

The amino acid sequence of human D2R was taken from the UniProtKB database [49] (PDB ID : P14416). Sequence similarity search was performed with the NCBI BLAST server [50]. Initial homology models of the D2Rs were built using MODELLER v9.12 program [51] from the sequence alignment that was achieved using the ClustalW algorithm [52],[53]. The parts with relatively low alignments scores (i.e., loop regions) were re-modeled with ROSETTA loop modeling protocol. [54] The ROSETTA *De Novo* prediction method has been adapted to study for extra-cellular loop (ECL2) modeling. This method is based on the assumption that the native state of a protein is at its global free energy minimum and a global search of the conformational space is carried out to select conformations that are especially low in free energy for a given amino acid sequence. *De novo* loop modeling protocol of ROSETTA was employed using fragment files retrieved from the ROBETTA fragment modeling server [55]. Then the residue-by-residue and overall structural quality is assessed by the PROCHECK [56] to evaluate the low-energy structures of D2R. The homology models were additionally validated by employing of Protein Preparation Wizard [57] which consisted of optimizing the hydrogen-bonding network and restrained minimization of the whole system using Optimized Potential for Liquid Simulations (OPLS) 2005 force field [58], before the ligand docking

simulations. The protonation process of the models at the physiological conditions is assigned employing the PROPKA [59] methodology.

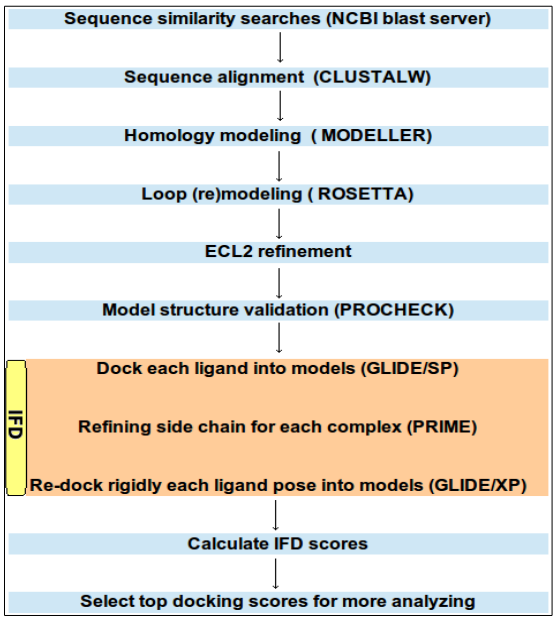


Figure 4.2 : Flowchart of homology modeling evaluation.

4.2.2 Normal Mode Analysis (NMA)

Normal mode analysis (NMA) is one of the most widely used time-independent simulation methods employed to search large-scale conformational changes in protein structures [60]-[62]. NMA is a fast and simple statistical method to calculate the vibration motion and flexibility of protein. In NMA analysis Cα atoms of protein were only considered. NMA of active and inactive models of D2R were performed using Bio3D and R programming language [63]. In this analysis second derivative matrix of the potential energy was calculated, V. The normal mode vectors were obtained by eigenvalue equitation.

$$A^T VA=\lambda \qquad \textbf{(4.1)}$$

The normal modes were described by eigenvectors (A_k) and their eigenvalues (λ_k). The eigenvalues are connected to the conformer transition of the protein along the specified eigenvectors.

4.2.3 Ligands data set

Structure files of ligands (antipsychotic drugs) that are shown in Figure 4.1, were retrieved from the ZINC database [64]. These structures were then protonated at

biological conditions (pH = 7.4) using LigPrep module of Maestro [65]. The conformational search for prepared ligands was performed by MacroModel [66], in order to find a set of low energy conformers via Systematic Pseudo-Monte Carlo (SPMC) method within 1000 maximum number of steps. The energy value for saving conformers was set to 21.0 kJ/mole. To eliminate redundant conformers, a maximum atom deviation cut-off of 0.5 Å was used. The OPLS-2005 force field [67] was used for the conformational search.

4.2.4 Molecular docking

Molecular Docking simulations were performed with the Glide Induced Fit Docking (IFD) [68] to conduct flexible docking. The IFD scoring algorithm applies reasonable hydrophobic, hydrogen-bonding interactions and penalizes steric clashes. [69] The IFD protocol is a multi-step processing that includes of (i) an initial Glide docking [70]-[71] of ligands during which the van der Waals radius of both the ligand and the receptor are scaled to 0.5 using partial charge cut-off of 0.15) (ii) Prime [53] refinement and minimization of the side-chains for each complex and residues within a 5.0 Å cut-off of each ligand pose. (iii) Then it uses Glide for re-docking of each pose. For all methods, the docking site was defined as an outer box of (28 × 28 × 28) $Å^3$, and an inner box of (10 ×10 ×10) $Å^3$ centered on essential amino acids at the binding site region (namely Asp114, Trp386, Phe390 and Tyr416). The homology modeling and docking protocols used in this study are illustrated in Figure 4.2.

4.2.5 Re-docking of crystallographically resolved ligands

Ligands derived from the crystal structures of respective complexes processed using LigPrep are re-docked into β2-adrenergic crystal structures employing the Glide docking software in the standard precision (SP) and extra precision (XP) modes and the induced fit docking (IFD) protocols. The active site was defined as an outer and inner boxes of (28 × 28 × 28) $Å^3$ and (10 × 10 × 10) $Å^3$, respectively (see above), which is defined by the centroid of the native crystallized ligands.

4.2.6 3D-QSAR

3D-QSAR approach was performed using PHASE [72] program of Schroedinger

suite. Fifty-two approved D2R inhibitors were employed in the format of ZINC database in present study. Activity of each ligand against D2R was valued using IC50 amount. IC50 values were submitted in QSAR calculation by converting to pIC50. All input structures of ligands were prepared and minimized in the biological pH (pH = 7) utilizing LigPrep [65] program. In order to provide more variation of conformers for input structures, conformational generating was applied for individual ligands using Monte Carlo Multiple Minimum (MCMM) method. The energy value for saving the conformers was adjusted to 21.0 kJ/mol. An RMSD cutoff of 1 Å was employed to remove same conformers. PHASE employs high active ligands in the training set to generate the pharmacophores. PHASE utilizes an analysis of k-point pharmacophores derived from conformational set of active ligands and then determines all spatial arrangements with pharmacophore features that are shared by those ligands. The functional interactions between receptor and ligand rely on conformational complimentarity between main groups placed in the ligand and orientation of residues in the active site. PHASE identifies these main interactions as hydrogen bond acceptors (labeled as A), hydrogen bond donors (labeled as D), hydrophobic groups (labeled as H), negatively charged groups (labeled as N), positively charged groups (labeled as P), and aromatic rings (labeled as R).

4.3 Results and Discussions

The closest sequence homology in GPCR structure to D2R which include both active and inactive conformers is the β2-adrenergic receptors. Initially, crystal structures of the active and inactive forms of β2-adrenergic receptors have been used as templates for the homology modeling studies of D2R. The structural models were built on the templates of the recently published active (PDB ID: 3SN6) [35] and inactive state (PDB ID: 3D4S) [73] structures of β2-adrenergic receptor which undergoes structural changes when agonists were linked to it [74]-[76].

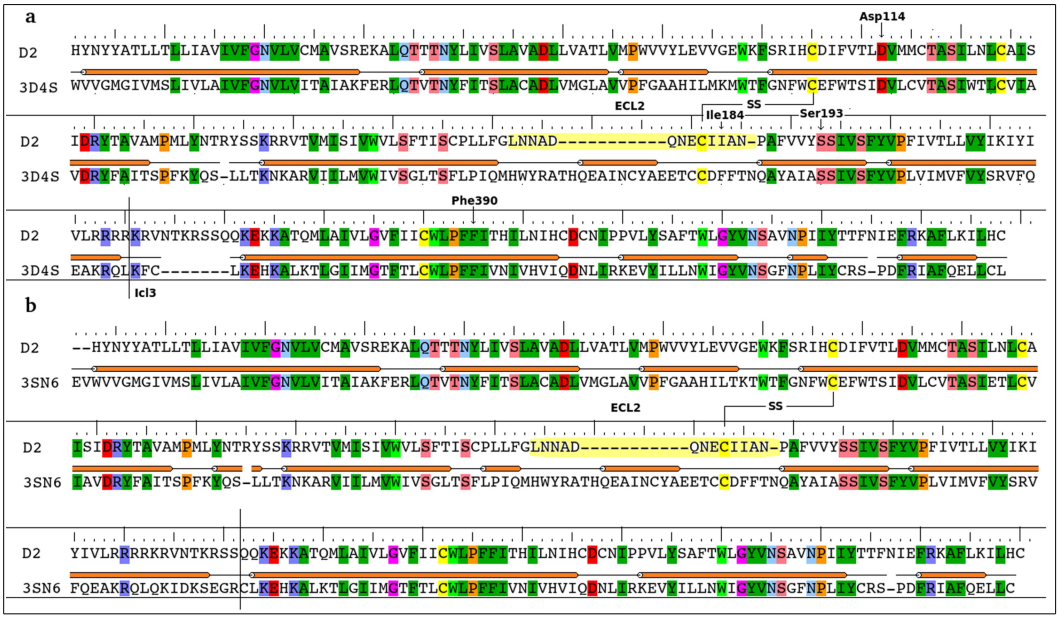


Figure 4.3 : Sequence alignments for **(a)** inactive and **(b)** active templates and D2R. The yellow highlighted parts indicate ECL2 domains.

Active-state structure differs from the inactive state by an outward movement of 5th and 6th helices on the intracellular domain which is necessary for receptor activation as it creates a suitable site for the binding of the G-protein. The sequence similarity between D2R and β2-adrenergic receptors was found to as 35% for the whole structure, 41% in the trans-membrane (TM) regions, and 57% at the binding pocket of the protein (Figure 4.3). The complete crystal structures containing the seven α-helical bundle and all originally occurring loops were used. Only the third intracellular loop (ICL3) at the β2-adrenergic receptors was removed as done in the literature [77],[78].

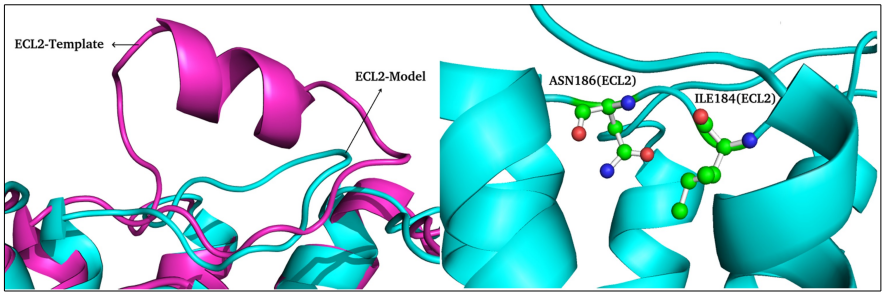


Figure 4.4 : (left) Superimposition of the second extracellular loops (ECL2) of D2R (blue) and the template (PDB ID: 3D4S) (purple) produced by the structural modeling. (right) Presentation of Asn186 and Ile184 residues at ECL2 of homology model that point into the binding-site.

100 possible structural models were generated for both active and inactive conformations and the top-10 lowest energy models ranked on the basis of Discrete Optimized Protein Energy (DOPE) [51] scores and Root Mean Square Deviation (RMSD) values were used for subsequent loop refinements.

Structure building of the flexible domains such as ECL2 was the most difficult part of the homology study. Reasonable conformational alignment between template and model was obtained for the backbone domain except in the ECL2 region. In this region, there is a short helical part at the template, so we chose to focus on ECL2 modeling of the protein because of its size and the critical role that it plays in ligand binding. In the template, this loop adopts a helical structure which consists of 24 amino acid residues. It plays a major role in ligand binding process [79]. The ECL2 loop in the D2R is 11 amino acid residues shorter than the one in the template. The D2R ECL2 loop residues were highlighted at Gly173–Asn186 region as shown in Figure 4.4. All monoaminergic GPCRs like D2R have a disulfide bridge (ECL2-SS-TM3) between two Cysteine residues in ECL2 (i.e., Cys107 and Cys182 in D2R). This bridge constrains the loop on top of the active site. Javitch *et al.* [79] reported that two residues (Ile184 and Asn186) located in ECL2 of D2R are responsible for the ligand interactions at the binding site (Figure 4.4). The residues Asp178-Asn186 in the ECL2 of the D2R were not aligned with the amino acids located in the short helix present in ECL2 of the template (Figures 4.4). According to the secondary structure prediction methods, there is no a stable α-helix organization in ECL2 of D2R [80]. For this purpose, Asp178-Asn186 residues were moved towards the N terminus of TM4, accordingly. The disulfide bridge ECL2-SS-TM3 in D2R was aligned with the corresponding disulfide bridge in the template sequence. The ECL2 residues Asn186 and Ile184 in D2R were aligned with two residues (Thr195 and Phe193) from the templates, which point inward to the binding crevice. Then, an extensive loop refinement was carried out by ROSETTA loop modeling protocols. In order to carry out an enrichment task on ECL2 domain, modeling of ECL2 have also been performed using ROSETTA 3.4. De novo fragment-based loop modeling tool were run to generate 20000 conformers. The points corresponding to the structures around the minimum of energy versus RMSD plot were searched. The disulfide bridge between two Cysteine residues in ECL2 (between Cys107 and Cys182) was

preserved. Finally, hydrogen atoms were added to the homology models and a short minimization was carried out with the all-atom ROSETTA force field. The top-100 models according to ROSETTA energy scores and heavy atom RMSD values were selected and the total number of the models were then reduced to one by comparing with the knowledge in the literature.

4.3.1 Model validations and preparation for subsequent ligand docking

Ramachandran plots are created in PROCHECK to check whether the models are folded correctly relative to the crystal structure of proteins solved in the PDB database. The PROCHECK statistics indicated 95.0% and 94.8% of residues of the D2R models of the active and inactive states, respectively, are in the most-favored regions. There is no residue of both conformers in disallowed regions at the Ramachandran plot (Figure 4.5).

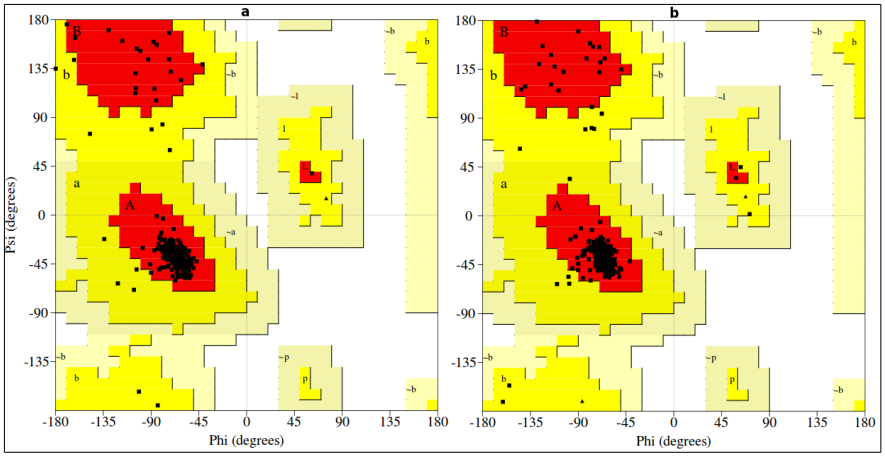


Figure 4.5 : Ramachandran plots of the (a) active (b) inactive β2-adrenergic receptor-based DRD2 models generated with PROCHECK.

The main differences between the inactive and active state homology models are (i) 14 Å outward movement of TM6 helix in the active state; and (ii) smaller outward movement and extension of the cytoplasmic end of the TM5 helix in the active state. (Figure 4.6) Comparing the pairwise binding site RMSD values for these two aminergic target receptors (PDB IDs: 3D4S and 3SN6), there are considerable deviations of the backbone atoms of the active site residues by activated conformer. (Figure 4.7)

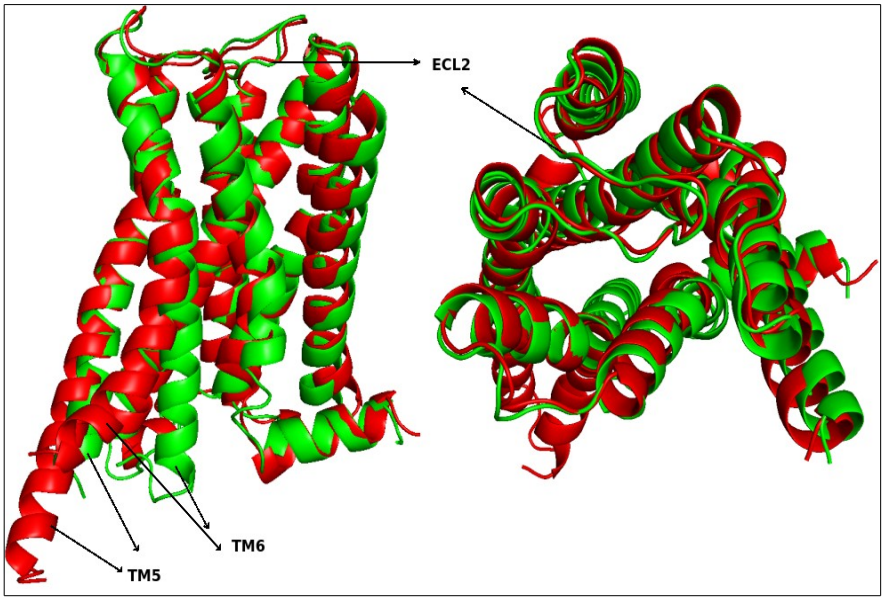


Figure 4.6 : Side (left) and top (right) views of superimposition of refined active (red) and inactive (green) state D2R model structures.

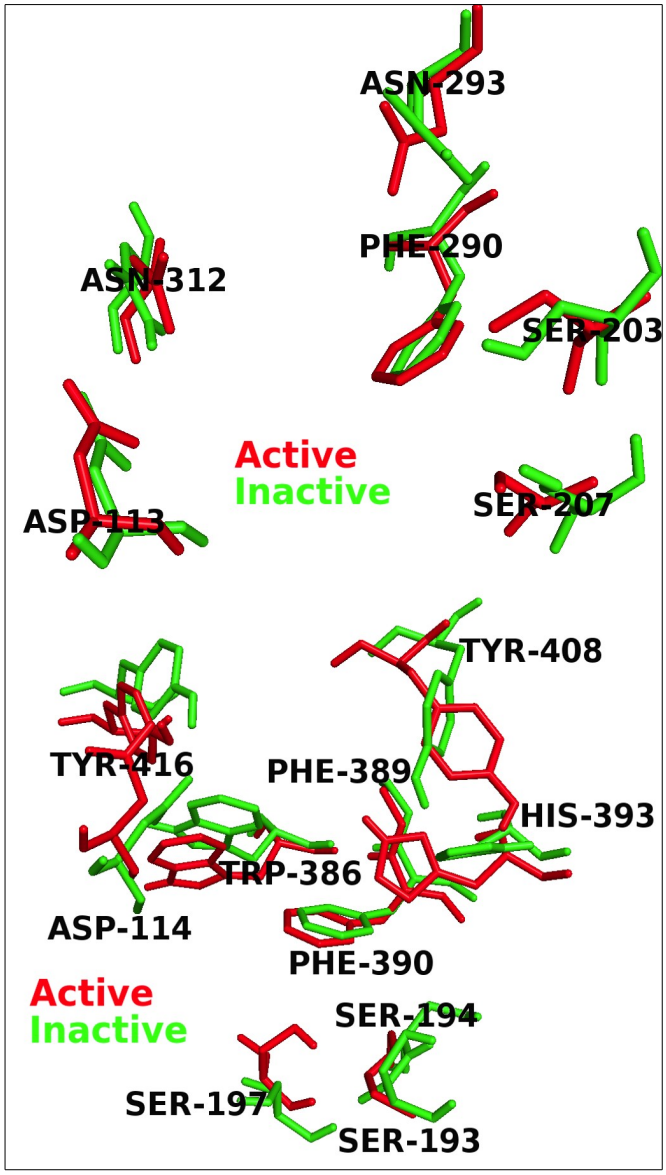


Figure 4.7 : Representation of the superimposition of binding sites of (top) X-ray crystal structures and (bottom) model-structures for the active (carbon atoms are shown with red) and inactive (carbon atoms are shown green) states). Hydrogen atoms are not shown.

4.3.2 Normal Mode Analyses (NMA)

To understand conformational basis of the active and inactive motions, the normal mode analyses (NMA) on the predicted D2R homology models were carried out. Individual amino acid residues fluctuation were calculated for both models, as shown in Figure 4.8. The residual flexibility graphs illustrated the amplitudes of the motions of each residues in the necessary modes. It was seen that terminal residues and loop domains displayed high fluctuation values for both states of the conformers and the

low flexibility belongs to the TM domains, which was a good agreement with experimental suggestions. Comparable stability analysis between two different conformers indicates a higher flexibility value for overall active D2R structure than inactive conformer. Less stability of active conformer is so anticipated upon an agonist binding. Particularly intra-cellular loops in active system show more flexibility than inactive system due to conformational transition in cytoplasmic side. Third intra-cellular loop in active system which connect TM5 to TM6 in cytoplasmic side accommodates G-protein to couple for signal transduction. In order to map position and degree of motions on predicted models, NMA was performed as shown in Figure 4.9. This comparative representation can clearly display the degree of dynamical activity on both structures, as expected, active model is so flex, even in TMs domains. NMA approach successfully displayed difference in stability for two predicted models, and suggested the influence of active conformer transition on overall motion of protein.

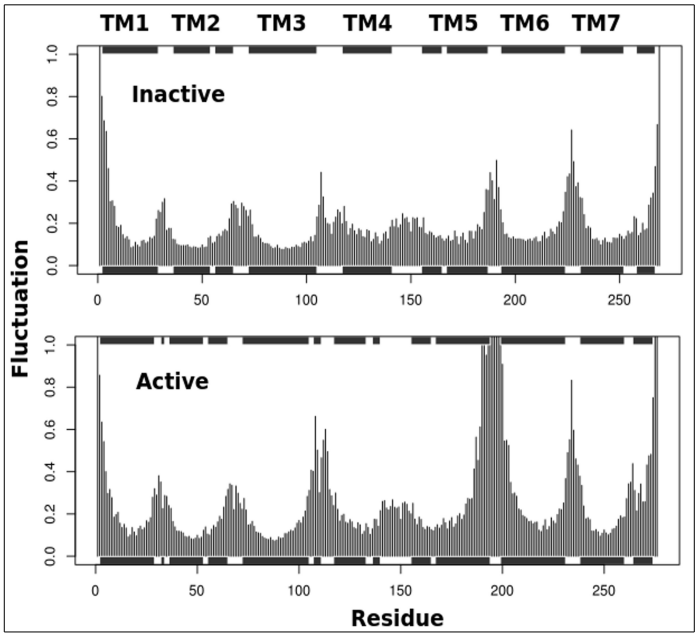


Figure 4.8 : The flexibility graphs for each residue index are shown using normal mode analyses (NMA) of D2R homology models for active and inactive states. The rectangular boxes and blanks represent alpha helices and loops, respectively.

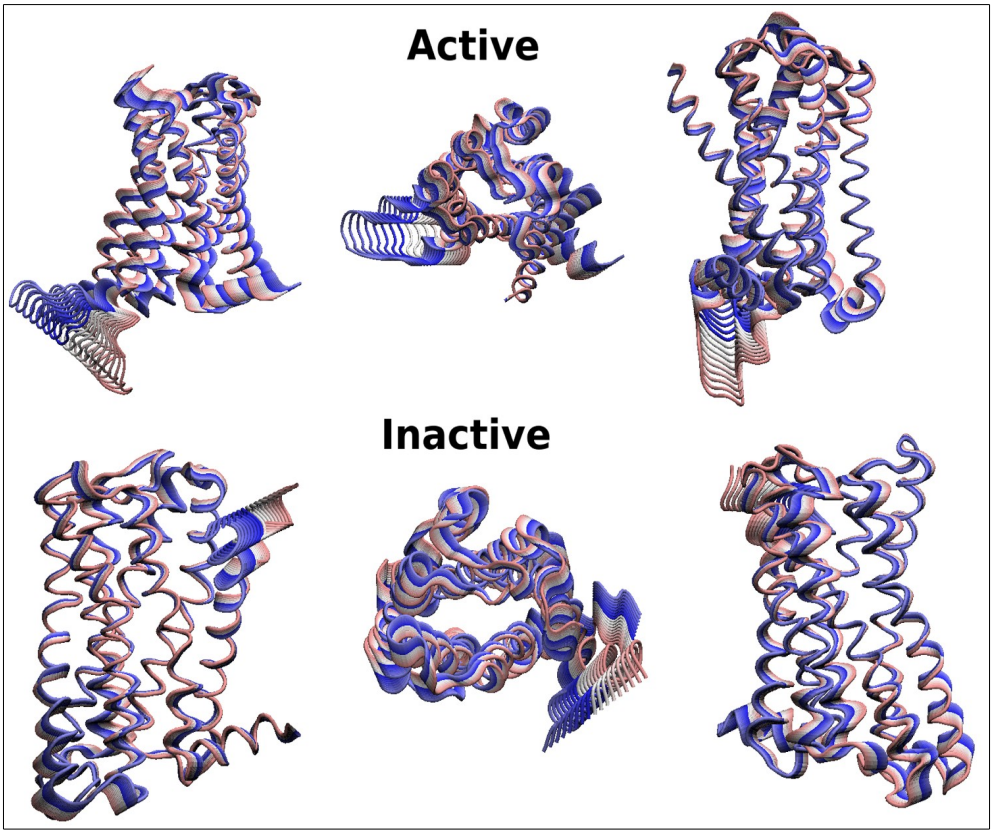


Figure 4.9 : Generated trajectory frames using NMA. Active state shows high fluctuations overall conformer than inactive system.

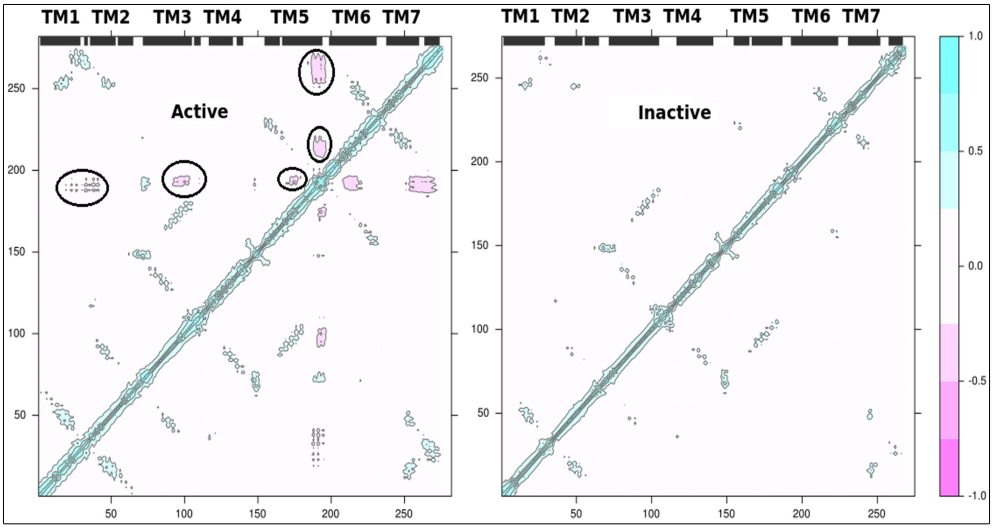


Figure 4.10 : Correlation maps for D2R homology models. Black boxes and blank represent alpha helices and loop domain, respectively. The color measure indicates from dark red (positive correlation) to dark blue (negative correlation).

4.3.3 Signaling pathway of D2R

In this section in order to identify and track the signal transduction provided by D2R, we performed residue-based interaction correlation method. Existing of two full active and inactive models provided us to shed light on signal transduction in the D2R due to the activation mechanism using correlation degree between amino acid residues. Directly or indirectly (signal transmitting by mediated residues) opposite correlations may establish between amino acids of TMs in deferent positions. Cross-correlation matrix was mapped for each model utilizing NMA calculations (Figure 4.10). Correlation profiles along both axes show the amino acid residue position and also secondary structure of each domain. Using this matrix provides us to understand pair residues correlation degree overall protein. In inactive conformer opposite pair residues correlations were not observed, but the active system established identified correlation between residues. These observed correlations are mainly associated to the activity treatments in structure of the D2R. In order to illustrate the critical residues which participated in correlations, identified pair residues were highlighted on active structure (Figure 4.11). Pair residues correlation was presented on each domain of the active conformer by red dotted line. As seen, all correlations were focused in TM5, TM6, TM7 and TM8. Cytoplasmic side of TM5 plays a main role in the center of correlation area. Arg219, Arg220, Val223, Asn224, Lys226 and Ser228 in the position of TM5 are the critical amino acid in signal transduction which establish correlation with specific residues in TM6 (Ile377, Leu379, Gly380, Val380, Phe382, Ile383 and Ile384), TM7 (Val421, Ile424, Ile425, Tyr426, Thr427, Thr428, Phe429) and TM8 (Asn430, Ile431, Glu432, Phe433, Arg434, Lys435, Ala436 and Phe437).

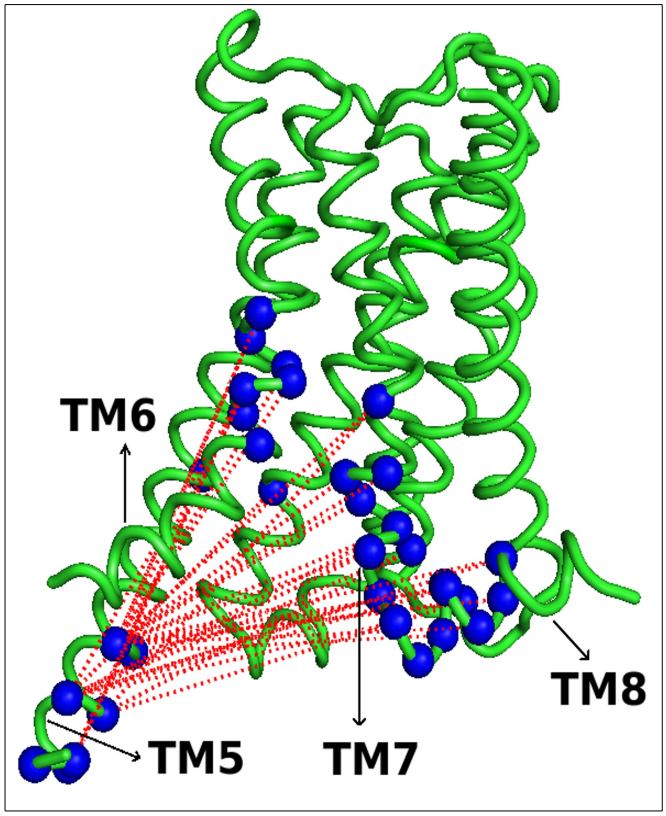


Figure 4.11 : Identification of signaling pathway on active D2R model. The main residues and domains were highlighted on model.

4.3.4 Validation of the accuracy and performance of Glide and IFD docking

In order to check the predictive power of correct binding conformations of poses with the Glide docking program, holo targets that involve conformers of timolol and BI-167107 ligands at the inactive (PDB ID: 3D4S) and active (PDB: 3SN6) states of the β2-adrenergic receptor of crystal structures are considered. The Glide/SP, Glide/XP protocols, and Glide/IFD, which allows conformational refinement within the receptor, are used. While the RMSD of heavy atoms between the Glide/IFD-generated docked pose and the conformer of timolol at the crystal structure was found to be 0.74 Å (Figure 4.12), the RMSD of heavy atoms between the Glide/IFD generated docked pose and the conformer of BI-167107 at the crystal structure is found to be 0.50 Å (Figure 4.13). Since Glide/IFD generated poses of timolol and BI-167107 have very good agreement with the conformations of ligands in the crystal structures (PDB IDs: 3D4S and 3SN6), the IFD module can be reliably employed to predict the binding interactions between docked compounds and D2R.

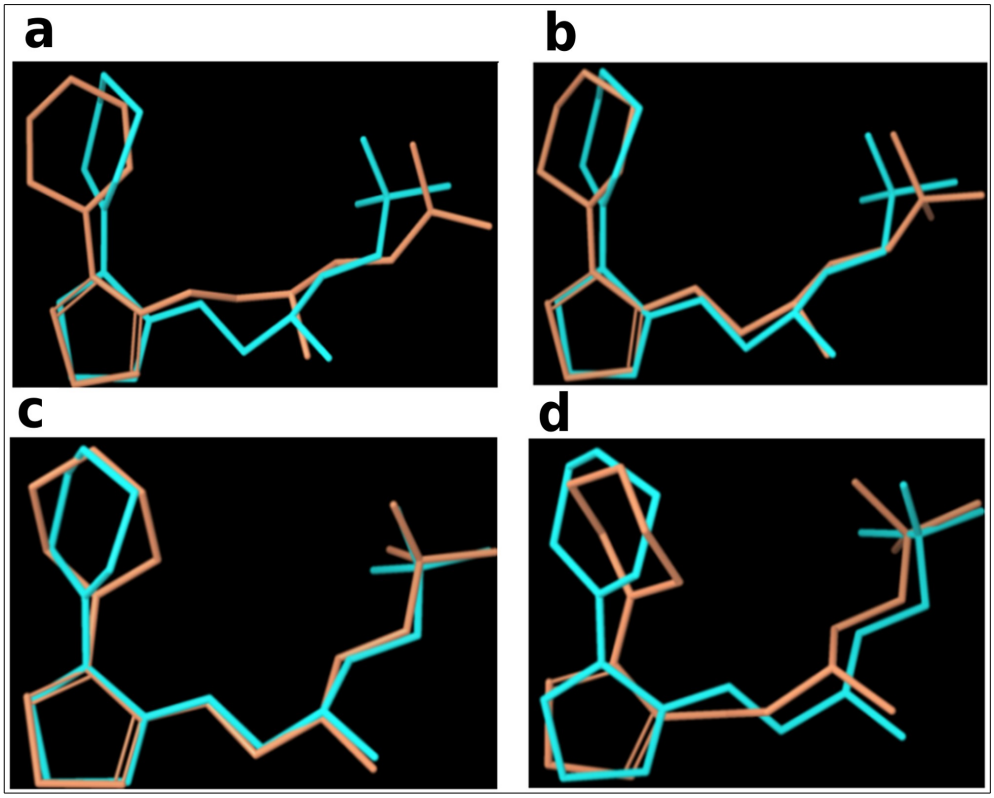


Figure 4.12 : The validation of accuracy and performance of Glide/SP, XP and IFD docking protocols for inactive state (PDB ID: 3D4S). The docked timolol (brown) and co-crystallized structure of timolol (blue) showed a root mean square deviation of (a) Glide/SP-0.69 Å, (b) Glide/XP-1.07Å, (c) Glide/IFD (SP) (re-docking with SP)-0.53Å, (d) Glide/IFD (XP) (re-docking with XP)-0.74 Å.

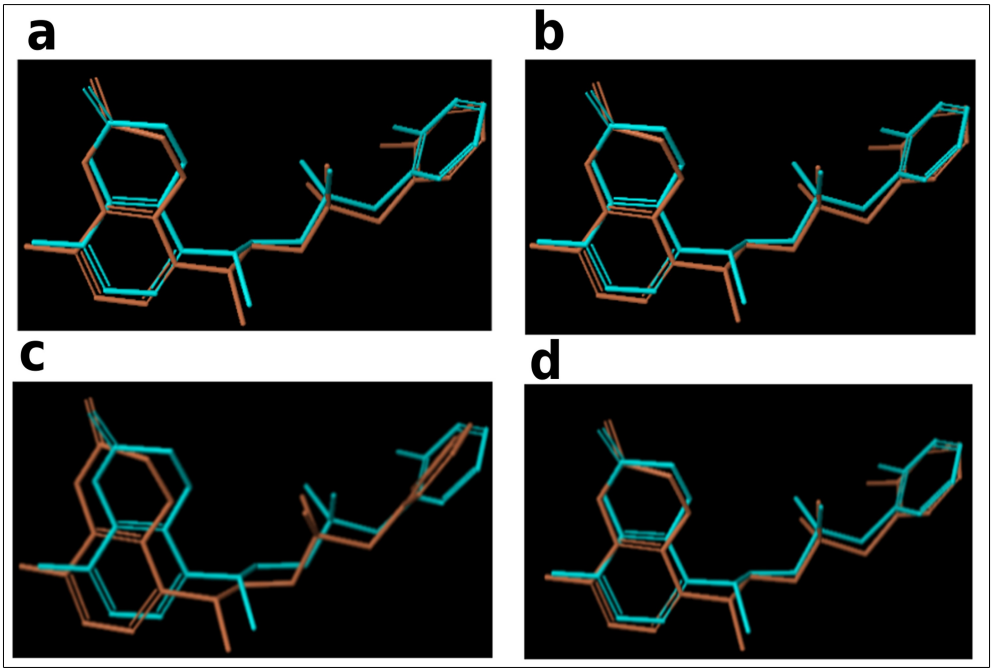


Figure 4.13 : The validation of accuracy and performance of Glide/SP, Glide/XP and Glide/IFD docking for active conformer (3SN6). The docked BI-167107 (brown) and BI-167107 at the crystal structure (blue) demonstrated a root mean square deviation of (a) Glide/SP-1.79 Å, (b) Glide/XP-1.44Å, (c) Glide/IFD (SP) (re-docking with SP)-1.09Å, (d) Glide/IFD (XP) (re-docking with XP)-0.50 Å.

4.3.5 Molecular docking and binding energy calculation

Several marketed drugs for schizophrenia are used as antagonists against the D2 receptor. (Figure 4.1) The D2R antagonists used are grouped in two classes: class-I (clozapine-like bulky antagonists) and class-II (antagonists that include two aromatic or ring connected by a rotatable connector with a protonated amine group as in ziprasidone) [81]. All six antagonist ligands considered in this investigation were individually docked into the active sites of the D2R in their presumed pharmacologically active and inactive conformations. One of the most difficult parts in molecular docking is the prediction of binding sites of small molecule compounds in homology model targets. IFD protocols are widely used in order to predict the binding affinities. The IFD method is aimed to be able to assist to find correct binding mode of small molecule inside the active site using induced-fit effects by the selection of a refined sample for the side-chain rotamers. The resulting poses were ranked based on IFD Score and Glide/XP GScore for each ligand. Accurate capture of specific binding interactions of poses that are not listed at the top-docking poses

were also selected for further analysis. It is very likely that most receptor antagonists share the same binding site, since they also share the ability to stimulate the receptor during the binding process. Table 4.1 shows the top-docking scores of ligands at the active and inactive states of the targets. In order to facilitate the comparison between docked poses and experimentally determined ligand binding studies and simple analogy of experimental results and calculated values, binding affinities are showed as binding energies. (Table 4.2) The Gibbs free energy of binding ΔG^0 is linked to the binding constant with "ΔG^0 = -RT lnKi". In silico docking experiments of this study and reported *in vitro* activity of the antagonist ligands show that class II antagonist can bind tightly to the receptor at two states rather than Class I antagonist. (Table 4.1)

Table 4.1 : Calculated binding energy (from IFD, kcal/mol) of known binder in to D2R. Experimental K_i (Exp. K_i, nM) (1) with respective references are also shown.

Ligands	Active E-binding	Inactive E-binding	Exp. Ki	Exp E-binding	Active Ki	Inactive Ki
Risperidone	-11.76	-12.76	2.20	-11.80	2.31	0.43
Ziprasidone	-11.60	-14.21	3.10	-11.59	3.05	0.04
Aripiprazole	-10.36	-11.75	4.40	-11.39	24.89	2.37
Clozapine	-9.58	-12.04	83.00	-9.65	92.57	1.46
Olanzapine	-9.87	-10.87	53.00	-9.91	57.08	10.42
Quetiapine	-11.05	-12.64	16.00	-10.61	7.69	0.52

(1) Average value from PDSP database.

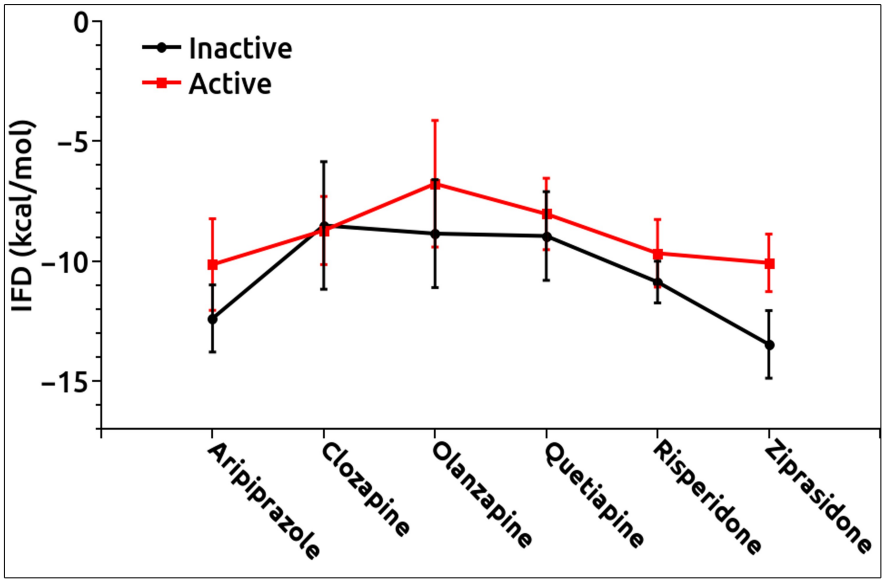


Figure 4.14 : Calculated IFD scores with their standard deviations for docked ligands against active and inactive modes.

IFD protocol provided several complexes for each ligand which differ in binding energies, ligand poses and orientations. Here we performed an average calculation for individual ligands and plotted them with inducing standard deviation values as shown in Figure 4.14. Higher binding affinities for docked ligands were observed against inactive conformer than active structure, which was anticipated because of D2R inhibitory treatment of the drugs. These results suggested the influence of conformational transition in cytoplasmic side on 7TM active cavity, which each conformer accommodates docked ligand with a deferent affinity. Active site residues and their types of interaction with commercially available drug ligands are summarized at Table 4.2. First, all D2R ligands known to date include a constrained nitrogen atom, which is protonated under physiological conditions. From thorough literature search and our current *in-silico* study in following Dopamine D2 antagonist binding site, particular properties necessary for activity have been determined (Table 4.2). These features consider: (i) the protonated nitrogen atoms are involved in a highly electrostatic interaction with a conserved aspartic acid residue in TM3 (Asp114), [82] the carboxyl group of the aspartic acid make a tight salt bridge with the primary amino group of all class I and II antagonists for both active and inactive conformers, as well as in all human biogenic amine receptors, mutation studies have implicated this residue in the direct binding of the D2R [83] and indicated the

significance of the Asp114 residue in aminergic GPCRs, due to its crucial interaction with the protonated nitrogen of the ligands, [83], [84] (ii) the second extracellular loop (ECL2) of the D2R includes Ile184, Ile183 and Asn186 residues that are positioned to face down into the binding pocket and contribute to the binding interactions with ligands (Figure 4.15), (iii) a hydrophobic interaction in TM6 (i.e., Trp386, Phe389, Phe390 and His393 residues) has also been recognized to be main for D2R antagonist ligands interactions. It should be noted that Phe390 is not only important for ligand binding, but it also has a role for activating D2R. This residue is found in all of the top-docking poses to take part in protein–ligand interactions, (iv) out of 13 residues at TM5, 5 of them (i.e., Ser193, Phe189, Phe198, Val190, Val191) are key-residues necessary for antagonist ligands binding. (v) Tyr408 and Tyr416 residues in TM7 make up a mostly hydrophobic pocket for antagonist ligands. Residues at the TM1 and TM4 helices do not play an important role for class I and II D2R antagonists binding.

It is observed that binding modes of some ligands (i.e., Aripipirazole) have a shorter salt bridge (~1.5 Å) compared to their conformers at the active state (~2.0 Å), (Figure 4.16). Aripiprazole constructs a hydrogen bond with Asp114 from central nitrogen atoms. The hydrogen bonds are formed with 2.5 Å and 1.5 Å at active and inactive states, respectively. Although docking pose of aripiprazole at the inactive state also construct another hydrogen bonding interactions with Glu95, it does not form this interaction at the active state (Figure 4.16).

Table 4.2 : Ligand protein interaction of D2R antagonists docked with IFD.

	Active state		Inactive state	
Ligands	**Hydrogen-bond**	**Hydrophobic interaction**	**Hydrogen-bond**	**Hydrophobic interaction**
Risperidone	Asp114, Ile184 (from backbone, NH)	Val190, Val115, Val111, Val91, Phe390, Phe389, Ile184, Ile183, Tyr408, Phe110	Asp114, Ile184 (from backbone, NH)	Val115,Cys118,Tyr416 Val91, Phe389, Leu94, Ile184, Ile183,Tyr408, Phe390, Val111, Phe110
Ziprasidone	Asp114, Ser193, Thr119	Ile183, Ile184, Phe389, Val191, Phe189, Tyr416, Phe390, Cys118, Val111, Tyr408, Phe110, Leu94, Val115	Asp114, Asn186, Ser193	Ile183, Ile184, Phe389, Val115, Trp386, Tyr416, Phe390, Cys118, Val111,Tyr408, Phe110
Aripiprazole	Asp114	Val111, Phe389, Phe390, Leu94, Ile184, Ile183, Trp413, Phe110, Val91, Phe110, Val115, Tyr408, Tyr416	Asp114, Glu95	Pro405, Ile183, Ile184, Phe110, Phe389, Tyr416,Val111, Phe390, Val115, Tyr416, Leu94
Clozapine	Asp114	Ile184, Phe389, Val115, Phe189, Tyr416, Leu171, Cys118, Val111, Val190, Tyr408, Phe189, Trp386	Asp114, Ser193	Ile184, Phe389, Val115, Phe189, Tyr416, Trp386, Phe390, Cys118, Val111,Tyr408, phe198
Olanzapine	Asp114, Ser193	Val111, Phe390, Phe389, Trp386, Ile184, Cys118, Phe189, Tyr416, Leu171, Ile122	Asp114, Ser193	Val115, Val111, Val190,Phe390, Phe389, Trp386, Ile184, Cys118, Phe198, Tyr416, Phe189
Quetiapine	Asp114, Tyr408, Cys182 (from backbone, CO)	Val115, Val190, Phe389, Ile184, Val91, Phe390, Tyr416, Leu94, Tyr408, Phe110	Asp114, Cys182 (from backbone, CO)	Val115, Phe189, Val111, Ile184, Cys118, Phe198, Tyr416, Leu94, Val91, Ile183

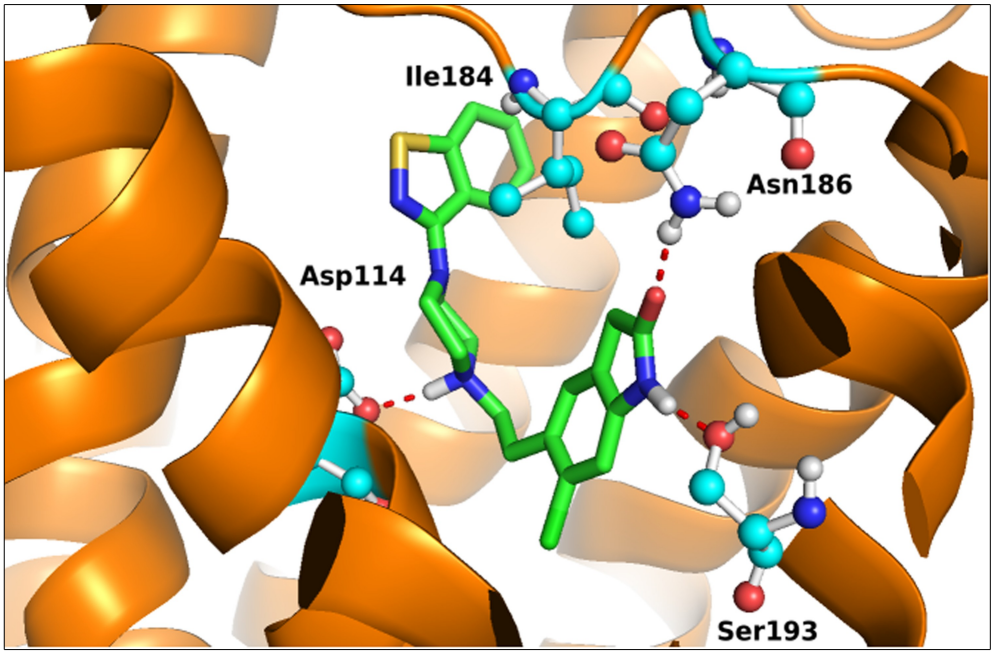


Figure 4.15 : Top-docking pose of Ziprasidone at D2R active model. Binding interactions of ECL2 residues (Ile184 and Asn186) and Ser193 (TM5), Asp114 (TM3) are shown. Dashed lines indicate salt bridge and HB interactions.

The IFD results show that all docked drugs bind to Dopamine D2 receptor mostly in a similar manner (Table 4.2). Our flexible receptor docking approach can be exemplified using the Dopamine D2 receptors active and inactive models. Risperidone (Figure 4.17) docking into the D2R (active and inactive) homology models show that several observed key interactions are consistent with site-directed mutagenesis data [85],[95]. Risperidone antagonist shows higher docking scores for D2R in the inactive conformer compared to active state (Table 4.1). The salt bridge between the protonated nitrogen of the risperidone and the conserved Asp114 (1.8 Å) and the hydrogen bonding between the carboxyl group on Risperidone and Ile184 (from backbone at ECL2) (~2 Å) are observed (Figure 4.17 and Figure 4.19). TM5 residues in positions of Ser193, Ser194, and Ser197, while not conserved throughout the aminergic GPCRs, are often involved in aminergic ligand-receptor interactions [83]. Risperidone also makes a substantial number of VDW contacts, particularly with the aromatic network that are listed at Table 4.2 and hydrophobic interactions with Ile183 and Ile184 in ECL2, adjacent to the conserved Cys182 and π-π stacking interactions with His393 for inactive conformer. The importance of the aromatic network has been also identified by site-directed mutagenesis study.

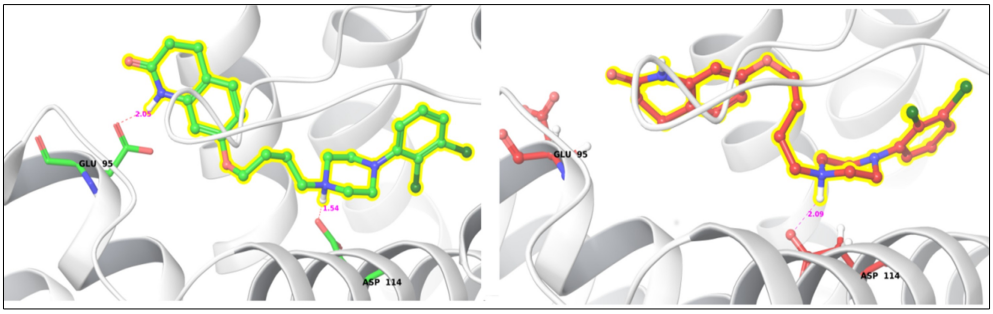


Figure 4.16 : The docking poses of Aripiprazole antagonist with D2R in inactive (left) and active (right) state models.

Docked complexes of Aripiprazole, Clozapine, Quetiapine, Ziprasidone, Olanzapine into the two states of targets also displayed consistent interactions (Figure 4.18). Clozapine and Olanzapine are the smallest molecules (Class I) studied here and different binding poses at the active site of targets can be observed. For example, conformers of Clozapine at the binding pockets of active and inactive targets have a RMSD value of 4.7 Å. This is not surprising since clozapine is a small molecule and it may form different binding modes both in active and inactive states of targets. While Clozapine forms a salt bridge with Asp114 (TM3) residue, and hydrogen bonding interactions with Ser193 (TM5) and Tyr416 (TM7) residues at the inactive target, these interactions are not observed at the active target. (Figure 4.18b). Our results also show that Ile184 residue from ECL2 in Dopamine D2 receptor at both conformers has a strong hydrophobic interaction with Clozapine antagonist (Table 4.2). In the case of Quetiapine, while at the active-state it forms π-π stacking interactions with Tyr408 residue, at the inactive target this interaction does not exist. Conformations bound ligands at active and inactive states have two distinct conformations (RMSD of 4.1 Å).

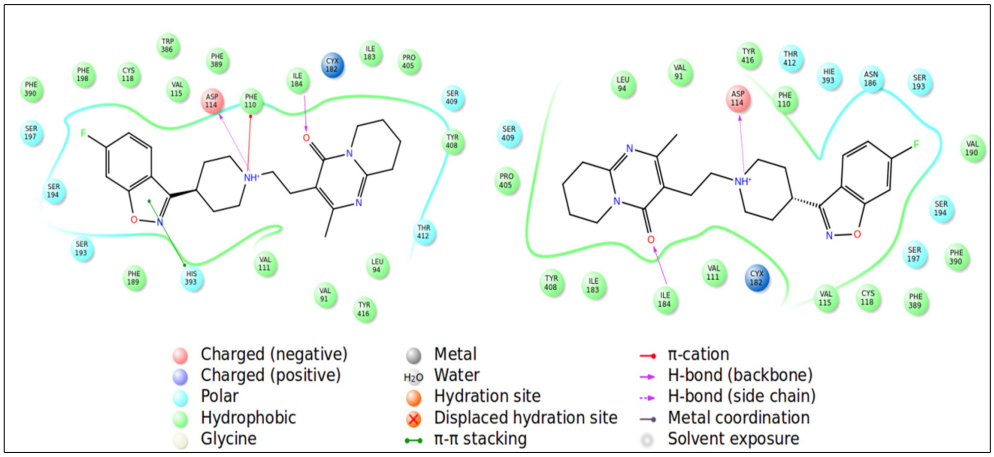


Figure 4.17 : Schematic 2D plots of protein-ligand interactions created for IFD: (a) Risperidone docked into the inactive receptor and (b) Risperidone docked into the active form of the D2R. Hydrogen atoms are omitted for clearance.

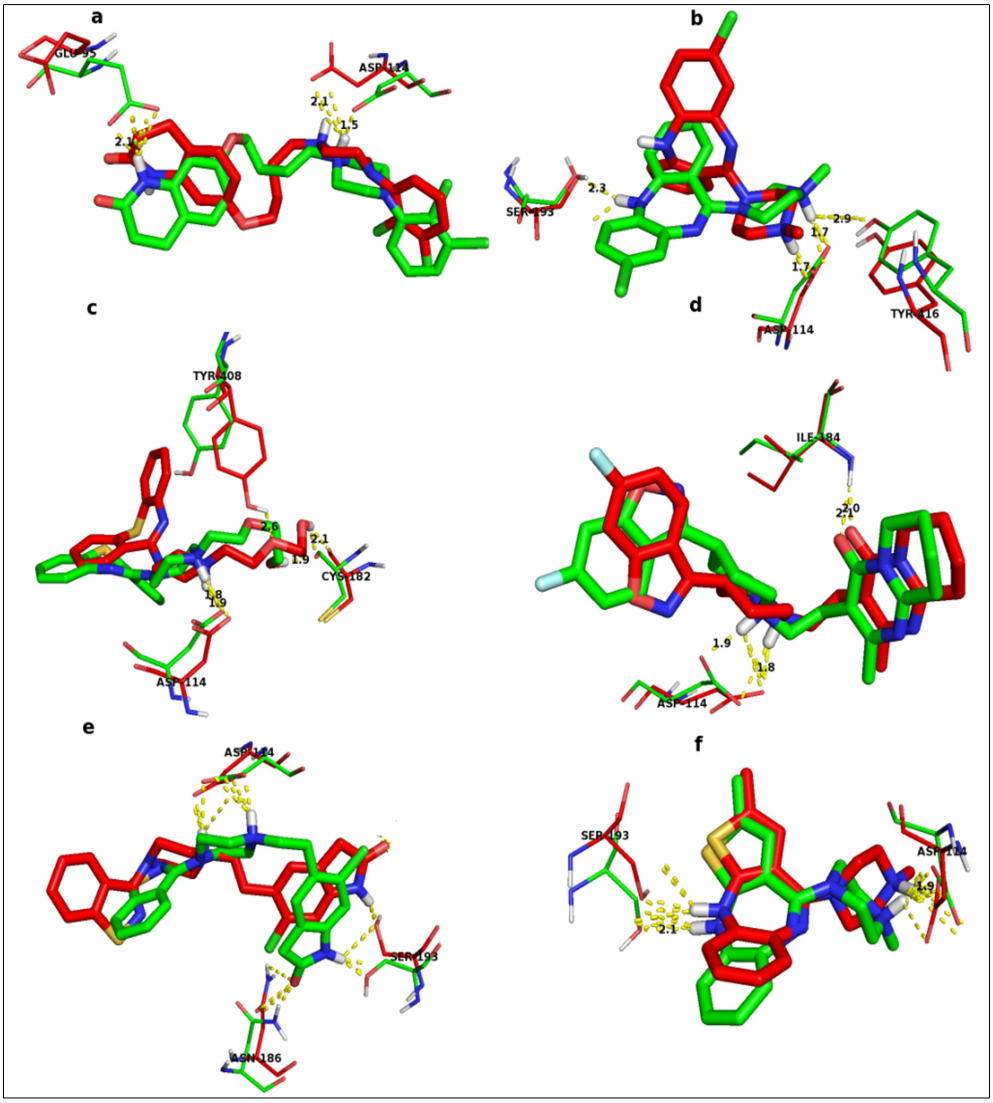


Figure 4.18 : Schematic view of the comparison of binding modes of **(a)** Aripiprazole, **(b)** Clozapine, **(c)** Quetiapine, **(d)** Risperidone, (**e**) Ziprasidone, **(f)** Olanzapine in the homology models for active (carbon atoms are shown in red) and inactive (carbon atoms are shown in green) conformers of D2Rs. Amino acid residues that formed hydrogen bonds with ligands have been also shown at the figure.

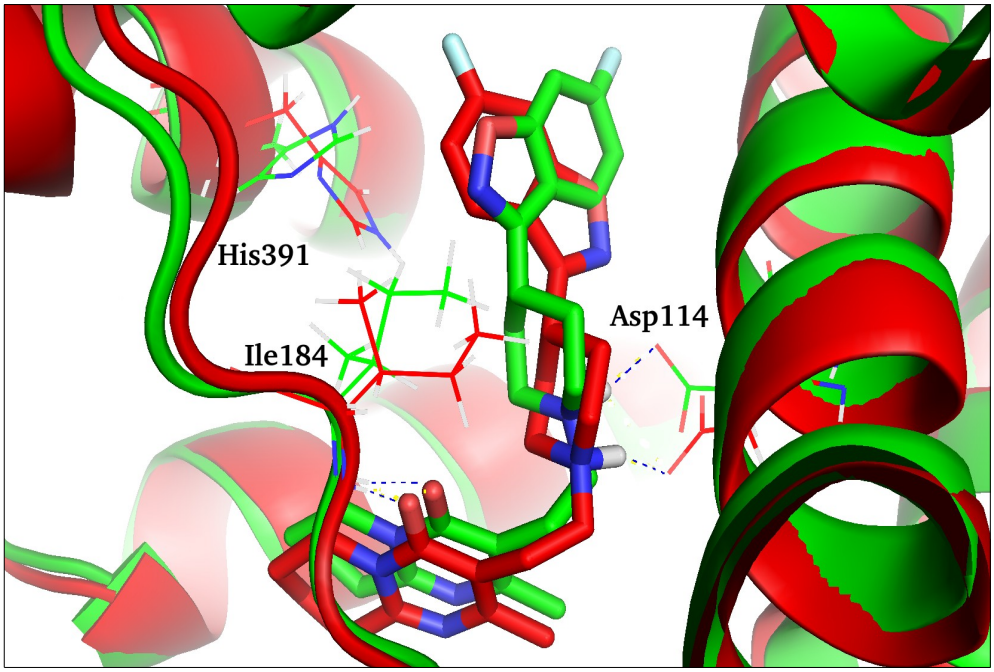


Figure 4.19 : Representation of the superposition of binding site of active (red) and inactive Dopamine D2 receptor interactions with Risperidone. (For clarity, non-polar hydrogen atoms on ligands were not shown and only residues that provide H-bond and π-π stacking interactions with ligands are shown).

4.3.6 Distance analysis

In order to elucidate the size of 7TM cavity in active and inactive D2R models and clear their difference in ligand binding domain, distance calculation between critical amino acid residues in the active site was performed. For this aim residues Ser194 (TM5), Phe390 (TM6), Asp114 (TM3), Tyr416 (TM7) were piked in both models and their distances with respect to each others were identified. Both models approximately share the same shape as binding pocket (Figure 4.20). The distance between Phe390 and Tyr416 in inactive state (13.2 Å) is longer than active system (12.8 Å). But in contrast Asp114 in inactive conformer is closer to Ser194 than active form. These different distances are associated to the distinct deviation of TM5 and TM6 in the cytoplasmic side of active conformer, which alters the orientation of ligand in the binding pocket, but despite of these deviation, the core of 7TM cavity is the same.

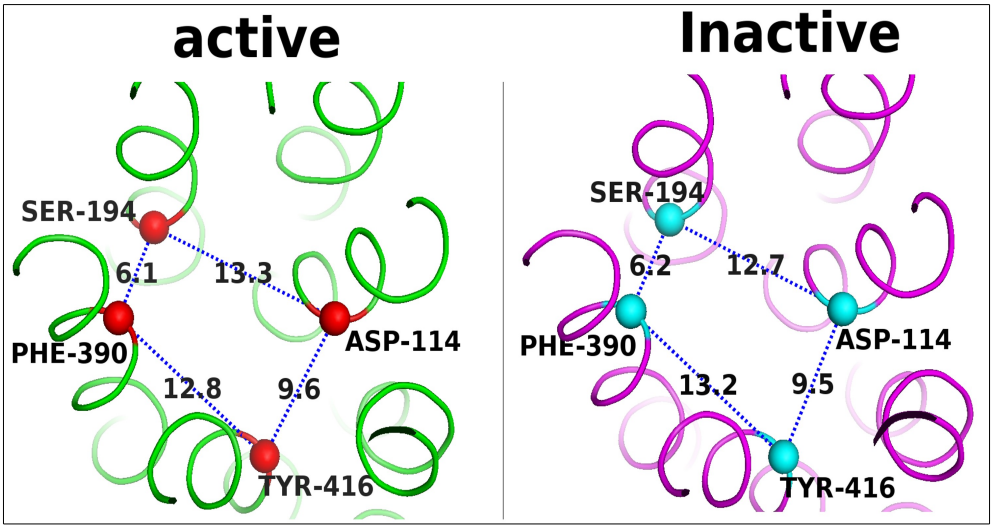


Figure 4.20 : Distance calculation on active sites of both D2R models.

4.3.7 Computational alanine scanning mutagenesis

Computational Alanine scanning mutagenesis studies of the residues in the binding site of the selected antagonist Clozapine (Class I) and Aripiprazole (Class II) are also employed. The Alanine scanning computations were performed to predict the energetically main amino acid residues in its interface and identifying the residues that are located in binding pocket of the wild type Dopamine D2 receptor (H-bonds, salt bridge, hydrophobic interactions) and mutating them to Alanine. *In silico* mutation studies show that Asp114 (TM3), Phe390 (TM6), Phe389 (TM6), Val115 (TM3) are crucial residues for ligand binding of class I antagonist ligands and Asp114 (TM3), Ile184 (ECL2), Tyr408 (TM7) are crucial residues for ligand binding of class II antagonist ligands which is consistent with molecular docking results (Table 4.3).

Table 4.3 : The change in relative binding energies for several alanine mutants relative to the D2R (Inactive) wild type binding energies.

	Aripirazole (Class II)	**Clozapine (Class I)**
Receptor	**Binding energy (kcal/mol)**	**Binding energy (kcal/mol)**
Wild Type	-10.68	-11.361
Asp 114 Ala	-7.94	-10.15
Val 115 Ala	-10.92	-10.72
Val 111 Ala	-10.20	-12.25
Tyr 416 Ala	-10.75	-11.04
Tyr 408 Ala	-9.68	-10.38
Phe 390 Ala	-10.40	-9.89
Phe 389 Ala	-10.06	-10.39
Leu 94 Ala	-10.54	-11.26
Ile 184 Ala	-9.24	-12.00
Ile 183 Ala	-10.62	-12.36
His 393 Ala	-10.65	-11.15
Cys 118 Ala	-10.46	-12.00

4.3.8 3D-QSAR modeling

In the remainder of present study we applyed 3D-QSAR approach which it is independent of any target structure. This insight is so useful for elucidation on D2R inhibitors in the lack of crystal structure. In order to construct common pharmacophore of D2R inhibitors, fifty two approved D2R inhibitors were submitted in 3D-QSAR calculation as shown in Figure 4.21. For each input structure, set of conformers were generated using Monte Carlo method. pIC_{50} values were ranged between 9.35-5.27, highest and lowest active compounds were connected to risperidone (ZINC00538312) and 1-Benzyl-4-(2-iodo-1H-pyrrol-1-yl) piperidine (ZINC20358060), respectively. To apply an activity threshold for ligands, pIC_{50} thresholds were set as $pIC_{50} > 7.2$ and $pIC_{50} < 6.2$ for active and inactive compounds, respectively.

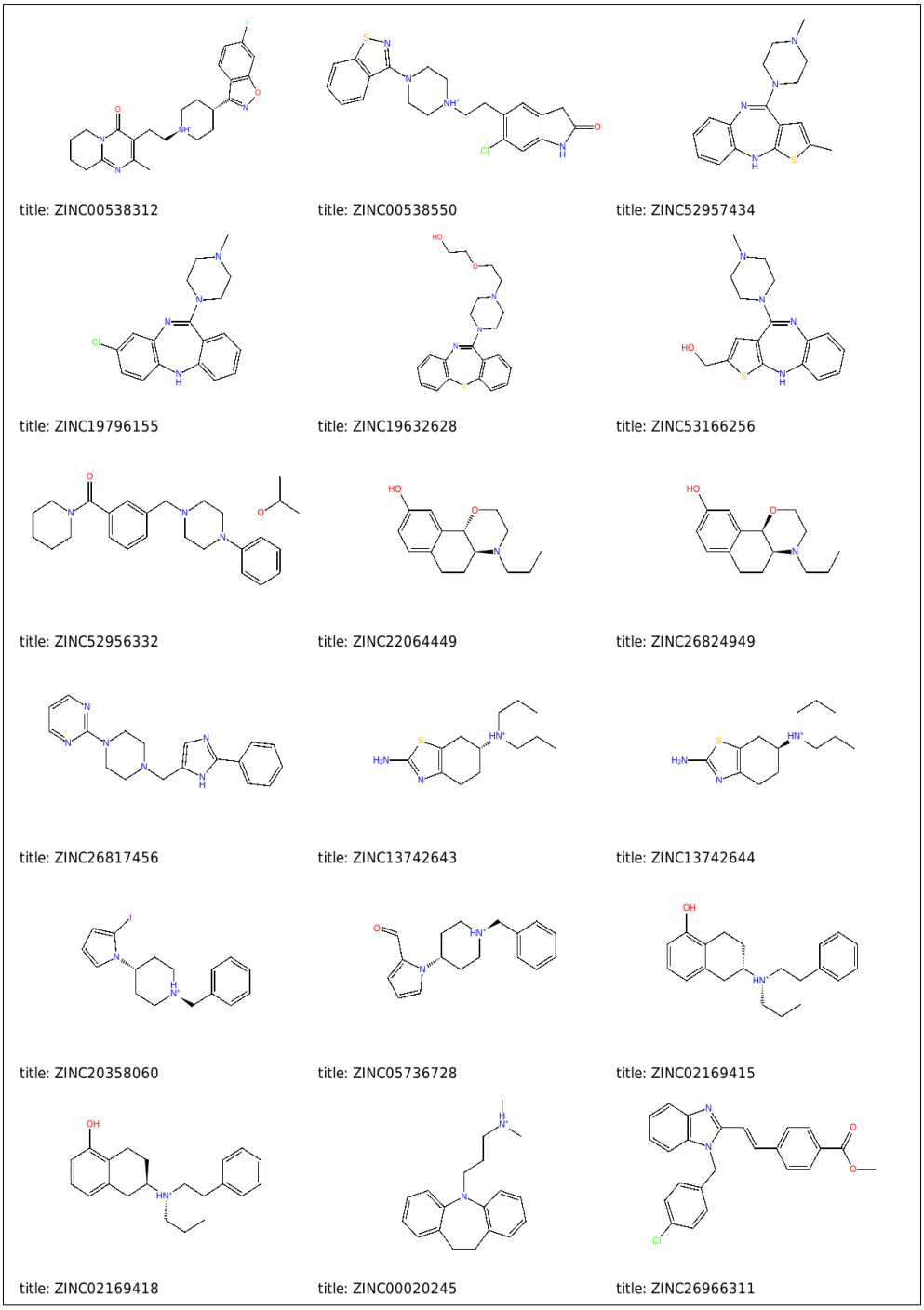


Figure 4.21 : Chemical structures of used ligands in 3D-QSAR study.

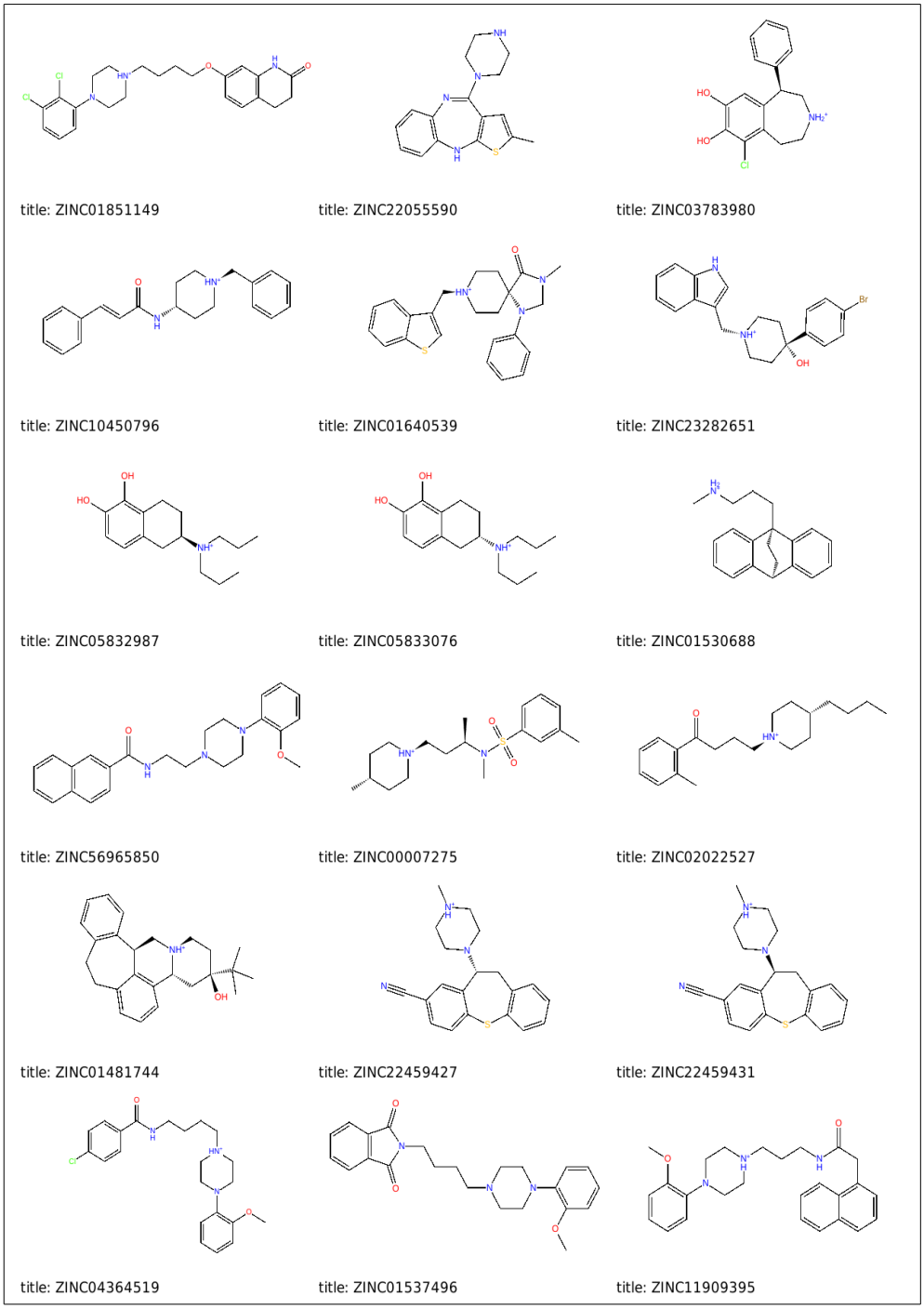


Figure 4.21 : Chemical structures of used ligands in 3D-QSAR study.

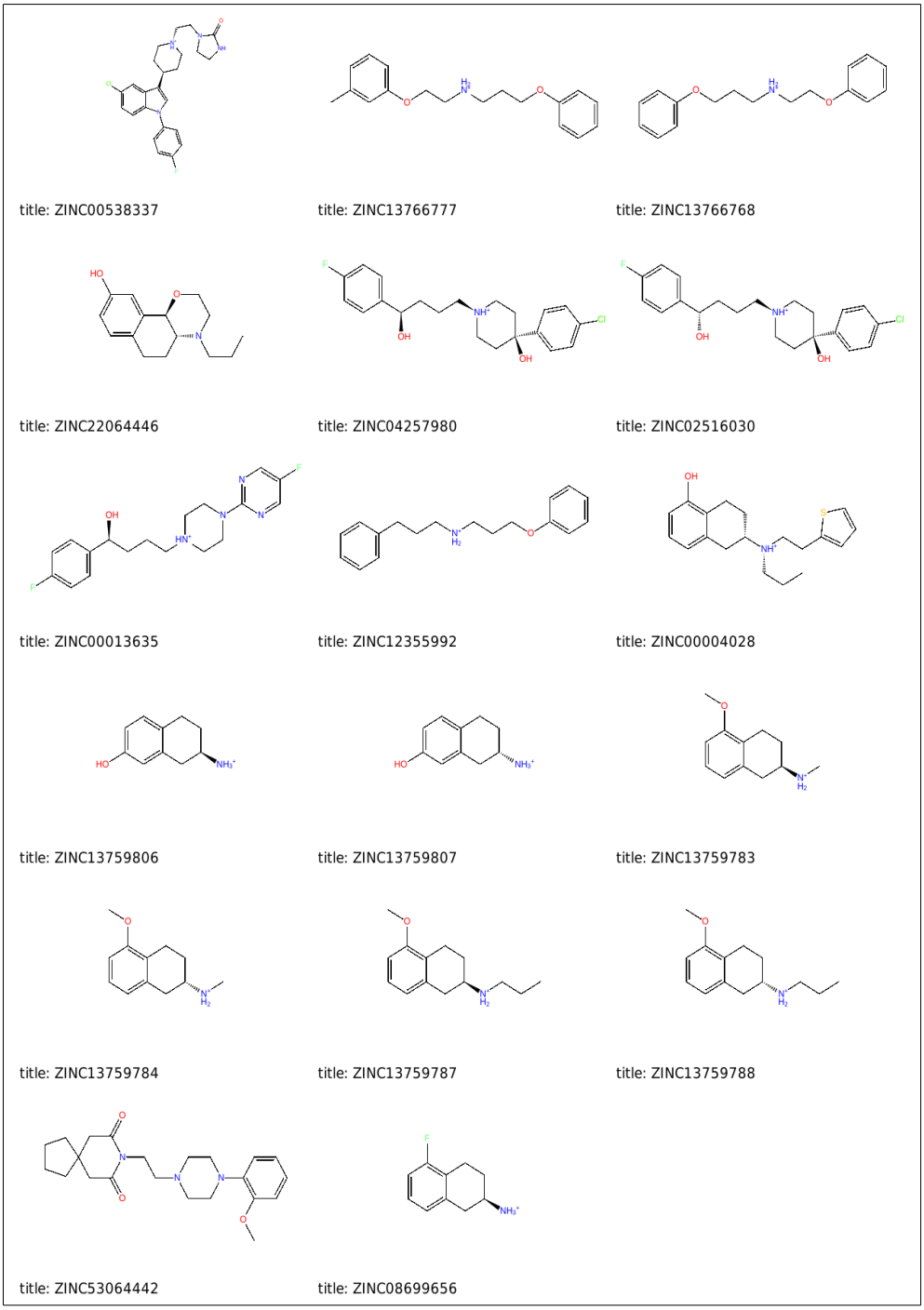


Figure 4.21 : Chemical structures of used ligands in 3D-QSAR study.

Compounds whose activity lies between the threshold were removed from our calculations. Using set of pharmacophore features, pharmacophore sites were created for all compounds. Phase defines six pharmacophore sites as follows; hydrogen bond acceptor (A), hydrogen bond donor (D), hydrophobic group (H), negatively charged group (N), positively charged group (P) and aromatic ring (R). Number of sites for

each pharmacophore was specified from 5 to 7. Found common pharmacophores for imported D2R inhibitors include of ADHRR, DHHPR, AHPRR, AAHPR, ADHPR, AHHPR, AAHRR, AAPRR, ADHHR, ADPRR, DHPRR and HHPRR, which were employed in 3D-QSAR modeling step. The regression was applied using a partial least squares (PLS) method, in which set of models were generated with an increasing number of PLS factors. In order to validate the created models, all collective compounds were divided into taring set (70%) and test set (30%). Statistical parameter values and derived scores for the best 3D-QSAR model AHPRR were listed in Table 4.4. R^2, SD, F, and P results were calculated to evaluate the taring set predictions; Q^2, RMSE and Pearson R values were employed to evaluate the test set calculations. These parameters were considered to rank the pharmacophore models (highest R^2, Q^2 and Pearson R and lowest RMSE, SD, and P values), finally AHPRR.1282 was suggested as a best pharmacophore model. Correlation of experimental and predicted pIC_{50} values for training set was plotted in Figure 4.22. Higher correlation coefficient ($R^2 = 0.90$) for generated pharmacophore model suggests the reliability of 3D-QSAR model. Figure 4.23 displays the alignment of top pharmacophore model AHPRR.1282 with it's reference (ZINC04364519), active (ZINC00538312/risperidone) and inactive ligand (ZINC20358060). Risperidone was introduced as a high active ligand in this study which has a reasonable alignment with our constructed model and in contrast compound “1-Benzyl-4-(2-iodo-1H-pyrrol-1-yl)piperidine” (ZINC20358060) as a high inactive ligand, established a low alignment with pharmacophore model. These results validate the reliability of our 3D-QSAR model. Created pharmacophore model can be employed for any ligand based virtual screening to discover new D2R inhibitors without knowing any information of D2R receptor.

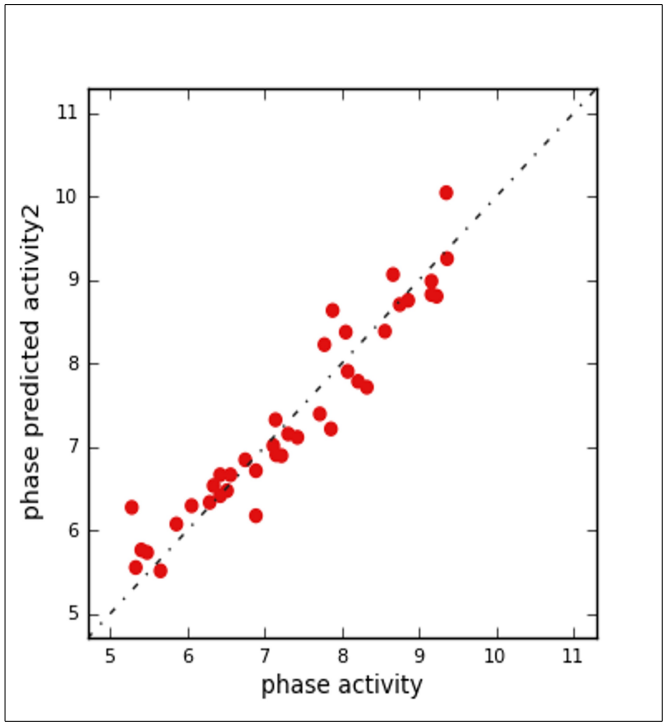


Figure 4.22 : Correlation between experimental and predicted activity value of contracted 3D-QSAR model.

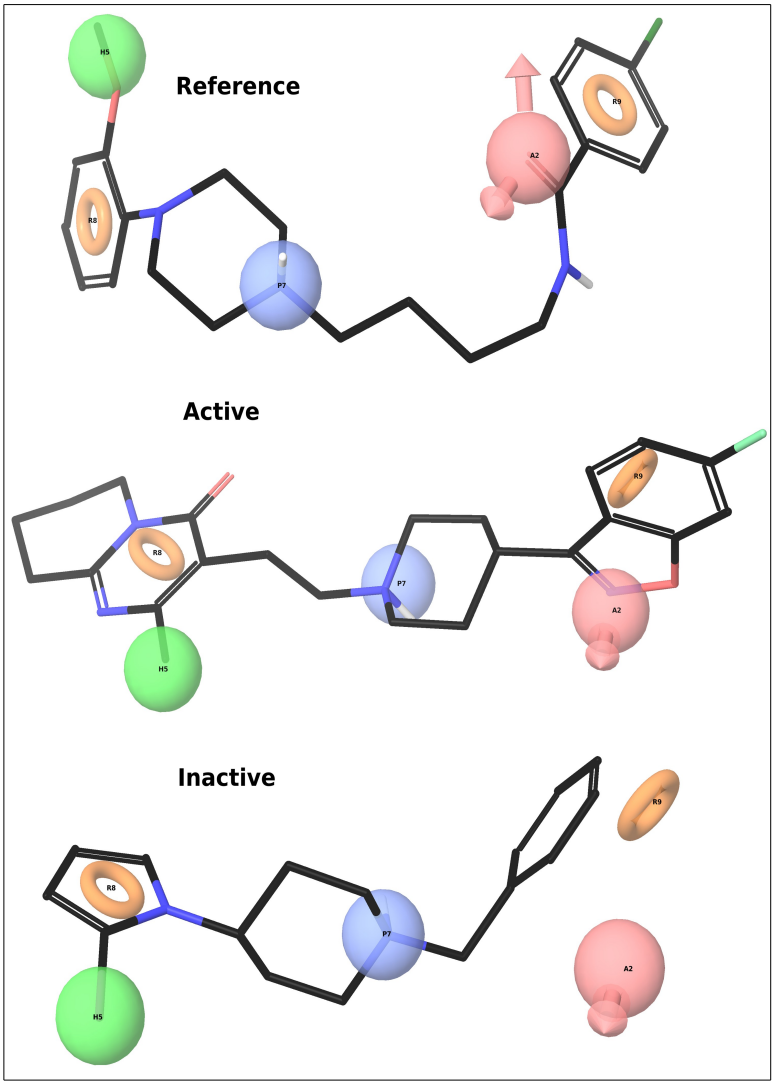


Figure 4.23 : Alignment of generated pharmacophore model with used reference, active and inactive compounds.

Table 4.4 : Statistical parameter values for the top 3D-QSAR model AHPRR and derived scores for the generated model.

PLS factor	SD	R^2	F	P	RMSE	Q^2	R-Pearson	Reference ligand
1	0.65	0.70	87.2	3.75×10^{-11}	0.71	0.63	0.87	ZINC04364519
2	0.38	0.90	157.6	3.14×10^{-18}	0.80	0.53	0.88	ZINC04364519
3	0.21	0.96	355.7	9.85×10^{-26}	0.76	0.58	0.88	ZINC04364519

4.4 Conclusion

In the section we modeled two different D2R models on the base of active and inactive templates. Generated models were then validated using docking simulations

and computational Alanine mutagenesis studies. Binding site refinement were performed using ligand screening protocols. The validated homology models that are derived in this study can be very useful at the virtual ligand screening investigations. The striking differences between the active and inactive forms of the model structure especially on the TM5 and TM6 sites, which are the sites responsible from the protein activity, were clearly indicated by the normal mode analyses. Molecular simulations combined with drug screening at the active sites of different states of same target may provide detailed insights into the ligand binding modes and also shed light into the interaction mechanisms of receptor proteins with targeted drugs at the molecular level. The derived models will serve as basis for the design of novel Schizophrenia drugs with enhanced activity and less side effects. Also signaling pathway of D2R was predicted using NMA and critical amino acid residues and domains in active conformer were identified. Finally, in order to find a ligand based approach on D2R inhibitors discovering, we constructed a common pharmacophore model AHPRR using 3D-QSAR methods. Our predicted 3D-QSAR model was reasonably validated using training and test set compounds and introduced as a useful model for any ligand based screening.

5. INHIBITORY TREATMENT OF CHEMOKINE RECEPTOR 5 (CCR5)

5.1 Introduction

Chemokine proteins belong to the G protein-coupled receptor (GPCR) family [97]. GPCRs have seven trans-membrane (TM) domains which were snaked through membrane bilayer and their cytoplasmic sides were linked to intracellular guanosine nucleotide-binding protein (G-protein) to transfer cellular signaling from outside into the cell during conformational activation [98]. The chemokine proteins were classified into four classes (C, CC, CXC and CX3C) with respect to the number and position of Cysteine residues in the amino acid sequence [99]-[102]. The CC chemokine receptor type 5 (CCR5) is a member of CC chemokine family and it plays a significant role at the HIV infection [103]. Mainly HIV proteins use CCR5 as co-receptor and couple it before entering into the cell. These proteins can also use other chemokine proteins such as CXCR4 as a co-receptor [104]. The CCR5-inhibitor drug maraviroc (brand-named *selzentry*, or *celsentri* outside the U.S.A.), was approved by FDA in 2007 [103]. Maraviroc is a non-peptide HIV fusion inhibitor. A number of small ligand CCR5 inhibitors were determined to have strong antiviral influences both in *in vitro* and clinical experiments [104] such as TAK-779 which is also non-peptide compound suggested as the initial CCR5 inhibitor [105],[106]. An antagonist that targets the CCR5 in the inactive state may inhibit the transmission of intracellular signaling [103]. However in the active state, they are stabilized to become eligible for intracellular signal transduction [103]. The X-ray structures of a few GPCR targets have been solved recently in both antagonist-bound inactive states [107]-[110] and agonist-bound active states [111]. Recently, the crystal structure of CCR5 in the presence of the anti-HIV drug maroviroc was crystallized successfully with resolution of 2.7 Å [112]. This achievement was a very big step and stimulated the anti-HIV drug development studies.

The V3 loop of envelope glycoprotein GP120 (or gp120) is critical in HIV fusion when it links to the co-receptor. Extra cellular (EC) domains of CCR5 participate at

the gp120-CCR5 coupling. Although chemokine receptors can function as viral co-receptors, the CCR5 target is one of the most physiologically important co-receptor during natural infection [114]. Despite of many potential investigations on HIV field, many questions regarding the interactions between gp120 and CCR5 is still not solved: How gp120 uses CCR5 as a co-receptor to enter the human cell? What is the molecular mechanism of this event? How anti HIV drugs in the position of CCR5 inhibitors protect the coupling of gp120 and EC domains of the CCR5? So far, most of the *in silico* studies on CCR5 were based on homology models [115]-[119]. Recently Tamamis *et al.* [120] used the CCR5 X-ray structure for investigation of the molecular recognition of CCR5 by a dual tropic HIV-1 gp120 V3 loop via short (20 ns) MD simulations. Here, in this study, in order to better understand the molecular mechanism of target-inhibitor interactions a long, 0.6 μs MD simulations in total, as well as post-processing analyses such as principle component analysis (PCA) and clustering approaches for both apo and holo states are performed.

MD simulations and their post-processing analyses provide significant insight into the structural and dynamical behaviors of biological systems at the atomistic level. In this work, we present quantitative results on the harmonic motion and the conformational transition of the CCR5 chemokine receptor. PCA and the clustering approach were used to eliminate the insignificant dynamic modes and the conformational changes throughout the simulations. We believe that clearing the very complex inhibition mechanism of CCR5 via long MD simulations will lead to discovery of novel potent antagonists inhibiting CCR5.

5.2 Materials and Methods

5.2.1 Hybrid computational services

All calculations were carried out on a 96 CPU cores AMD opteron (6174 2.20 GHz) computers at ULAKBIM High Performance and Grid Computing Center (TR-Grid). MD trajectory analyses have been performed utilizing Ubuntu Linux based operating system (with the properties of 12 Intel(R), Core(TM), i7-4960X, CPU; 3.60GHz and 2 GPU/NVIDIA graphic card) and with over 64 GB of RAM.

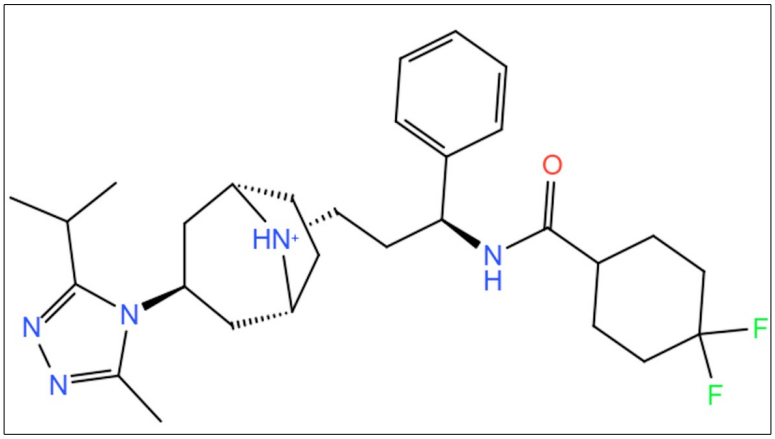


Figure 5.1 : Chemical structure of maraviroc used as co-crystallized ligand in holo system.

5.2.2 The modeling of apo and holo proteins

The crystal structure of CCR5 chemokine receptor with a co-crystallized antagonist (maraviroc) with a resolution of 2.7 Å was retrieved from the PDB server (Protein Data Bank (PDB) ID: 4MBS) [112] and it is used for further preparation procedures. The chemical structure of co-crystallized ligand was shown in Figure 5.1. Rubredoxin was removed from structure and the missing amino acids Cys224, Arg225, Asn226 and Glu227 in the position of third intracellular loop (IC3) were modeled using Modeller 9.13 [51]. The new CCR5 receptor was prepared using Protein Preparation Wizard [122] implemented in the Schrodinger Maestro molecular modeling package. Protonation states of the target were adjusted using PROPKA [59] at physiological pH of 7.4. In order to compare the inhibition efficiencies of the CCR5 antagonist at the apo (ligand-free) and holo (ligand-occupied) states, apo and holo forms of the receptor were considered. Both ligand-free and ligand-bound CCR5 complexes were merged with a 1,2-dipalmitoyl-sn-glycero-3-phosphocholine (DPPC) membrane bilayer and orientation of the target protein at the lipid bilayer was adjusted using Orientations of Proteins in Membranes (OPM) server [123]. The membrane bilayers have been modeled by utilizing VMD [124] Membrane Builder plugin tool. The CCR5 chemokine crystal structure involves 4 Cysteine residues. They form two disulfide bonds, between Cys20-Cys269 and Cys101-Cys178 residues. These essential disulfide bonds were constrained using the patch DISU of the VMD. Then, the membrane embedded proteins were solvated with TIP3P [125] explicit water models employing the Helmut Grubmuller's Solvate 1.0 program.

Finally the systems were neutralized (by 0.15 M of KCl solution) using VMD's Solvate plugin and located in a box of water having thickness of 15 Å. The total number of atoms involved were around 58000. (Figure 5.2)

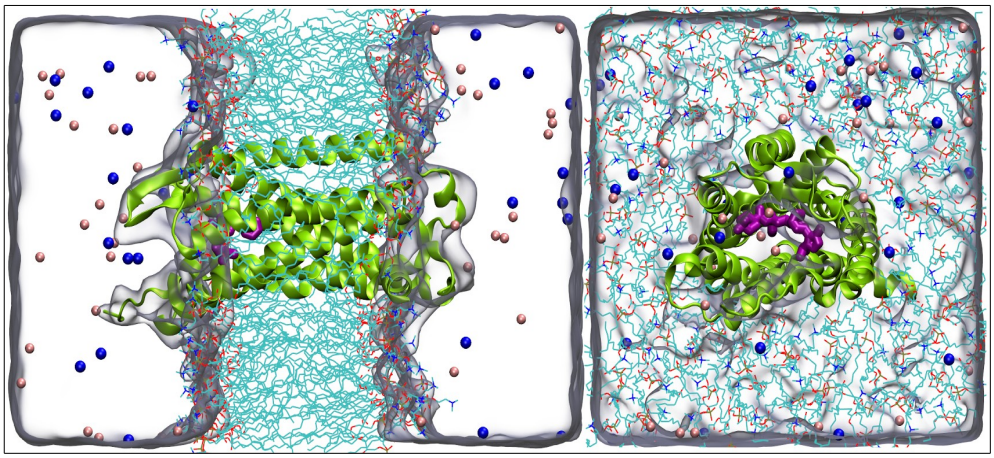


Figure 5.2 : Simulated systems which is consist of embedded CCR5 chemokine (CCR5 is represented as a green cartoon) complex into lipid bilayer (DPPC, shown with stick representation), waters (shown as quick surface) and counter ions (K^+/Cl^-, shown with blue and pink balls, respectively).

5.2.3 Classical molecular dynamics (cMD) simulations protocol

All cMD simulations were carried out using the NAMD 2.9 [126]. The CHARMM36 [127] force field was used for the CCR5 membrane protein and DPPC lipid bilayer. ParamChem [128] server was used to generate force field for maraviroc molecule. All covalent bonds between hydrogen and heavy atoms were constrained using the SHAKE algorithm. In order to simulate the isothermal–isobaric ensemble (NPT) and control the used temperature (310 K) and the pressure (1 bar), individually, Langevin dynamics and Langevin piston methods were used. The Langevin damping coefficient and the piston period were set to 1.0 ps^{-1} and 0.05 ps, respectively. 3D periodic boundary conditions were used and for long-range electrostatic interactions, a cut-off distance of 12 Å was used with Particle Mesh Ewald (PME) approach. A time step of 1 and 2 fs was used for equilibration and production MD run, respectively.

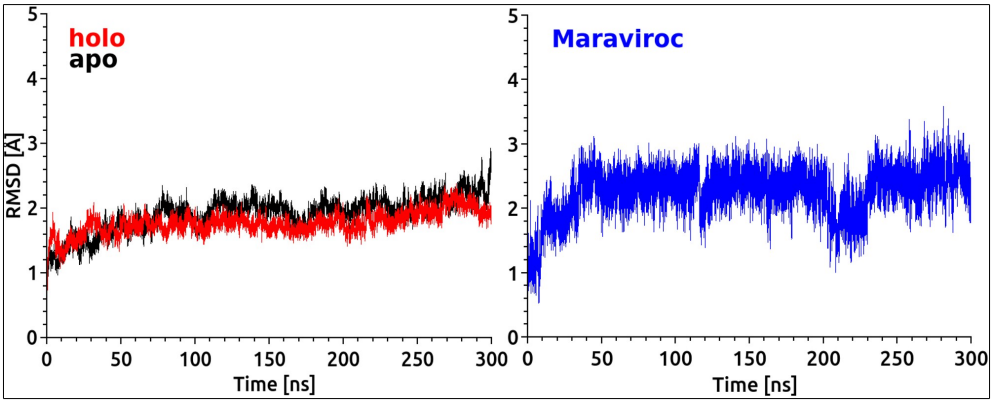


Figure 5.3 : The Root mean squared deviations (RMSD) of Cα atoms of comparative apo and holo forms in the course of 0.3 μs MD simulations (left). The RMSD of heavy atoms of the maraviroc during MD simulations (right).

5.2.4 Minimization and constrained equilibration

The systems were minimized and equilibrated before performing the production MD runs. This procedure was carried out as follows: i) in order to achieve the equilibrium of lipid tails, 10^4 steps of minimization and 2 ns isochoric-isothermal (NVT) MD simulations with all atoms fixed except atoms of lipid tails was performed, ii) $2x10^4$ steps of minimization and 2 ns NVT simulations were used with constrained protein, iii) Final equilibration was carried out with all atoms released through 4 ns under NVT ensemble, (iv) Finally 0.3 μs production MD simulations under isothermal-isobaric (NPT) conditions were performed for each *holo* and *apo* states (total 0.6 μs). During the MD simulations, the coordinates of all atoms were recorded for every 10 ps for further analyses.

5.2.5 Calculations of non-bonding interaction energies

The average interaction energies between the amino acid residues in the binding cavity and inhibitor were calculated using $3x10^4$ trajectories. NAMD energy plugin implemented in VMD and CHARMM36 force field were used for this aim. The cut-off distance and switch distance were set to 12 Å and 10 Å, respectively.

5.2.6 Principal Component Analysis (PCA)

PCA [129]-[130] is a popular statistical data-processing analysis for the decreasing of large-dimensional observations sets onto collective data. In other words, PCA is a process of determining models in data, and describing the data as to focus on their

likenesses and distinctions.

5.2.7 Applying PCA on MD simulations

A standard MD trajectory involves the coordinates of overall atoms stored during the simulation. For a systems of N atoms, the input data set for PCA can be a statistical data matrix and each column of the matrix indicates Cartesian coordinate for a particular atom at every frame. Before starting the PCA, each frame should be aligned with respect to the initial frame because not the displacement and rotations of the structure but the fluctuation of the atoms are considered.

Mathematically obtaining PCs for MD trajectories includes two important stages:

i) generation of the covariance matrix (C),

$$C_{ij} = < \left(x_i - < x_i > \right) \left(x_j - < x_j > \right) > \tag{5.1}$$

ii) the next stage is diagonalization of the 3N×3N covariance matrix C that can be calculated by eigenvalue decomposition (EVD) [131],[132] as

$$C = V \Lambda V^T \tag{5.2}$$

where Λ describes the diagonal matrix containing the eigenvalues and V describes a matrix including eigenvectors. The eigenvalues display the mean squared displacements (MSD) of atoms (C_α atoms in this study) throughout the used eigenvector. In this study, PCA was applied utilizing the bio3D package in R [63].

5.2.8 Graphical facilities

MD trajectory visualizations, plots, profiles and documents for this work were obtained utilizing Visual Molecular Dynamics (VMD) software [124], PyMOL molecular visualization system program [133], R statistical program [134], LibreOffice powerful office suite, GNU Image Manipulation Program (GIMP), Maestro 9.7 molecular modeling environment and Mendeley as a reference manager [135].

5.3 Results and Discussions

Represented analysis at the current work includes several insights. Firstly, the effect of inserted rubredoxin molecule in the position of IC3 on overall protein is investigated. Since rubredoxin was placed in IC3 (locating between TM5 and TM6),

the conformational transition on the amino acid residues in these domains was focused. The representative structure (the structure that has the lowest RMSD value) taken from 0.3 μs MD simulations was superimposed to X-ray crystal structure, and the mismatching domains from initial structure (target structure from X-ray data) were analyzed. In order to improve potency of entry blockers as anti HIV drugs, here we have also examined structural and dynamical changes of maraviroc at the CCR5 binding pocket by long MD simulations. The inhibition mechanism of CCR5 and the effect of inhibitors on the protein conformation upon ligand-binding were studied using the combination of MD simulations and PCA .

5.3.1 MD equilibration

Root mean square deviation (RMSD) calculations of protein based on backbone atoms as well as RMSDs of heavy atoms of the ligand were performed using the RMSD plugin of VMD to determine the structural stability. (Figure 5.3). It is obvious that both apo and holo forms have reached stable conformations during 0.3 μs MD simulations. While the average deviation value of RMSD for Cα atoms in holo form was 1.77 Å, this value was 1.97 Å in the apo form. During simulation holo form shows slightly a more structural stability than apo form, this result is anticipated upon inhibitor binding effect. RMSDs of the ligand during the simulations show that heavy atoms reached to equilibrium after 30 ns of simulation and it remained stable for the rest of the time except a small deviation was observed in the period of 210 and 230 ns. The first 30 ns trajectory frames is excluded from post-processing protein-ligand interaction analysis.

5.3.2 Fusion facilitates influence on CCR5 conformer

Obtaining of well-diffracting X-ray structures of GPCR is one of the most challenging issues in GPCR studies [136]. Because of this problem only a less number of GPCRs were identified using crystallization methods. This difficulty was connected to the small size of polar surface in GPCR [136]. A strategy by Kobilika *et al*. was suggested to solve this problem during crystallization of the beta 2 adrenergic receptor (B2AR) [110]. T4 lysozme (T4L) was fused to the cytoplasmic side which was connected TM5 and TM6 domains. Fused T4L is effective to other seven TM helical domains [137]-[142]. The other used GPCR-fusion molecules consist of

rubredoxin, cytochrome b562 RIL (Bril, bRlL, BRIL) and flavodoxin [143]. In this study, the used X-ray crystal structure involves rubredoxin as fused partner in cytoplasmic side between TM5 and TM6. In order to understand the effect of this GPCR-fusion partner on CCR5 conformer, we excluded rubredoxin from initial structure and then missing amino acid residues of IC3 (Cys224, Arg225, Asn226 and Glu227) were engineered. Holo and apo states of the final structure (CCR5 without rubredoxin) was then subjected to a very long MD simulations (0.6 μs, in total). Here, we mostly focused on conformational changes on TM5 and TM6 domains which were more associated with IC3 domain. In order to examine conformational transitions which were contributed to cytoplasmic side of TM5, two residues (Val131 (from TM4) and Leu222 (from TM5)) which are positioned in the terminal domains of cytoplasmic side of TMs) were considered. The distance between these residues are highlighted and their evolution distances from each other was plotted (Figure 5.4). During the first 100 ns of the simulations, no significant change in the distance between two residues was observed compared to their initial positions. This suggested us that 100 ns MD simulations might not be sufficient to observe the conformational changes in CCR5. In the second 100 ns simulations, TM5 (cytoplasmic end) started to change its conformation and the distance between two terminal residues changed around 4 Å. During third 100 ns simulations, the distance between two terminal residues reached to 8 Å (Figure 5.4). A representative structure of $3x10^4$ MD trajectories was generated and superimposed with crystal structure of CCR5 including rubredoxin molecule (Figure 5.4). Change in the positions of terminal residues throughout the simulations can be easily seen from the Figure 5.4. Superimposition of initial structure with representative structure from MD highlighted another distinct displacement in the EC domain of TM6 (Figure 5.4). The rubredoxin that is used for easy crystallization of CCR5, effected the conformation of target structure CCR5. Thus usage of the TM domain of CCR5 without any refinement via MD simulations might lead misleading results. We believe that the derived target structure after a very long MD simulations carried out in this work, was a reasonable target for further investigations of drug-receptor interactions.

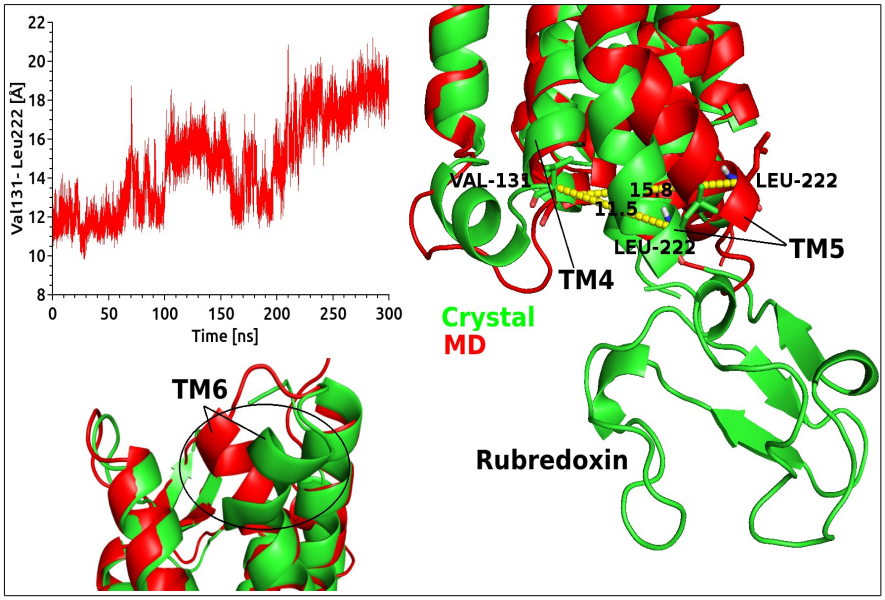


Figure 5.4 : Distance analysis between Val131 (cytoplasmic side of TM4) and Leu222 (cytoplasmic side of TM5). Superimposition of representative structure from MD (red) with crystal structure (green).

In the rest of study, interactions between CCR5 and anti-HIV drug maraviroc as well as conformational changes of the target upon binding of inhibitor were investigated. In order to elucidate the effect of the drug, a control system (using same MD protocols with holo system) was also prepared for the apo state and MD simulations were carried out.

5.3.3 Non-bonded interactions

Non-covalent interactions between amino acid residues at the binding pocket and the inhibitor were estimated by calculating the interaction enthalpies (Figure 5.5). In addition, hydrogen bond (H-bond) occupancy value as percentage was identified by applying the criteria of cut-off for the proton donor and acceptor atoms (i.e., distance ≤ 3.0 Å; angle ≥120 degree). H-bonding interactions between ligand and the key amino acid residues at the binding pocket is also investigated. As displayed in the Figure 5.5, Glu283 at the binding pocket makes a strong and populated H-bond during the simulations. It displays a high H-bond occupancy degree (61.1%) throughout the 0.3 μs MD simulations. (Figure 5.5) The importance of this residue has been also pointed out in the experimental studies [144]-[148]. The binding of inhibitor from the central basic nitrogen atom to the carboxylic acid group of the Glu283 amino acid may stabilize the complex. Two other residues Lys26 and Tyr37

at the binding pocket could not establish stable H-bonds with the inhibitor during the simulations. They showed low occupancy degrees (4.3% and 8.8%, respectively). Two other polar active site residues, such as Tyr89 and Tyr251, did not participate in H-bond interactions with the inhibitor.

The per-residue interaction analysis is also performed for the CCR5-maraviroc complex system using $3x10^4$ trajectories (Figure 5.5). Derived results from our MD analyses showed a good agreement with previous experimental studies [144]-[148].

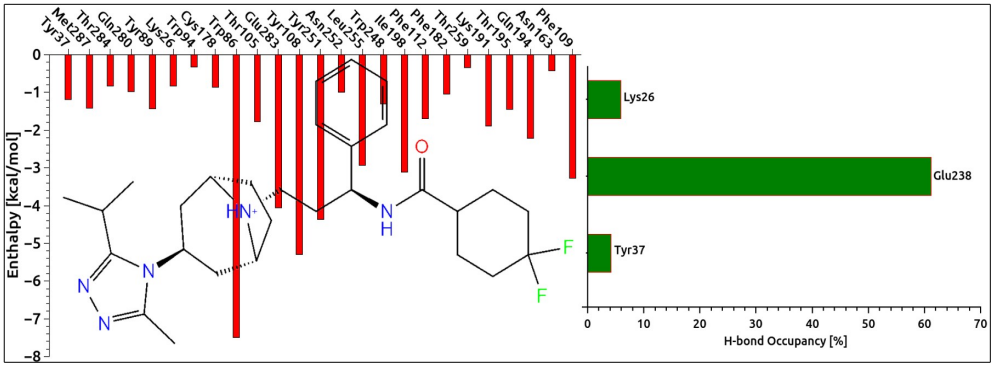


Figure 5.5 : Non-covalent bond interactions between the amino acid residues at the binding pocket with the inhibitor (left). In order to identify individual amino acid residues participate in interaction with each segment of the ligand, the 2D chemical structure of maroviroc was inserted into the profile. The occupancy in percentage of each residue participating in H-bonding with the inhibitor (right).

Figure 5.6 shows the representative structure of CCR5-maraviroc complex system from $3x10^4$ trajectories. While Tyr251 constructed a π-π stacking type interaction with the inhibitor, the nitrogen atom of the tropane group of maraviroc formed a stable H-bond with the Glu283 at the binding pocket. These two interactions between CCR5 and maraviroc were suggested as key interactions for the anti-HIV treatment of the antagonists by Imamura *et al*. [149] The binding cavity of the CCR5 is mainly hydrophobic because of existence of several nonpolar amino acids (i.e., Trp86, Trp94, Phe109, Phe112, Phe182, Thr195, Ile198, Trp248, Leu255 and Met287) in the pocket [150]-[152]. It was suggested that the binding of gp120 to CCR5 was dependent to several nonpolar amino acid residues such as; Trp86, Trp94, and Trp248. [150]-[152]. In the protein-ligand complex, the ligand placed at the bottom part of CCR5 cavity which was identified by key amino acids from membrane

helices TM1 (Ile28-Asn57), TM2 (Met64-Gln93), TM3 (Asn98-Val130), TM5 (Lys191-Gly216), TM6 (Arg230-Leu255) and TM7 (Gln277-Tyr297). In addition to EC loops of CCR5, amino acid residues in the TM domains (i.e., Tyr37) were reported to be included in the linking of gp120 [153] This amino acid was conserved at overall CC-chemokine proteins and our results are in good agreement with the experimental results in showing the importance of this amino acid residue at the binding pocket.

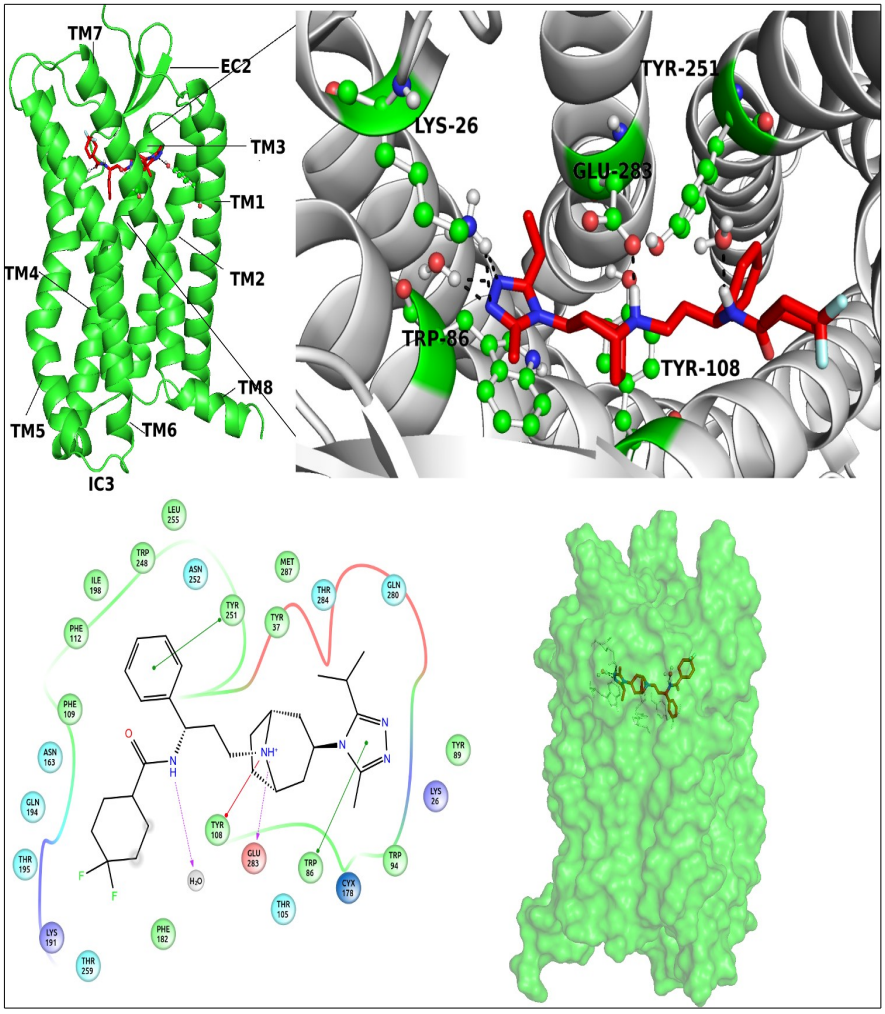


Figure 5.6 : Representative complex from 30000 derived frames after MD simulations has been shown. 2D and 3D ligand interaction diagrams show key interactions at the binding site.

Although the inhibitory mechanism of CCR5 is not fully understood so far, an experimental study reported that inhibitors blocked HIV entry via allosteric regulation [154]. CCR5 inhibitors were placed in the binding cavity formed by the

TM domains close to the EC side of CCR5. The gp120 links to the outer surface (EC loops) of CCR5 [155]. EC loops of CCR5 plays a critical role in HIV entry [155]. In order to see the effect of HIV inhibitor on the conformation of EC2 loops, H-bonding occupancies between amino acid residues at this loop were investigated during the simulations (Figure 5.7). Although an H-bond was established between Thr167 and Arg168 in the apo state, this bond was not observed at the holo state. On the other hand, although another H-bond was formed between Thr177 and Glu172 at the holo state, this bond is not exist at the apo form.

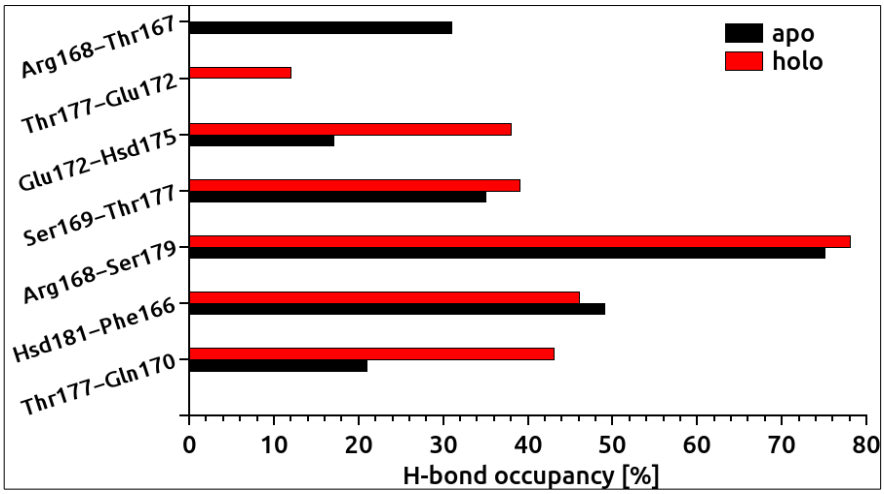


Figure 5.7 : H-bond occupancy of second extracellular loops (EC2) amino acids residues in percentage. A comparative analysis is performed for two states.

H bonds between Glu172 and His175 as well as Thr177 and Gln170 were more stable at the holo state. In the absence of maraviroc, % H-bond occupancies between these amino acids decreased dramatically. H-bond occupancies for other amino acid residues at the EC2 were similar for holo and apo states. The average H-bond occupancy at the EC2 loops were observed as 36.5% and 32.5% for holo and apo states, respectively.

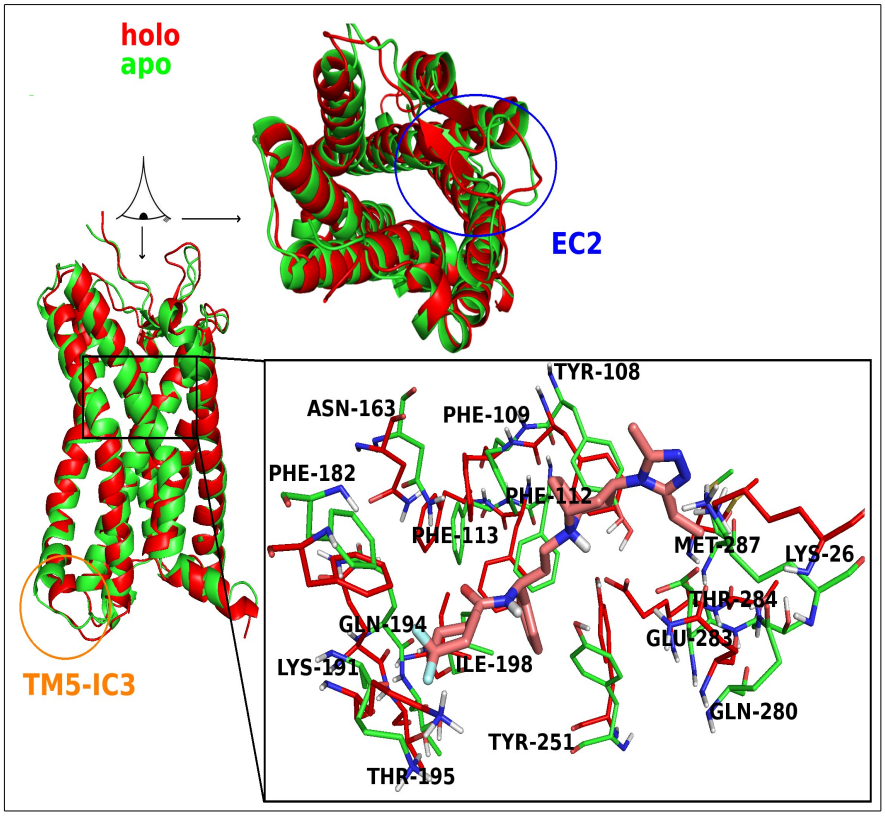


Figure 5.8 : Superimposition of representative apo and holo forms. Upper panel shows extra-cellular side and lower panel display 7TM active cavity.

Different studies in literature have suggested that in most situations the second (IC2) and third intracellular loops (IC3) of GPCRs are the main domains for protein to couple with G proteins. The amino acids in these domains are the primary determinants for G protein linking [156]. The recent work reported additional proof that the first IC loop is not mainly included in the linking of chemokine receptors to G proteins [156]. GPCR activation process identified by the flexibility and movement of its TM near the cytoplasmic side and three intracellular domains [156].

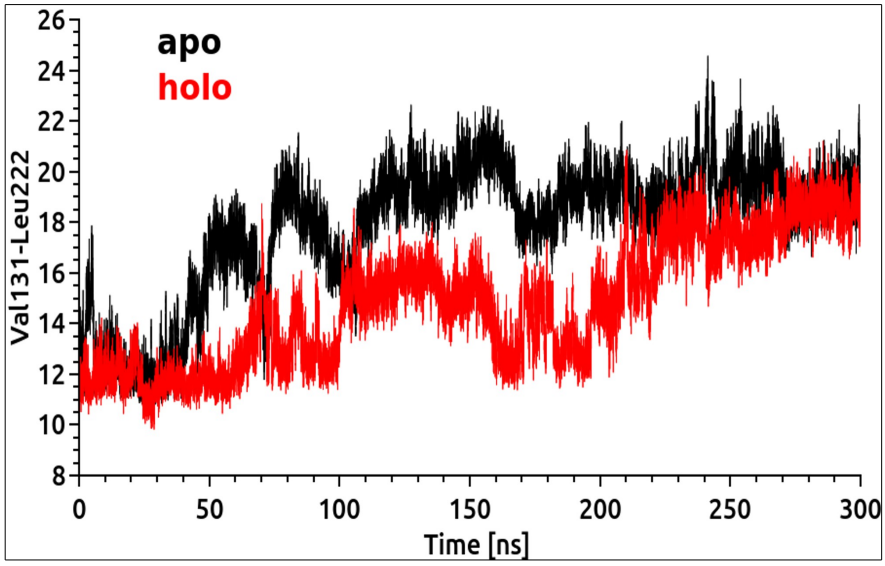


Figure 5.9 : Distance plot shows the distance evolution between Val131 (TM5) and Leu222(TM6) amino acid residues respect to MD time.

Representative structures (i.e., the frame that has the smallest RMSD from average structure) of apo and holo states from each 30000 MD trajectory frames were superimposed. (Figure 5.8) A distinct difference between apo and holo states were observed at the EC2 domain. This result was anticipated and it displayed the influence of maraviroc on EC2 conformer which was critical domain on binding of gp120. Effect of inhibitor on amino acids at the binding pocket was also examined and illustrated in this figure (Figure 5.8). Not only side-chains, but also backbone topologies of amino acid residues were effected. Particularly Lys26 and Phe182 in holo state have been departed from apo partner. In the position of TM5-IC3 linker (cytoplasmic side of TM5), apo conformer displayed largely compared to holo form upon ligand binding (Figure 5.8). In order to show the change in distance between TM5 and TM6 in the cytoplasmic side for both apo and holo forms, two amino acids (Val131 from TM5 and Leu222 from TM6) were selected and the distance between them was plotted during the simulations. (Figure 5.9) In the first 60 ns, holo form was so stable whereas change in distance between two residues was started to change for apo conformer at 40 ns and it was increased about 8 Å during 0.3 μs. Distance between two residues for both states were initially at ~12 Å and they increased to ~20 Å at the end of the simulations. Although both states showed similar distances between two residues at the end of the simulations, their distance paths during the simulation were not the same (Figure 5.9).

The RMSD values of apo and holo MD representative conformations of CCR5 with respect to their initial conformers was found as 2.0 Å and 1.9 Å, respectively.

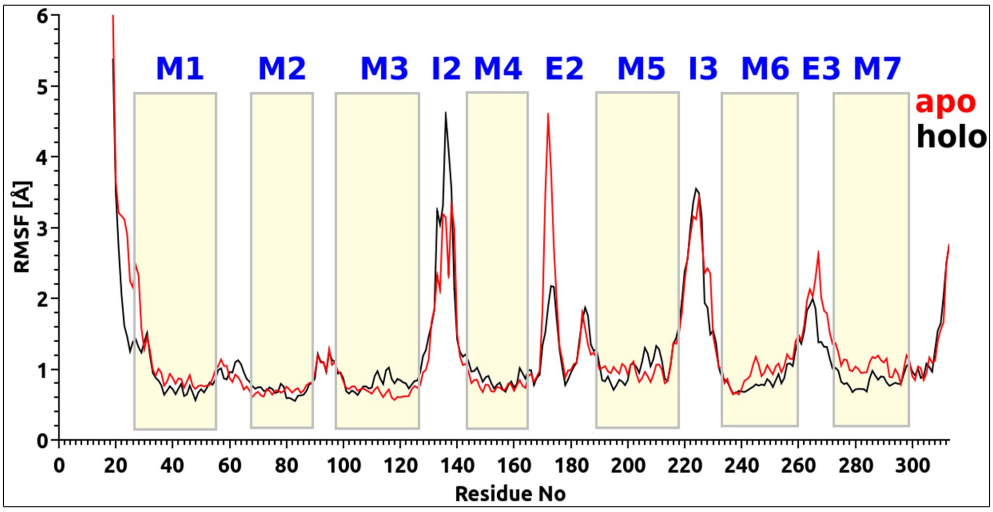


Figure 5.10 : RMSF values of Cα atoms versus residue numbers during 0.3 μs MD simulations. Fluctuation of each TM and loop domains are indicated and compared between the ligand bound- and ligand-free CCR5 chemokine.

5.3.4 Root Mean Square Fluctuation (RMSF) Calculations

In order to investigate the effect of inhibitor on the overall CCR5 target, average fluctuation values were calculated for individual amino acid residues during the simulations. $3x10^4$ trajectory frames from MD simulations were used for RMSF calculations. While TM helices showed high stability for both apo and holo states (around 1.0 Å RMSF), IC and IC linkers showed higher fluctuation values (up to 4.0 Å) (Figure 5.10). It is well known that N terminus domain at the co-receptor (i.e., Thr171, Glu172 and Lys173 amino acid residues at the EC2 domain) is crucial at the gp120 binding and this region needs to undergo a conformational change before HIV entry to the nucleus. EC2 region of the target structure fluctuated more in apo state (~4.0 Å) when compared to inhibitor-bound holo state (<2 Å). First two TMs were stable for both states and the inhibitor did not affect the topology of first two TMs. However, higher fluctuations were observed in cytoplasmic regions of TM3 and IC2 linkers in the presence of maraviroc. RMSD plots for EC2 loop based on Cα atoms for apo and holo states during the simulation has been represented at the Figure 5.11. While no large differences on RMSD's of apo and holo states at EC2 has been observed up to 150 ns, after this time a dramatic shift in RMSD between these two

states has been seen. (Figure 5.11)

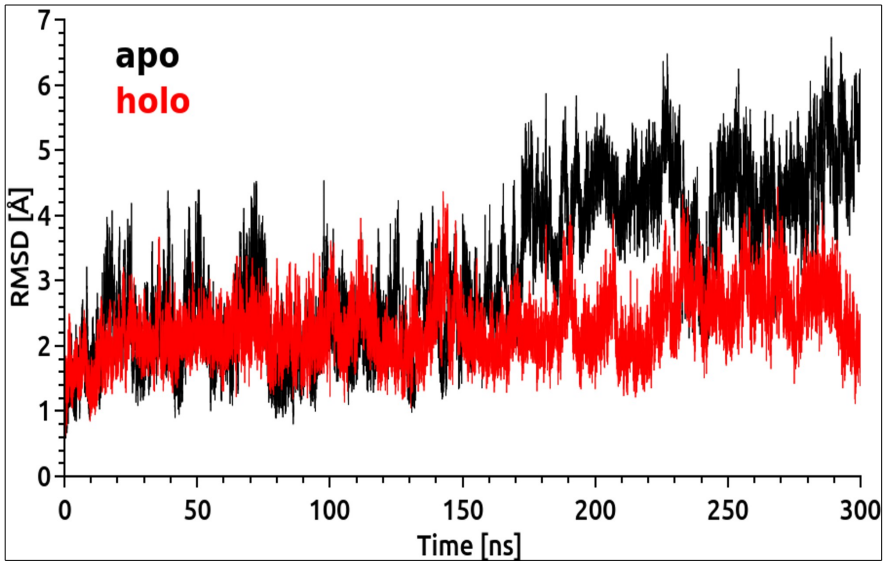


Figure 5.11 : RMSD evolution of EC2 amino acid residues with the base of Cα atoms for apo and holo systems.

5.3.5 Clustering analysis

Clustering calculations for maraviroc antagonist at the binding cavity of CCR5 was performed to characterize more populated conformational variation in the course of MD simulations. The criterion for the clustering calculations was the 2 Å RMSD threshold of heavy atoms of the ligand for $3x10^4$ maraviroc conformations. A relatively high stability of the ligand was observed during the simulations (Figure 5.12).

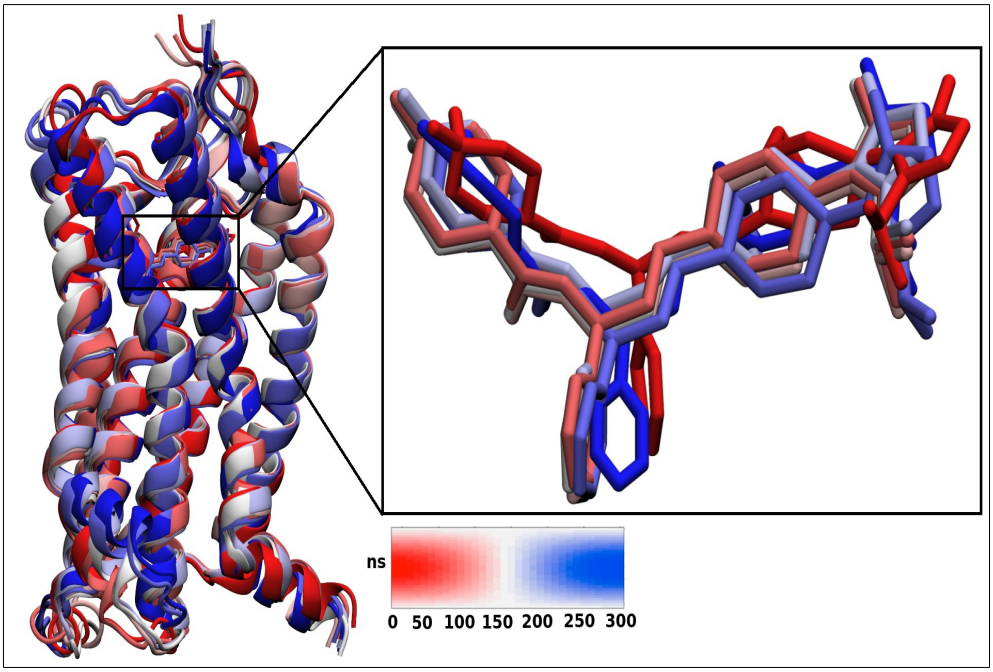


Figure 5.12 : Clustering analysis of the maraviroc conformation into the CCR5 chemokine receptor cavity during MD simulations. A color code is inserted (red: initial, blue: final frames).

RMSD histogram profiles for both states was compared at Figure 5.13. The comparatively high RMSD values for ligand-bound CCR5 were mostly occurred by fluctuation of the amino acid residues of TM5 and EC2 as mentioned at previous sections.

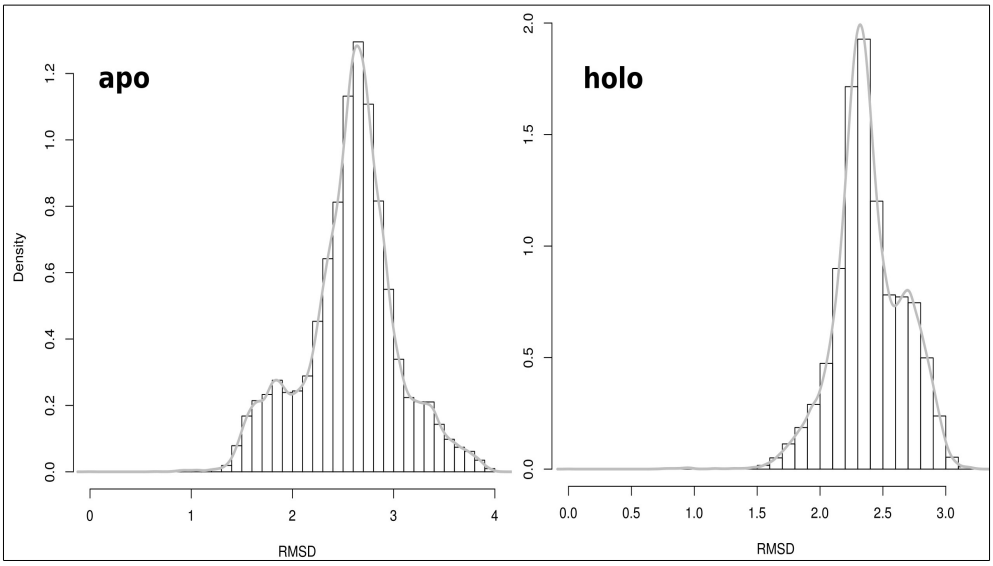


Figure 5.13 : Histograms over Cα atoms RMSD values (Å).

5.3.6 Dynamic cross-correlations

A cross-correlation analysis can be utilized to display how the atomic motion of different domains of the structure are coupled. Here we carried out a dynamic cross-correlation map (DCCM) analysis based on of Cα atoms for both apo and holo states of CCR5 during MD trajectories in order to investigate motion correlations at the protein. The DCCM profiles for the both ligand-bound and ligand-free systems have been represented at the Figure 5.14. The correlated dynamics identified in the both states are not showing similar profiles and the positive and negative correlative motions were importantly altered between apo and holo states. Following correlation results were observed: i) correlated motions between amino acid residues in the EC domains of TM1, TM2 and TM3 positions and residues in TM5 for holo state. This correlations were not observed at the apo state; ii) residues at TM2, TM3, TM4 and EC2 revealed strong anti-correlated motion with residues at TM7 and TM6, which were mostly connected to the extremely flexible state in the apo form. This anti correlation motions do not show similar profiles with holo state.

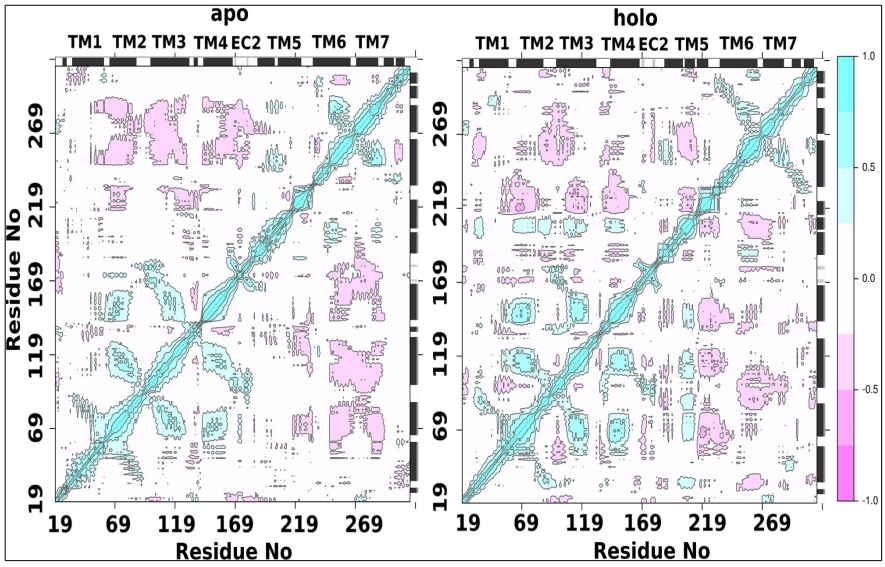


Figure 5.14 : Cα-residue dynamics cross correlation map for the ligand-free and ligand-bound CCR5. The color measure operates pink (-1 to -0.75) to white (-0.25 to 0.25) to cyan (0.75-1). Negative amounts (pink) show that Ca atoms displace in opposite way, called anti correlated motions, but positive amounts (cyan) display correlated motions happening at the one way.

5.3.7 Principal Component Analysis (PCA)

In order to describe the total norm of receptor motion, we performed PCA based on Cα atoms. This approach aided to determine the overall combined motion of the Cα atoms in the protein denoted by the eigenvectors of the covariance matrix which is argued by its coincident eigenvalues [157]. The frequency of the eigenvectors with large eigenvalues can usually represent the total concerted motion of the protein correlated to the protein function. The increasing sum of eigenvalues as a function of number of eigenvalues derived from the collected MD frames during 0.3 μs has been shown in Figure 5.15. The eigenvalue spectrum displayed the PC calculation's profile which showed the proportion of variances versus the eigenvalues for apo and holo systems. Scores for the first PCs of ligand-free and ligand-bound CCR5 are 22.3% and 31.5% of the total motions, respectively. Scores for the second PCs for apo and holo states were individually 15.3% and 10.7%, respectively. The third PCs (last main PCs) had scores of 12.8% and 8.3% for ligand-free and ligand-occupied systems, respectively. The initial three PCs all at once defined 50.4% and 50.5% of the overall motion for apo and holo systems, respectively.

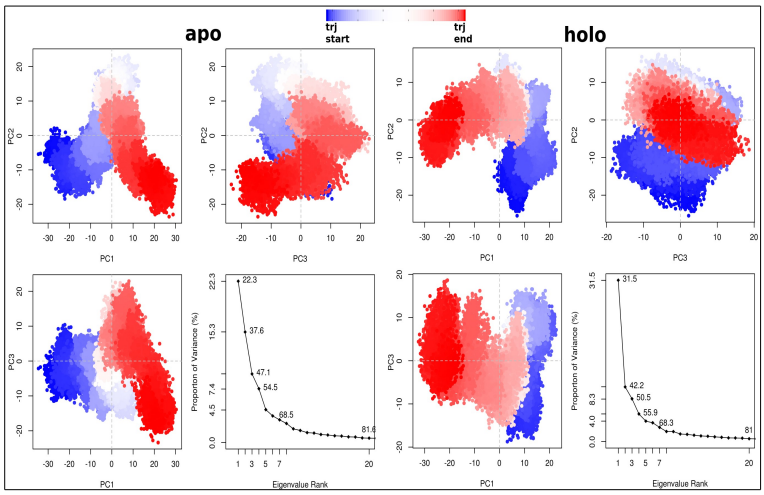


Figure 5.15 : Clustering profiles of average-linkage algorithm on different subspace dimensions projected by first three PCs. Clustering was performed on the overall (except first 20 ns) MD trajectory frames. Percentage of increasing eigenvector participation to the overall CCR5 motion by the apo and holo state.

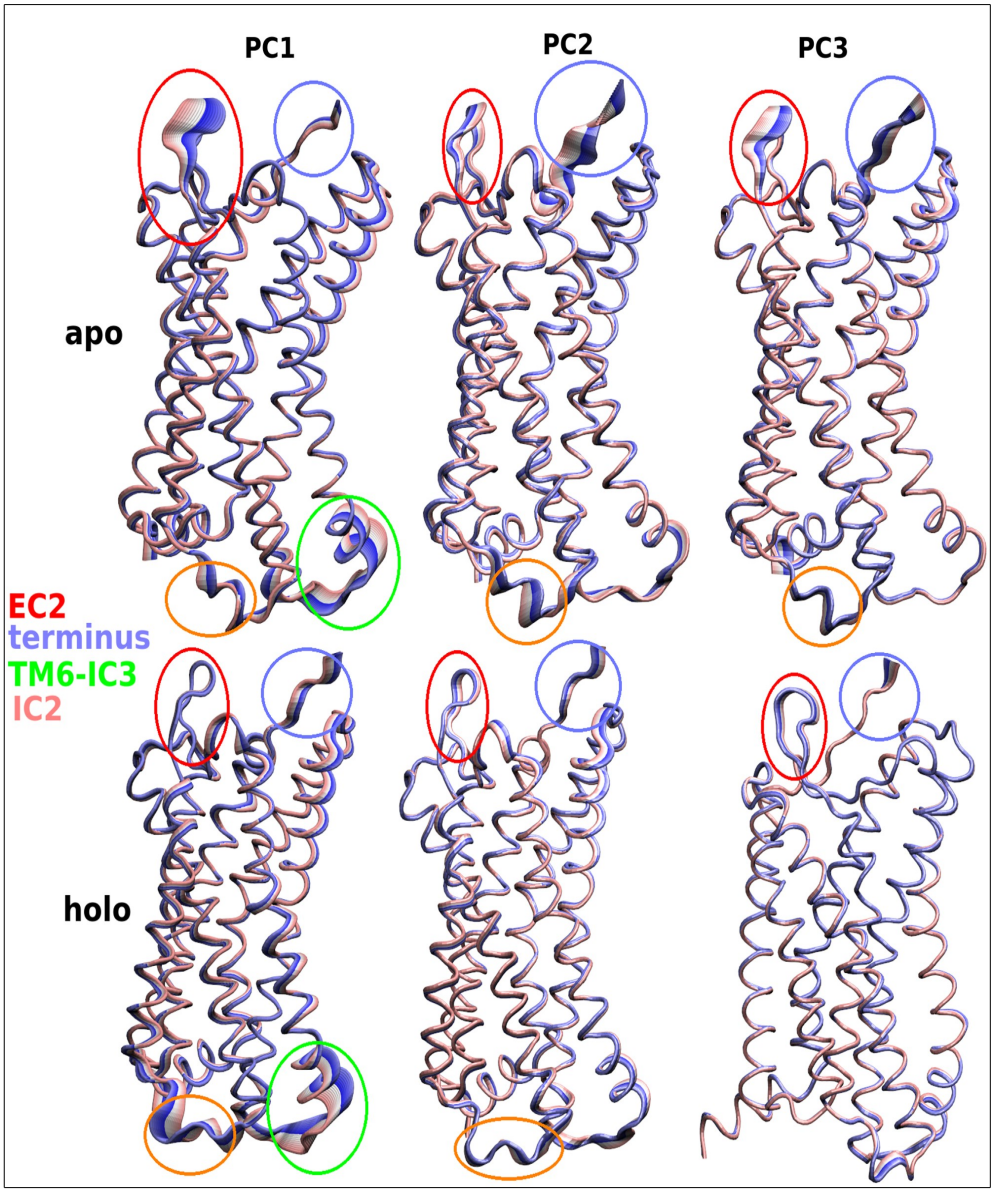


Figure 5.16 : Domains, directions and degrees of motions respected to the first three PCs were illustrated. The main motion are indicated by broadened tubes (color was changed with the course of time step). First and second columns display the apo and holo state of CCR5, respectively.

5.3.8 Conformational clustering respect to main PCs

Although PC calculations display the important motions included in MD simulations, it does not split the frames into different structural groups. This approach can be obtained by performing clustering analysis over the PC results. Clustering determines various conformational forms generated along the MD simulations by clustering protein structures into subsets depend on their structural similarity [158]. In the present work, totally $3x10^4$ conformers for each apo and holo

states were clustered using the first three PCs as shown in Figure 5.15. Clustering of generated conformers were plotted in three cross profiles for each state. Color scale tracks the trajectory numbers from blue to red. The side-chains were excluded from this calculation and only Cα atoms were considered. Figure 5.15 displays the cross-plots of PC1-PC2, PC1-PC3 and PC2-PC3 for both systems. The distribution of dots (frames) throughout the *x* and *y* axes, represented the comparative contribution to the whole dynamic from each PC. According to our results, regular and organized set of conformations were observed in the cross-plots of apo and holo forms which were corresponded to the first and second PCs. Semicircle shapes are reveled by the first two PCs. As reported by Hess et al. [159]-[160] such a model likely displays random diffusion within the system. But conformational of apo and holo systems were distributed in two various situation which was attributed to the inhibitor. Also different conformational distribution was observed with respect to the other main PCs (PC2-PC3 and PC1-PC3) as shown in cross-plots.

In Figure 5.16, MD frames of atomic deviations in the course of the first three PCs were visualized In rows 1, 2 and 3, PCs conformers were overlaid for both systems, respectively. A broadened tubes in these profiles displayed displacement, while slim tubes displayed domains that stay almost rigid. Dynamical variations between apo and holo states can be clearly shown from the Cα atoms motion projection onto the first three PCs. In agreement with our stability analysis that suggested a large amount of flexibility in EC2 for the ligand-free CCR5 simulations, the first PC explained a distinctive displacement at the EC2 for apo state, but in the presence of the inhibitor, this loop motion was not occurred at the EC side. The first PC was influenced by other distinguishing motion within N-terminus domains for both systems. Also the other main motion that came from PC1 was occurring at high degree of flexibility in the cytoplasmic side of TM5 and IC3 for two systems (as our previous discussion, this motion was directly attributed to the lack of fusion partner). The second and third PCs were controlled by a high motion inside the N-terminus and IC2 domain at apo system. It is clear that the presence of the inhibitor has a main influence on the conformational space of EC2 in complex.

5.4 Conclusion

In this study, PCA analysis and clustering approach for a marketed drug was performed using a long MD simulations. To the best of our knowledge, this work presented here was the most exhaustive study on CCR5-inhibitor interaction starting from a high resolution crystal structure, so far. Similar works have been issued before to investigate atomic interaction between CCR5 inhibitors and CCR5 on the base of homology models, not on the solved crystal structures. One of the aims of this study was to elucidate the role of rubredoxin molecule in CCR5 structure, and our study showed that it effected the protein structure as a whole ,particularly the cytoplasmic side of TM5.

Results of the present work were commonly in agreement with experimental results and some new key ideas were suggested: gp120-co-receptor activity was inhibited by anti-HIV drug maraviroc and it's inhibitory effect on EC2 was identified during long MD simulations. Here the majority of EC2 in protecting of HIV infection was explored and the critical residues (Thr171, Glu172 and Lys173) were identified. The derived results along with a through PCA and MD trajectory analyses highlighted important structural and dynamical differences at *apo* and *holo* forms of the target, are quite striking, and they suggest a greater future role for simulations in deciphering complex patterns of mechanisms of action of the inhibitor.

6. INHIBITORY TREATMENT OF DOPAMINE D2 RECEPTOR

6.1 Introduction

G-protein coupled receptors (GPCRs) constitute 7 trans-membranes (TMs), which play critical roles in physiological and pathophysiological processes [161]. GPCRs are responsible for cellular signal transduction from outside of cells. They are targets of nearly 30% of all of marketed drugs [31]. GPCRs frequently exist in equilibrium between inactive and active conformations [162],[163].

Drug binding to GPCRs investigations were extremely difficult for a long time because of the lack of high-resolution crystal structures in their active and inactive states. Solvation of the first X-ray structure of rhodopsin at the beginning of 2000s has opened a wide avenue for discovering and designing of novel agonist/antagonist ligands against GPCRs [164]. Crystallized conformer of GPCRs are used as templates for modeling of unsolved structure using homology modeling approaches and protein engineering studies.

In the present study, we focused on an important dopamine receptor from GPCR family, which is known as human dopamine D2 receptor (D2R). There are five sub-type of dopamine receptors, D1, D2, D3, D4 and D5 [165]. The D1 and D5 types constitute D1-like family, whereas D2, D3 and D5 belong to D2-like family [165]. Also there are some reports that suggest the existence of D6 and D7 receptors, but these evidences were not clearly determined, yet [165]. Dopamine receptors play critical roles in endogenous neurotransmitter in nervous systems and neurological processes including emotion, memory, lust, love, motivation, addiction, attention and pleasure [43]. The neurotransmitter dopamine is a primary agonist for dopamine receptors [166]. Dopamine (3,4-dihydroxyphenethylamine) is a hormone which is responsible for signal transmission between neurons in human brain [166]. Two main diseases, Schizophrenia [167] and Parkinson’s disease [168] are connected with dysfunctions of the dopamine system. Many investigations conclusively reported that Schizophrenia involves high level of dopamine activity and most of the anti-

psychotic drugs that are frequently used to treat Schizophrenia have a inhibitory effect on dopamine activity by targeting the dopamine D2 receptor [169]. D1 receptor is the most populated dopamine receptor in nervous system, D2 receptor is the second most populated one and D3-D5 receptors are at lower levels [170]. As many biological active hormones, dopamine couples to and activates the inactive state of D2R [170]. Dopamine functions as an agonist against D2R located on surface of cells and it leads to signal transmission via a second messenger system. [170] GPCR activation process includes distinct conformational transitions particularly in cytoplasmic side via coupling of G-protein to intra-cellular loops of GPCR [171]. The active state of β2 adrenergic receptor in complex with an agonist at the active site of the TM domains together with G-protein was determined by Rasmussen et al. [35] In this X-ray structure, outward movements in the cytoplasmic side of 5th and 6th TM helices were observed . Existence of the active state of GPCRs opens new avenues for agonist-based drug design as well as elucidation of the activity mechanism in these membrane proteins. So far only one active conformer was identified and other states were solved in inactive forms.

In the current study, 3D structure of unsolved D2R is derived using homology modeling approaches. Recently inactive X-ray structure of D3R was determined in complex with a D2R/D3R selective antagonist [47]. More than 70% amino acid residue identity score between D3R template and D2R target structures made this solved D3R structure as a reasonable template for prediction of 3D structure of D2R. Also Platania *et al*. have been modeled D2R structure on the base of D3R structure [172], in this study there is no inhibition mechanism analysis. Our main objective is to investigate the inhibitory effect of D2R inhibitors in the term of classical MD simulations. For this aim several atypical anti-psychotic drugs which antagonize D2R were selected and docked against our predicted model to create initial complexes. MD simulations are essential tools for identifying the physical base of the structure and function of biological systems. MD simulations facilitate us to generate thousands of time-depended conformers by initiating from a rigid structure/complex. In order to understand and elucidate the behavior of individual D2R antagonists in binding pocket of receptor and even illustrating any conformational transitions on overall protein structure, all complexes were submitted to MD simulations. We

therefore hope that, in the light of explained D2R inhibitory mechanism by long MD simulations, novel and potent D2R antagonists may be designed and they may lead to discovery of high potential anti-psychotic drugs with less side-effects.

6.2 Methods

6.2.1 Homology modeling

X-ray structure of D3R with a resolution of 2.89 Å was retrieved from Protein Data Bank server (PDB ID: 3PBL) [47] and employed as a template to predict the 3D of unsolved D2R structure. Chain A of dimer crystallized structure was considered and submitted to protein preparation procedure. There was not any missing heavy atom in backbones and side-chains of amino acid residues in overall TM domains. Third intra-cellular loop (ICL3) residues in the solved crystal structure has been replaced by lysozyme fragment to stabilize the structure along crystallization process. This part was removed from template structure. Amino acid sequence of D2R in *fasta* format (UniProt ID: P14416) was prepared from UniProt sever [49] *fasta* file was modified by removing ICL3 domain residues and only residues in the neighborhood of TM5 and TM6 were kept. ClustalW [52],[53] method was applied to align the amino acid residues of template and target. Combined MODELLER software [51] and ROSETTA [54] loop-modeling protocol were performed to build and refine the 3D structure of D2R. Predicted model was submitted to validation process using PROCHECK [173] software and ProSA-web server [174]. Ramachandaran and Z-score [175] profiles were plotted to show reliability of the predicted models.

6.2.2 Ligand preparation

All chemical structure preparation procedure for used ligands in this work were performed using MarvinSketch software. Consequence ligand preparations steps are follow as; i) 2D structure of each ligand was sketched, ii) 3D structures of all ligands were generated using molecular mechanical (MM) geometry optimization approach, iii) all ligands were then set to the physiological pH (pH = 7.4) at the protonation step.

6.2.3 Induced Fit Docking (IFD)

Since there is no any co-crystallized data of used ligands in complex with D2R, in order to predict accurately the D2R structure complexes with these inhibitors, induced fit docking (IFD) [176] protocol of Schrodinger suit was performed. IFD procedure was established in three consequence stages which involves; i) docking of all ligands into the generated model, ii) refining of amino acid residues within 4 Å of docked poses, iii) re-docking of docked ligands against refined protein. Docking score values for each complex were listed in Table 6.1.

6.2.4 Embedding of predicted model in membrane bilayer

Protonation properties of the protein were adjusted using PROPKA [59] at physiological pH (pH = 7.4). Each ligand-free and ligand-bound D2R complexes were merged with a 1,2-dipalmitoyl-sn-glycero-3-phosphocholine (DPPC) membrane bilayer and orientation of the target protein at the lipid bilayer was constructed using Orientations of Proteins in Membranes (OPM) [177] server. The membrane bilayers have been created using VMD [124] Membrane Builder plugin tool. D2R model forms one disulfide bond, between Cys107-Cys182 residues [178]. This disulfide bond was constrained using the patch DISU of the VMD. The membrane embedded proteins are then solvated with TIP3P explicit water models using the Helmut Grubmuller's Solvate 1.0 program. Finally the systems are neutralized (by 0.15 M of KCl solution) using VMD's Solvate plugin and located in a box of water with 15 Å thickness between the receptor and boundaries of the box. The overall number of atoms were almost 57000.

6.2.5 Molecular dynamic (MD) simulations

All classical MD (cMD) simulations are carried out using the NAMD 2.9 [126]. The CHARMM36 [127] force field was used for the D2R protein and DPPC lipid bilayer. ParamChem [128] server was used to generate force field for ligands. All covalent bonds between hydrogen and heavy atoms were constrained using the SHAKE [179] algorithm. In order to simulate the isothermal–isobaric ensemble (NPT) and control the used initial temperature (310 K) and the pressure (1 bar), Langevin dynamics [180] and Langevin piston methods were used, respectively. The Langevin damping coefficient and the piston period are set to 1.0 ps^{-1} and 0.05 ps, respectively. 3D

periodic boundary situation were used and in order to treat long-range electrostatic interactions with a cut-off distance of 10 Å, Particle Mesh Ewald (PME) [181] method was applied. A time step of 1 and 2 fs was used for equilibration and production MD processes, respectively.

6.2.6 Minimization and constrained equilibration

The systems are minimized and equilibrated before performing the production MD simulations, this procedure was carried out as follows: i) in order to equilibrate the lipids tails, initially 10000 steps of energy minimization and 2 ns isochoric-isothermal (NVT) MD simulations is applied to all constrained atoms except the lipid tails, ii) 20000 steps of minimization and 2 ns NVT MD simulations is applied with constrained protein, iii) Final equilibration was carried out with all atoms released through a 4 ns under NVT ensemble. Finally 0.1 μs production MD simulations under isothermal-isobaric (NPT) were performed for holo and 6 apo states (in total 0.7 μs). Along the MD simulations, the coordinates of all atoms are recorded in the .dcd trajectory file for every 10 ps (i.e., 10000 frames).

6.3 Results and Discussions

6.3.1 Homology modeling

Initial objective of our work was prediction and modeling of the 3D structure of unsolved D2R. For this aim, a comparative modeling approach was performed on the base of crystal structure data of D3R as a template structure with a high amino acid sequence identity score (>%70) respect to the target. Figure 6.1 shows residue alignment between D3R and D2R, also topologies of 7 TMs, ECL2 and ICL3 were indicated. As expected, all TM regions display a high residue similarity. This generated alignment data was submitted in structure building using MODELLER software. The loop domains were then remodeled and refined using ROSETTA loop modeling protocol. 2000 conformers of loop regions were generated and examined based on the total energies of derived conformers. The conformer that has the lowest energy as well as includes a constrained disulfide bond at the position of ECL2 within 2000 conformers is selected for further analysis. It is well-known that there is an important disulfide bridge between ECL2 and TM3 (i.e., Cys107-Cys182), this

covalent bond has an essential role at the formation of stabilization and low energy conformations of ECL2 atoms which is also associated directly to the active site of the binding cavity [178]. Therefore, during the overall modeling processes, this critical disulfide bond was mainly considered [178]. After the selection of the conformer within 2000 models, in order to validate the generated model, Z-score profiles as well as Ramachandran plot are generated and have been shown in the Figure 6.2 and 6.3 at the Supplementary Material, respectively.

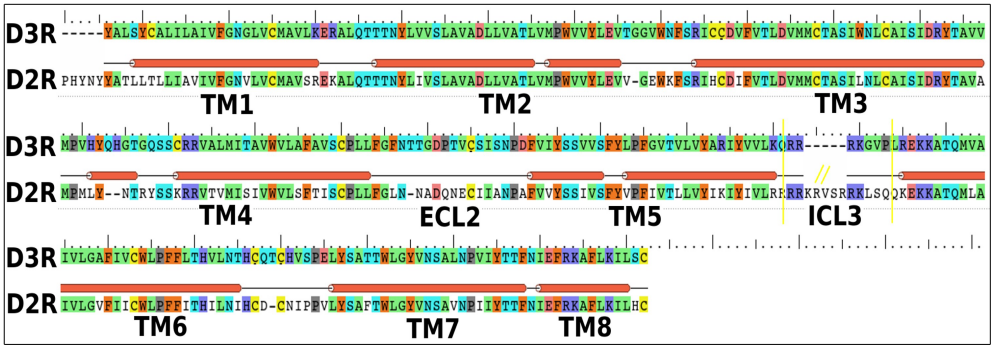


Figure 6.1 : Amino acid sequence alignment of D2R and D3R. TM and loop domains are indicated by tube and line, respectively. Similar residues from template and target are highlighted with the same colors. The ICL3 part was removed from template and it was artificially modeled, this loop domain is not effective to TM domains.

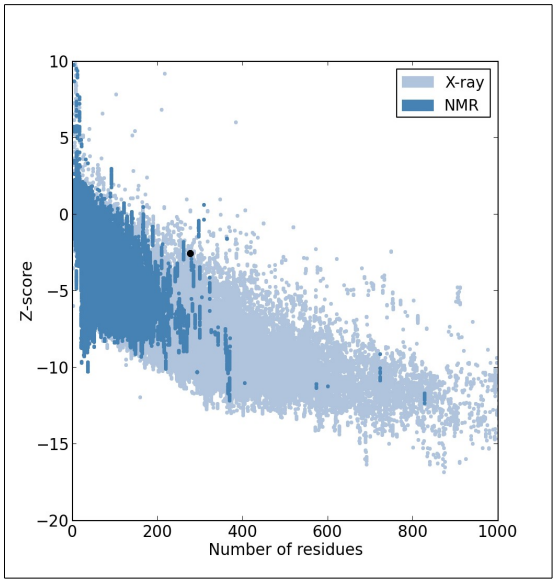


Figure 6.2 : Z-score plot of predicted D2R model.

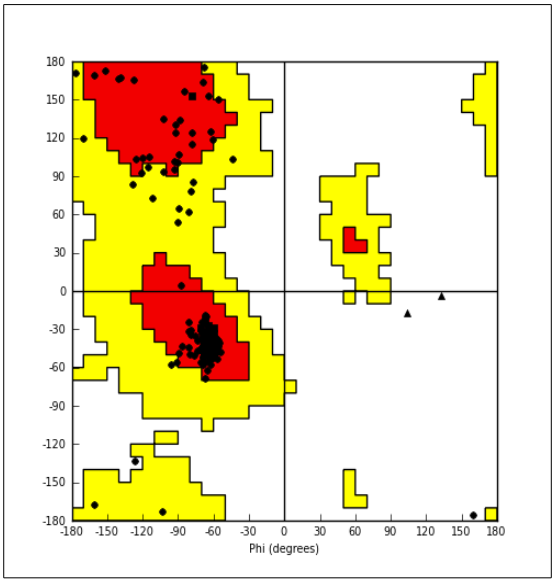


Figure 6.3 : Ramachandran plot of D2R model.

6.3.2 Molecular docking of known drugs at the derived D2R model

Six different atypical anti-psychotic marketed drugs as shown in Figure 6.4 (risperidone, ziprasidone, aripiprazole, olanzapine, clozapine and quetiapine) are selected and docked into the binding pocket of the derived D2R model using Induced-Fit Docking protocol. (Table 1) All docked compounds are approved as D2R inhibitors and mostly used to treat Schizophrenia. These six different approved D2R blockers which efficiently antagonize Dopamine D2 receptor, provided us better understanding of molecular mechanism of D2R inhibitory by relevant antagonists in binding pocket.

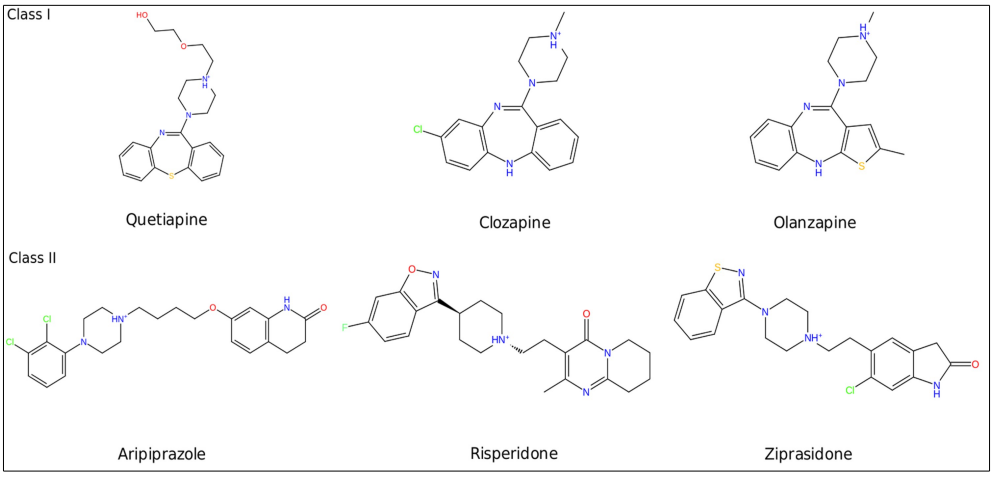


Figure 6.4 : 3D chemical structure of used ligand in this work.

6.3.3 Molecular dynamics (MD) simulations

In this study, we tried to understand the inhibitory mechanism of D2R using different marketed anti-psychotic drugs. For each drug we instructed a ligand-protein complex (six complexes in total) independently, as well as in order to identify the effect of the ligand to the structure of the target protein, a ligand-free D2R system was constructed as a control system. All complexes and apo form were submitted to classic MD simulations, totally 0.7 μs in length (100 ns for each system) is performed. Trajectory frames were considered every 10 ps and 10000 conformers were saved for the each complex.

6.3.4 Protein and ligands flexibility analysis

In order to identically determine influence of inhibitors on stability and conformational space of D2R structure (especially on TM domains), flexibility analysis were applied using MD trajectory frames. Root mean square deviation (RMSD) on the base of Cα atoms of amino acid residues from initial conformer were individually calculated for all ensembles (flexible loops and N-terminus domain were not included in this calculation only membrane domains were considered). Evolution of RMSD variations in function of time (100 ns MD simulations for all systems) was displayed to clearly understand the influence of inhibitory treatment on global conformational space over all receptors (Figure 6.5). Although all systems showed less than 4 Å RMSD but the different deviation of Cα atoms of ligand-free system (apo) conclusively shows the effect of an absent inhibitor in the binding site cavity as expected. Approximately after 40 ns, apo system exhibited distinct conformational transition compared to other ligand-bound systems. It displayed less stability during simulation compared to holo systems. Quetiapine and olanzapine-bound systems show a high stability compared to other systems. Clozapine-bound complex revealed high deviation from initial conformer after 60 ns. In the case of GPCRs, achieving a complete conformational stability in a short time (ns time scale) was not expected, due to the fact that GPCRs activation includes two consequence stages, as follows; i) agonist/antagonist binding slightly echo to overall structure (this can be occurred in ns timescale); ii) distinct conformational transitions which are only associated to the cytoplasmic side of TM5 and TM6, upon G-protein coupling to

ICL2 and ICL3 (this phenomena happens in ms timescale through a complex cycle consist of several unclear intermediates) [38]. All conformers of holo complexes roughly shared the same RMSD evolution in function of MD simulations time which suggest similar effect of these inhibitors on D2R structure. Moreover, RMSD calculation was carried out for active site residues of model as shown in Figure 6.6. Clozapine-bound system revealed a high flexibility in 70 ns. Model in complex with Quetiapine exhibited a higher stability in compare to other systems.

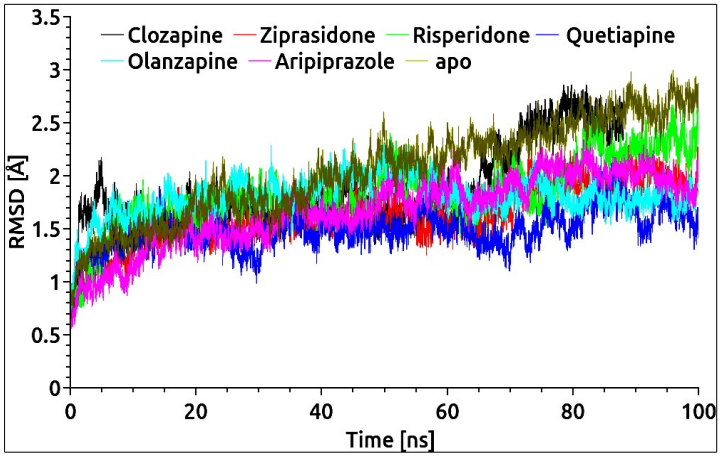


Figure 6.5 : Cα RMSD evolution of TM domains for all apo and holo systems respect to MD times. Each complex and apo form are shown by various colors. Apo system revealed the lowest conformer stability.

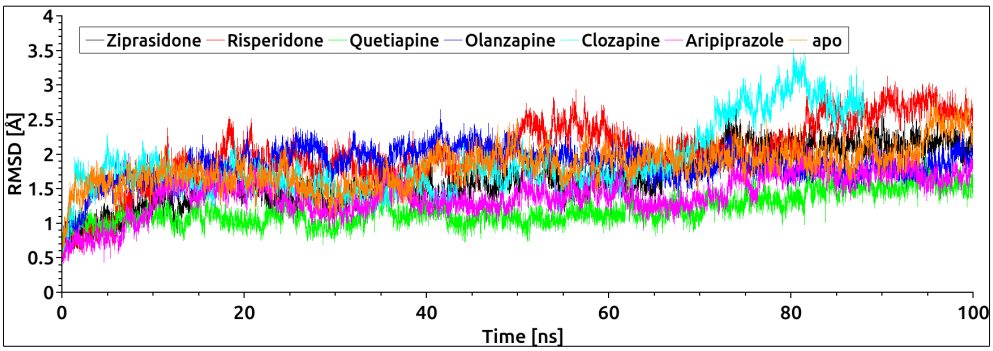


Figure 6.6 : RMSD plot of active side residues.

In order to see the effect of the studied compounds on the topologies of the target structure, root mean square fluctuation (RMSF) calculations were carried out on the base of Cα and side chain atoms which were shown in Figure 6.7 and Figure 6.8, respectively. The RMSF in positions of the Cα atoms for TM regions are very stable

throughout the simulations (< 2 Å). The most flexible elements (EC and IC linkers) display larger fluctuations of up to 6 Å from average structure. This range of fluctuations for the mobile element of the structure is not surprising. A large fluctuation (>2 Å) was observed for the apo states (<1 Å) compared to ligand-bound forms, at the cytoplasmic side of TM6, which is associated to G-protein coupling domain and it clearly demonstrates the effect of inhibitors in stability of the cytoplasmic side of TM6 that prevents regular accommodation of the G-protein. Aripiprazole-bound system exhibited significantly high flexibility compared to other studied systems in the position between TM3 and TM4. Interestingly, this complex shows a more stable form and exhibited different dynamic properties compared to other systems in the position of ICL2. These events may connected to different chemical structure of aripiprazole inhibitor. Aripiprazole is the highest extended compound in this class which involves four CH_2 groups at the central chain. Its capacity to have different conformations may lead forming and breaking of several hydrogen bonds between TM3 and TM4 upon ligand binding in this complex, and it may cause distinct deviations in cytoplasmic side of D2R. In the case of apo form high RMSF values are observed in EC parts of TM4 domain which is connected to ECL2. In the position of ECL2 and TM5, risperidone exhibited different and higher fluctuations compared to other systems. Since TM5 and ECL2 amino acid residues play critical role in ligand-binding pocket any deviations or conformational changes on these domains from initial position can be mainly associated with the inhibitory mechanism of D2R. Moreover, to identify the compactness of D2R model in complex with different antagonist, radius of gyration (gyradius) of D2R was calculated on the base of Cα atoms for all systems and the results were plotted in Figure 6.9. As anticipated, ligand-free conformer revealed a higher and different compactness treatment during MD simulation in compare to holo systems. Among holo conformers, clozapine-bound system exhibited higher gyradius values than others.

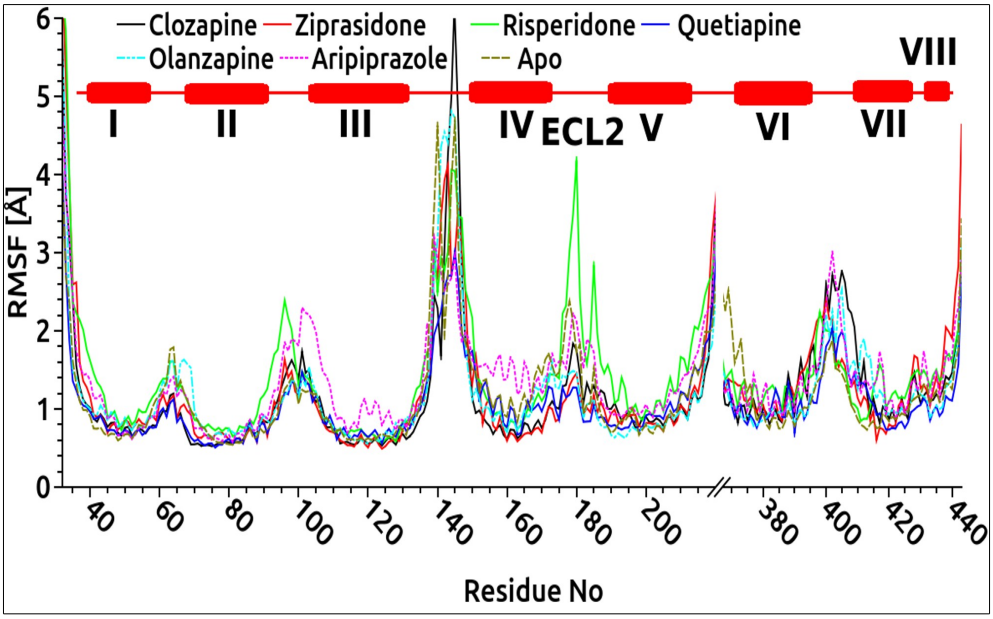


Figure 6.7 : Average RMSF values for individual amino acids (only Cα atoms are considered) during MD simulations. Helical and loop domains of D2R models are indicated by tube and line, respectively. The ECL3 domain is broken.

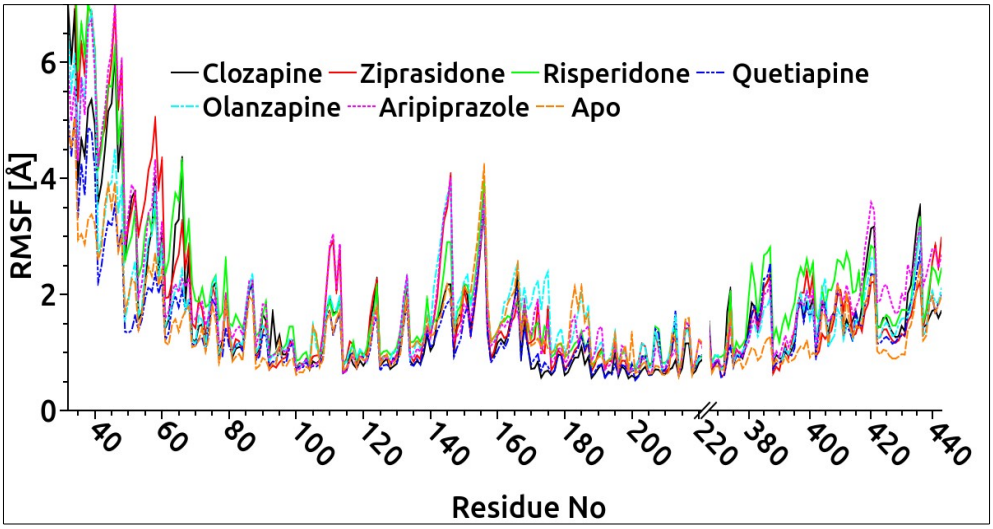


Figure 6.8 : RMSF plot of individual amino acids with the base of side chains.

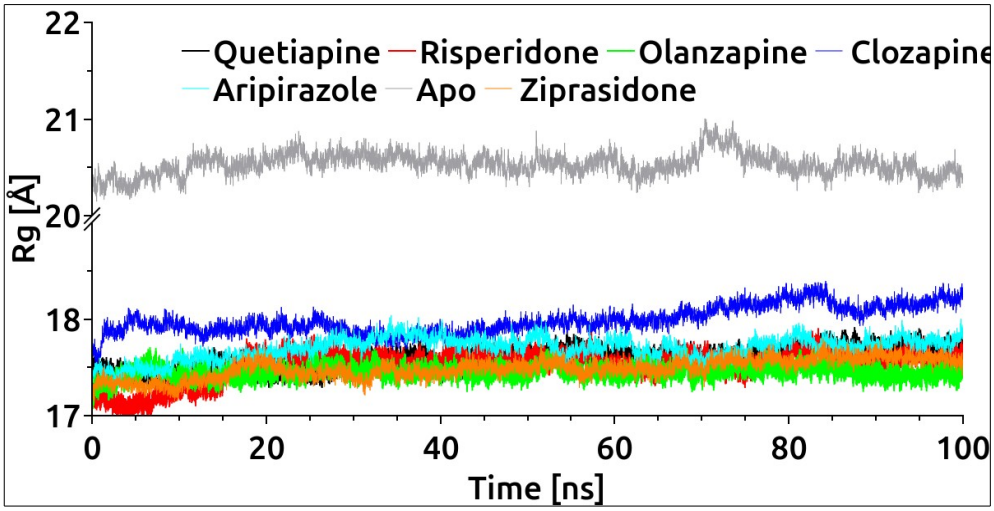


Figure 6.9 : Cα radius of gyration values for overal apo and holo systems.

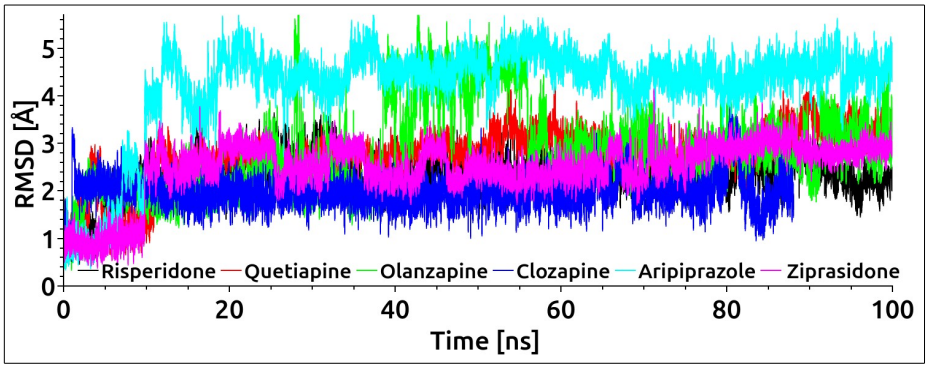


Figure 6.10 : Heavy atom RMSD evolutions of D2R inhibitors along MD simulations.

In order to investigate structural and dynamical profiles of studied ligands throughout the MD simulations, their RMSD evolution have been examined compared to initial conformers based on heavy atoms. (Figure 6.10). Kalani et al [81] have been classified these atypical anti-psychotic ligands in two groups, class-I which involves olanzapine, clozapine and quetiapine and class-II consists of risperidone, ziprasidone and aripiprazole. The first and second class compounds form bulky and extended chemical structures, respectively. In early time of MD simulations (~10 ns), distinct fluctuation were observed in some cases which connected to deviations from docking poses. Aripiprazole particularly displayed a high degree deviation (> 4 Å) from its initial pose (IFD position). Olanzapine and aripiprazole inhibitors showed larger change in conformations compared to initial position. In order to visualize evolution positions of ligands during simulations in 7TM cavity, all compounds were

incorporated in conformational clustering and their positions individually were illustrated in Figure 6.11. Evolution of MD time was indicated in function of color scale (red to blue) for each ligand. Red sticks represent initial or docking position of ligands and other colored sticks display popular positions of compounds along simulation. This figure helps to easily observe the conformational change of compounds during MD simulations. A detailed insight into clustering results suggested high conformational stability in polar binding domains of the inhibitors which was associated to constrain interaction of protonated nitrogen which is positioned in center of structure with charged Asp114 residue. This de-protonated amino acid plays a critical role in stabilizing of D2R inhibitors, as our results have demonstrated conclusively the importance of this critical hydrogen bonding (see details in hydrogen bond analysis section).

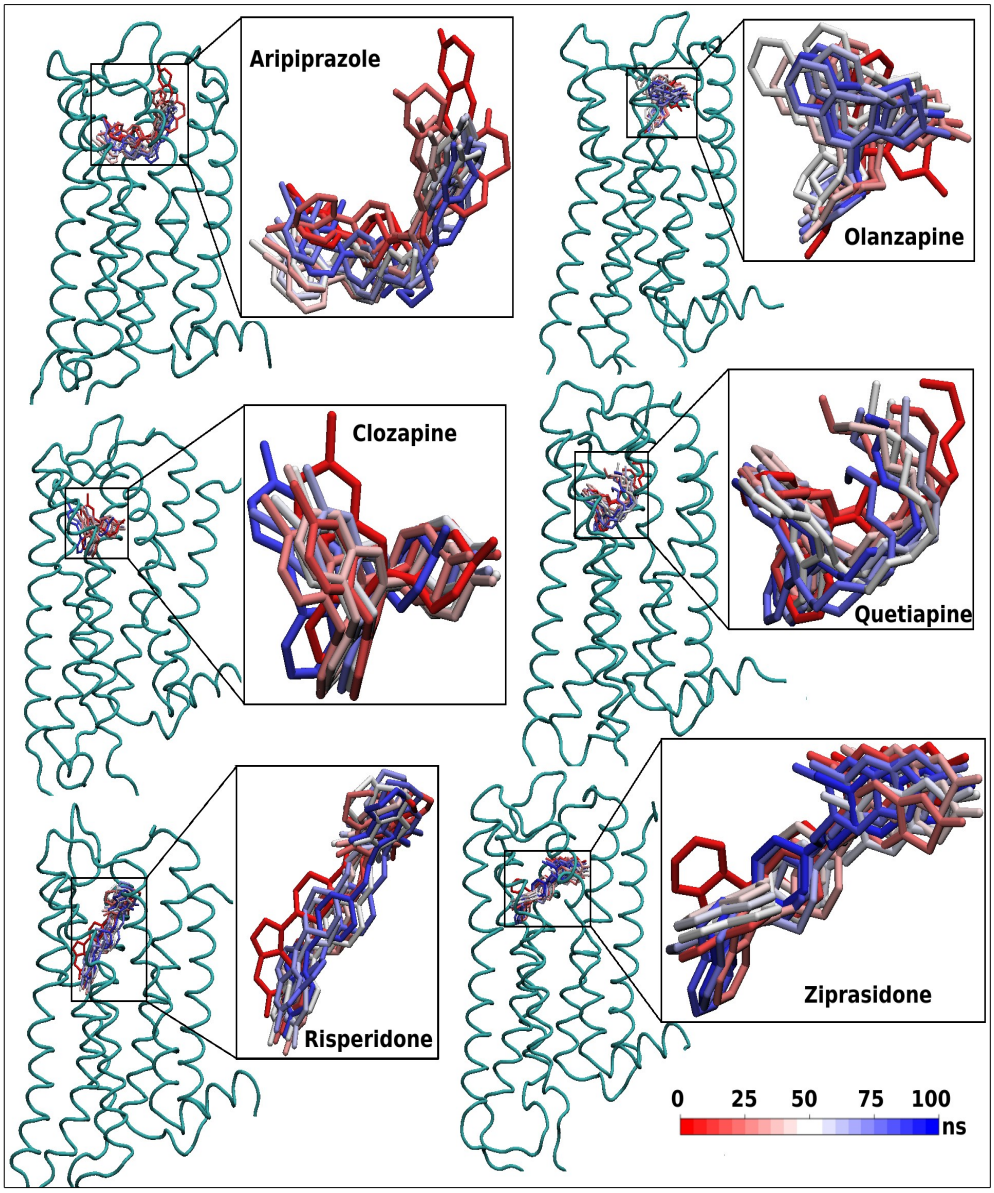


Figure 6.11 : Clustering analysis of D2R inhibitors during MD simulation into the 7TM binding cavity. MD color scale is initiated from dark red (corresponds to docking pose) to dark blue, 100 ns in length. Each panel clearly shows the evolution of ligand position respect to the MD time. The positions are clustered (threshold of >2 Å was applied) and popular conformers are considered.

6.3.5 Hydrogen bond analysis

Salt bridge and hydrogen bond interactions play an important role in ligand pocket of aminergic GPCRs, these bonds assist the stabilization of ligands and signal transduction through complex intermediates. In this section we identified overall established hydrogen bond occupancy values (expressed in percentage) between receptor and ligand with respect to all six complexes using totally 60000 MD

trajectory frames. Popular hydrogen bonds and their occupancies were profiled in Figure 6.12 Asp114 amino acid is participated in the formation of salt bridge of all complexes (except quetiapine-bonud D2R) and identified as a common charged residue in providing polarity of active site. In the case of D2R in complex with quetiapine, no any H-bond interaction has been observed in our assigned H-bond criteria (≤3 Å distance between donor and accepter atoms and 20° angle cut-off) but it dose not mean that there is no other polar interactions between quetiapine and Asp114 in the position of TM3. Highest H-bond occupancy (60%) is observed for the risperidone. The second highest H-bond occupancy has been observed for olanzapine (54%). Colzapine and aripiprazole approximately share the same H-bond occupancy (~50%). Interestingly among these inhibitors, only aripiprazole has established a strong H-bond interaction with Tyr408 residue (TM7). Also we noticed that ziprasidone has formed H-bonds with Tyr37 and Glu95 residues with the occupancy of 10% and 20%, respectively along simulations. Quetiapine forms H-bonding interaction with His393 residue in the position of TM7 with around 20% H-bond occupancy throughout the simulation.

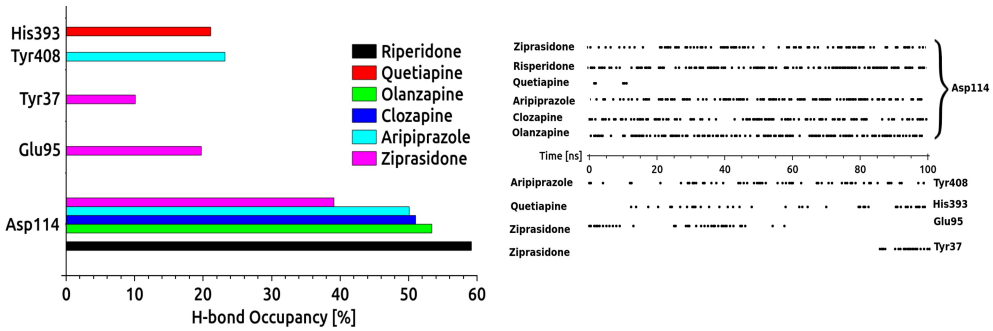


Figure 6.12 : H-bond occupancy analysis of ligand-protein interactions (left), For each ligand-bound system occupancy (%) of H-bonds between ligand and receptor are estimated using 10000 MD trajectory frames. Evolution of the H-bond forming and breaking between active residues and inhibitor during MD simulation for each complex (right).

6.3.6 Non-bonding energy calculation

In order to shed light on overall main non-bonding interactions between ligand and receptor which were established in 7TM active cavity, all inhibitor-bound complexes are submitted for van der Waals (vdW) and electrostatic interactions. All amino acid residues of D2R within 4 Å distances of inhibitors (twenty-one residues) were

selected and NAMD-energy calculation is then employed. All non-bonding energies between twenty-one residues (individually) and six inhibitors are calculated using 60000 MD trajectory frames and average total energy values are plotted in Figure 6.13. In order to clearly profile energy results for all residues, Asp114 residue data was excluded from column plot and expressed additionally within the Figure 6.13. Asp114 residue shows the lowest total non-bonding energy values for all mentioned systems in compare with other residues. In addition to Asp114 there are other important amino acid residues in D2R active binding pocket which were considered and described in-depth for individual complexes as following:

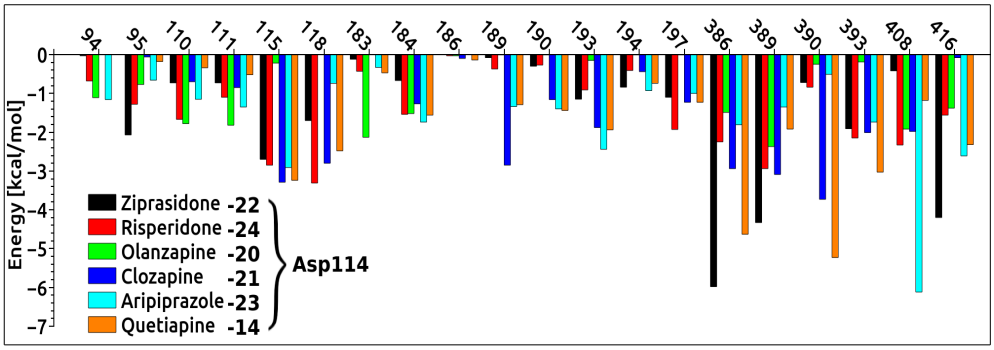


Figure 6.13 : Non-bonding interaction analysis for all systems. Active ligand binding residues were selected and their average interaction energy values in six complexes with inhibitors were estimated during MD simulations. To make clear, energy values of Asp114 are excluded from column plot and represented as text.

6.3.6.1 Risperidone

The extended structure of risperidone was accommodated well during MD simulations by D2R active site and significantly established polar and non-polar interactions with corresponded residues. As energy plot in Figure 6.13 suggests, Val115 (TM3), Cys118 (TM3), Ile184 (ECL2), Ser197 (TM5), Trp386 (TM6), Phe389 (TM6), His393 (TM6), Tyr408 (TM7), Tyr416 (TM7) and Glu95 (TM2) residues strongly participated in interaction with the ligand. Representative 2D structures (i.e., the structure that has the lowest RMSD value based on average structure during the MD simulations) of D2R in complex with studied compounds are illustrated in Figure 6.14. Protonated nitrogen of risperidone has formed a constraint salt bridge with charged oxygen of Asp114. (Figure 6.15) According to the non-bonding energy analysis and representative results, TM1 and TM4 residues

are far from risperidone and they do not responsible in ligand binding interactions. Moreover, aromatic amino acid residues such as Tyr408 (TM7), Tyr416 (TM7) and Phe389 (TM6) play main roles in ligand binding at the active pocket. Risperidone is the only compound among other six inhibitors that participated in pi-pi stacking interaction with His393 residue, as obviously shown by Figure 6.14.

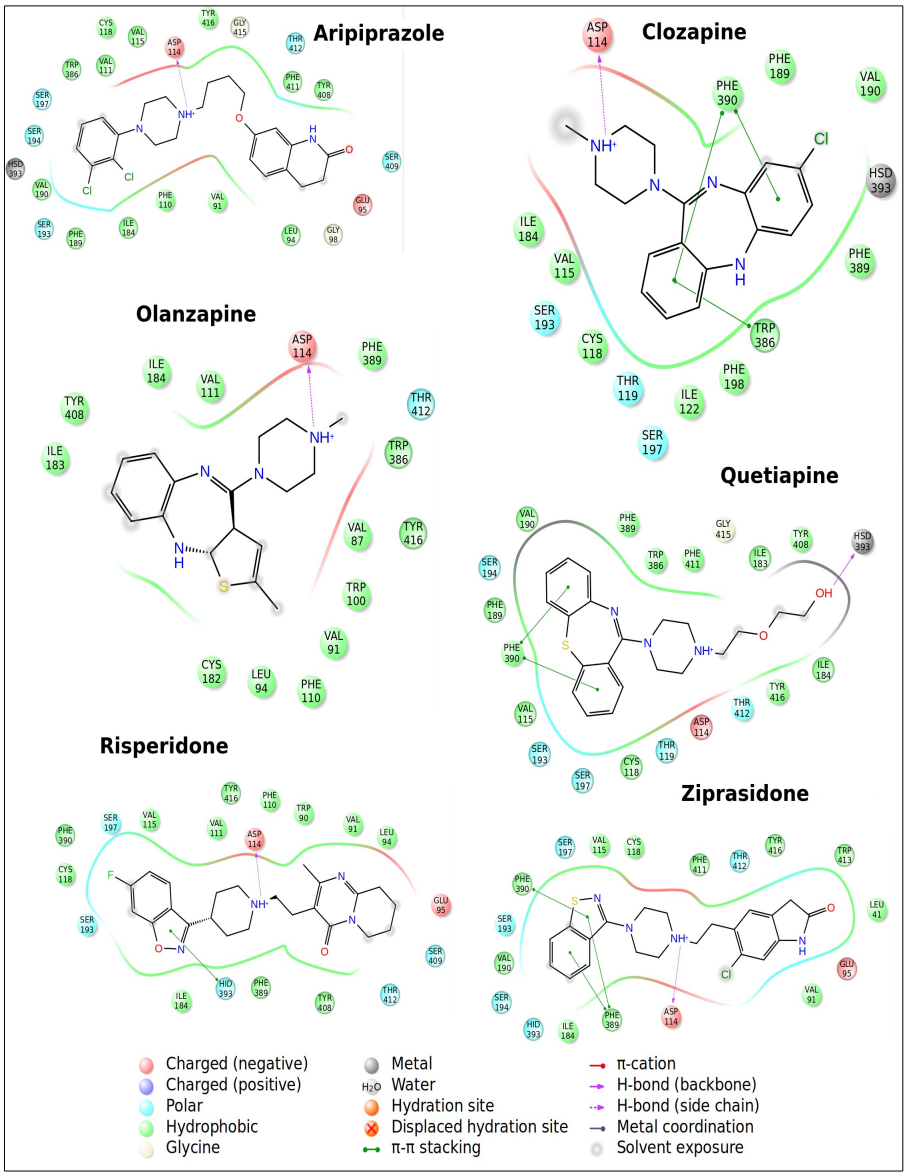


Figure 6.14 : 2D representative structures of D2R inhibitors into binding cavity. H-bond (salt bridges), hydrophobic, polar and π−π stacking interactions are shown by their symbols (as displayed in legend). Phe390, Trp389, His393 and Trp386 residues have participated in π−π stacking interactions. Asp114 is a constrained residue which establishes strong polar interactions with protonated nitrogen of inhibitors.

6.3.6.2 Ziprasidone

In the case of ziprasidone, an effective anti-psychotic drug with a extended structure which exhibited high affinity towards Glu95 (TM2), Val115 (TM3), Trp386 (TM6), Phe389 (TM6), His393 (TM6) and Tyr416 (TM7) residues in D2R cavity as shown in energy plot. These residues except Glu95 mostly form a hydrophobic pocket for ziprasidone. 2D and 3D binding mode of ziprasidone was represented in Figure 6.14 and 6.15. Amino acids residues in the position of TM1, TM5 and TM4 did not show any direct effect to ligand binding.

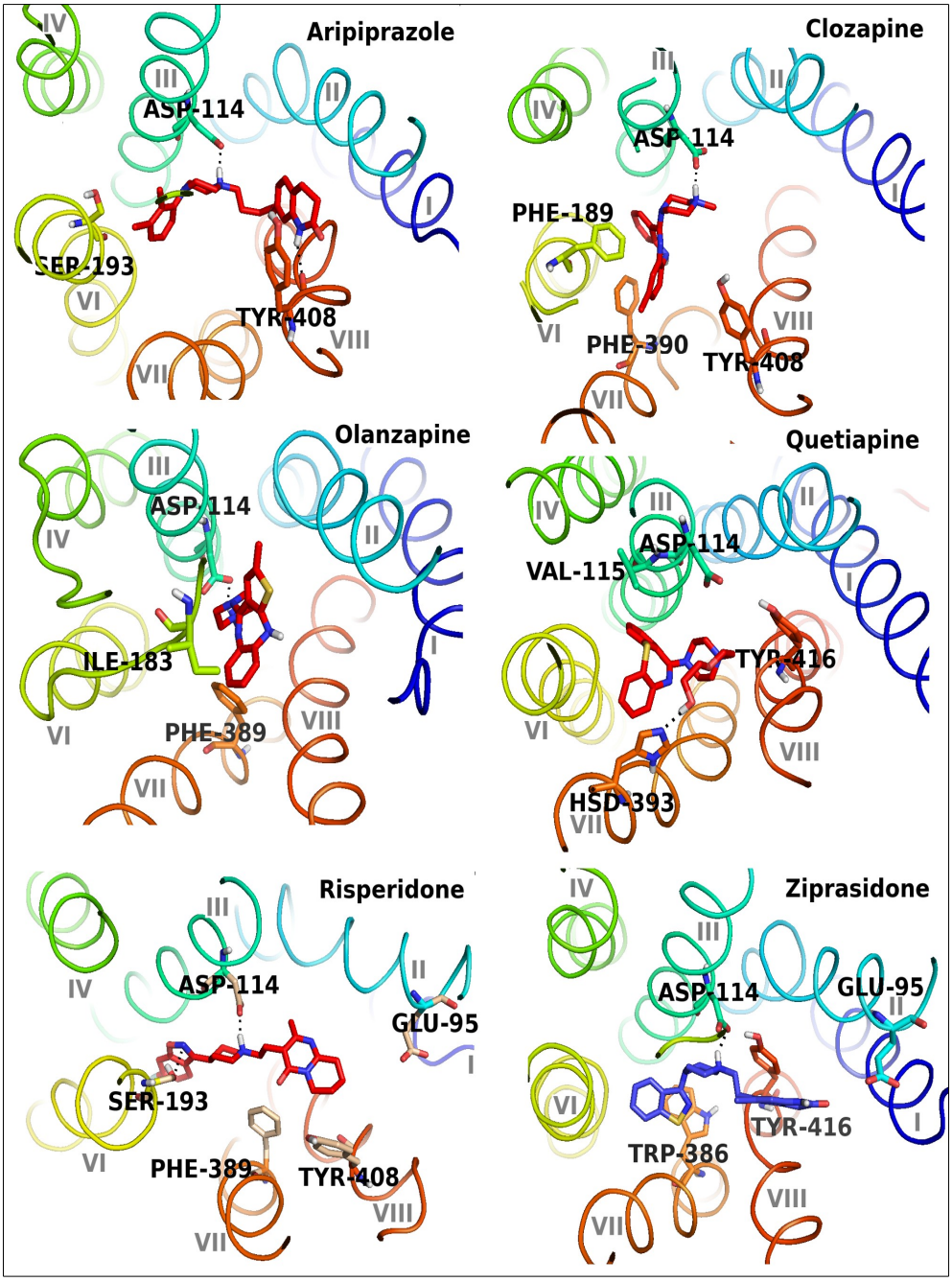


Figure 6.15 : Representative 3D pose of D2R inhibitors in 7TM cavity. Ligand positions of six representative complexes are displayed, and also their ligand-protein interactions (main residues are included) are indicated. TM numbers are displayed on each helical part (TM1-7) and colorized on the base of their positions. H-bonds are shown by black dash line, Asp114 is constrained in all complexes.

6.3.6.3 Aripiprazole

According to our binding energy calculations, aripiprazole in D2R model tightly bonded with Val115 (TM3), Ile184 (ECL2), Ser193 (TM5), Phe386 (TM6) Tyr408

(TM7) and Tyr416 (TM7) residues of active domain. 3D mode of this antagonist was pictured in Figure 6.15 This class-II inhibitor occupied the region between TM3, TM5, TM6, TM7 and ECL2 domain. Among other considered inhibitors only aripiprazole form hydrogen-bond interactions with backbone carboxyl of Tyr408 as discussed before. In addition to the H-bonding interactions with Tyr408, this residue also has an essential role in forming of hydrophobic interactions from its aromatic ring at the side chain with the antagonist. The role of polar environment in this pocket is higher compared to other inhibitor-bound active sites. This ligand has formed minimal interactions with residues of TM1, TM2, and TM4, particularly in contrast to the other antagonist (i.e., Phe389 and Phe390 are not directly participated in this binding cavity, this suggests less hydrophobicity at the aripiprazole binding pocket).

6.3.6.4 Clozapine

For class-I antagonist, such as clozapine, we have found the following residues to be critical in ligand-binding pocket: Val115 (TM3), Cys118 (TM3), Phe189 (TM5), Ser193 (TM5), Trp386 (TM6), Phe389 (TM6), Phe390 (TM6), His393 (TM6) and Tyr408 (TM7). Representative pose of this antagonist in ligand cavity of D2R was displayed in Figure 6.15 Clozapine has occupied the region between TM3, TM5, TM6 and TM7 and established minimal interactions with TM1, TM2 and TM4 residues. This bulky antagonist located mostly in hydrophobic binding pocket and form tight bonds with critical Phe390 residue. Moreover, pi-pi stacking interaction play a sub-maximal role in clozapine-bound D2R by Phe390 and Trp386 residues as clearly shown in Figure 6.14, two aromatic rings of clozapine participated in this hydrophobic interaction.

6.3.6.5 Olanzapine

Non-bonding energy analysis with olanzapine suggests that Phe110 (TM3), Ile183 (ECL2), Phe389 (TM6), Phe393 (TM6), and Tyr408 (TM7) residues to be located in the active site of D2R. Representative 3D pose of olanzapine in Figure 6.15 displays that this small-size antagonist has been accommodated between TM3, TM6 and TM7 residues. Olanzapine binding cavity has exhibited hydrophobic characteristic with aromatic residues to be located particularly in TM6 and TM7 like other class-I

antagonists-bound complexes. In addition to Ile184, olanzapine is the only antagonist in our study which has hydrophobic interaction directly with critical Ile183 residue in the position of ECL2.

6.3.6.6 Quetiapine

As our binding energy analysis suggests, Val115 (TM3), Cys118 (TM3), Ile184 (ECL2), Ser193 (TM5), Trp386 (TM6), Phe390 (TM6), His393 (TM6) and Tyr416 (TM7) residues has participated directly in the formation of the quetiapine binding pocket. The chemical structure of this antagonist has a polar tail which was linked to the protonated nitrogen at the central ring, thus it may affect the polarity of this nitrogen atom.

6.3.7 Binding energy comparison of six standard drugs

In this section, we performed a comparative elucidation analysis on the binding affinity degrees of individual D2R antagonists against the derived D2R model using MD trajectory frames. Electrostatic, van der Waals and total non-bonding interaction energies were shown for each complex at the Table 6.1 (represented results are the average values from 10000 frames). Table also shows experimental dissociation constant (Kd) values as well as IFD docking scores for six ligands. Both docking results as well as NAMD non-covalent bonding energy analysis shows parallel results with experimental values. In general, compounds at Class-II have better binding interactions compared to Class-I compounds. As it can be seen from Table 6.1, this prediction is conserved at the *in-silico* calculations.

Table 6.1 : Binding enthalpy energy and IFD score of D2R model with atypical anti-psychotic drugs and also their experimental binding affinity values.

D2R antagonist	ΔH^{vdW} (kcal/mole)	ΔH^{elec} (kcal/mole)	ΔH^{tot} (kcal/mole)	K_d (nM)[1]	IFD score (kcal/mole)
Quetiapine	-45.52	-16.71	-62.23	180	-9.86
Aripiprazole	-45.67	-23.82	-69.50	1.8	-15.41
Clozapine	-36.63	-19.03	-55.66	113	-10.75
Olanzapine	-31.30	-20.87	-52.16	17	-8.12
Risperidone	-41.04	-25.15	-66.19	0.44	-10.62
Ziprasidone	-44.57	-25.32	-69.89	2.8	-12.20

1. http://zinc.docking.org/

6.3.8 Shift of the TM5 from IC site during simulations

Representative structures (the structure that have the smallest RMSD from the average structure during simulations) of six ligand-bound forms are superimposed with the apo state. (Figure 6.16) Distinct conformational deviations are observed in cytoplasmic side of TM5 upon antagonist binding (i.e., allosteric effect). The smallest shifting is observed when there was no any ligand at the active site (apo form). The largest shift is observed with aripiprazole binding. This shifting at the cytoplasmic side of TM5 plays a critical role in GPCRs in the activation process. Moreover, in order to understand the effect of antagonist over D2R conformation in depth, the key residues involved in D2R binding pocket are individually superimposed as shown in Figure 6.17. In all poses, aripiprazole-bound residues adopted different behavior compared to other systems.

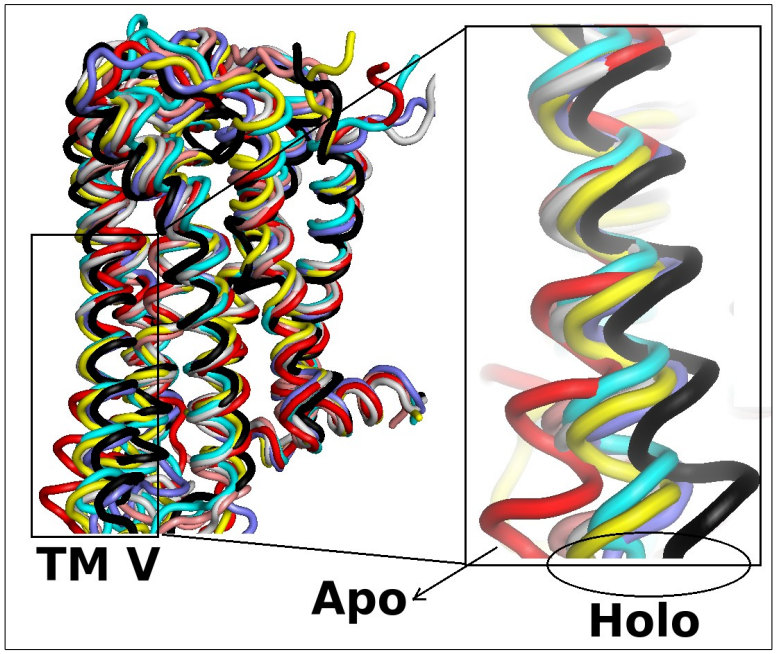


Figure 6.16 : Conformational deviations of TM5 in different systems. Representative conformer of all apo and holo receptor are superimposed and TMs5 are focused for the better analysis. Dark red helical is responsible for apo form and the other colors display holo conformers. TM5 of aripiprazole-bound revealed a higher displacement from apo form, the other holo conformer have approximately shared the same deviations in the position TMs5.

In order to apply a distance analysis between TMs during MD simulation, the residues which establish H-bonding with each other were selected and submitted in H-bond occupancy analysis and the results were reported in Table 6.2. These results suggests us that distance betweenTM3 and TM5 was increased upon inhibitor binding, this phenomena is more sensitive in risperidone and aripiprazole. Moreover, in the case of distance between TM2 and TM7, risperidone revealed a different treatment and decreased the distance between these TMs as H-bonds occupancy between Glu95 and Ser409 suggested.

6.3.9 His393 dihedral angle

His393 plays a critical role in D2R activation process, the D2R inhibitors induce different conformation to His393 residue and differ its dihedral angle during MD simulation. Here in order to shed light on this phenomena, we analyzed the dihedral angle changing of His393 in all apo and holo systems in the course of MD simulation, the results were plotted in Figure 6.18. In the case of apo form, average

dihedral angel of His393 is 150° and exhibited a stable state, the other holo systems respect to the ligands which antagonize the receptor show different dihedral deviation. Particularly aripiprazole, risperidone and olanzapine-bound receptors exhibited distinct dihedral angle deviation from apo conformer for this residue. His 393 residue has a high capacity for establishing pi-pi stacking interaction with aromatic rings of D2R antagonists, as examplfied by risperidone, this antagonist underwent a pi-pi stacking interaction with His393 residue.

Table 6.2 : Hydrogen bond occupancies (%) between amino acid residues from different TMs.

	Apo	Quetiapine	Aripiprazole	Clozapine	Olanzapine	Risperidone	Ziprasidone
Thr119-Ser197	26	19	9	18	22	4	24
His393-Ser194	0	0	0	0	0	0	3
His393-Tyr408	15	4	4	0	0	12	3
His393-Thr412	0	0	0	0	0	0	0
Glu95-Ser409	0	3	0	0	1	25	0

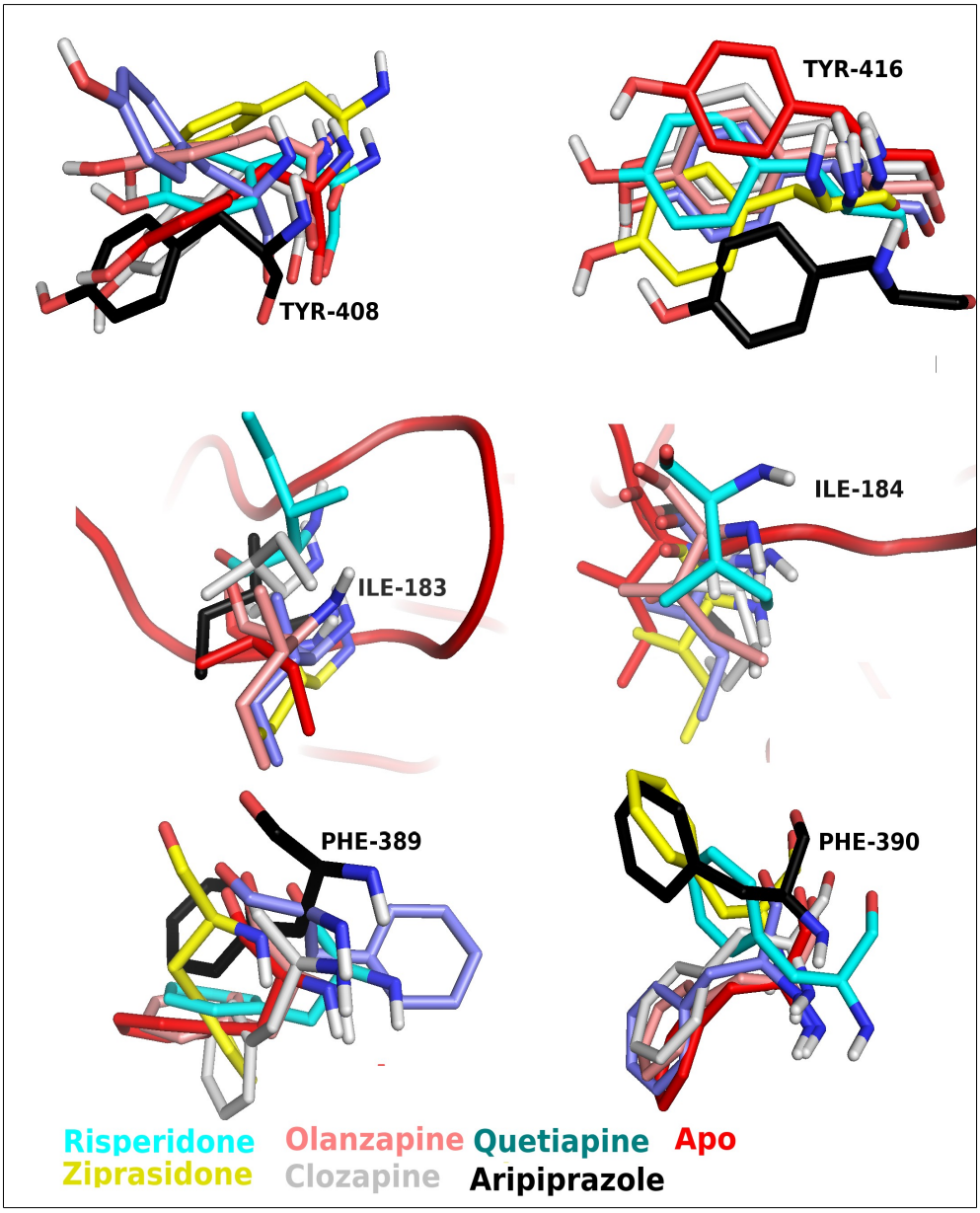
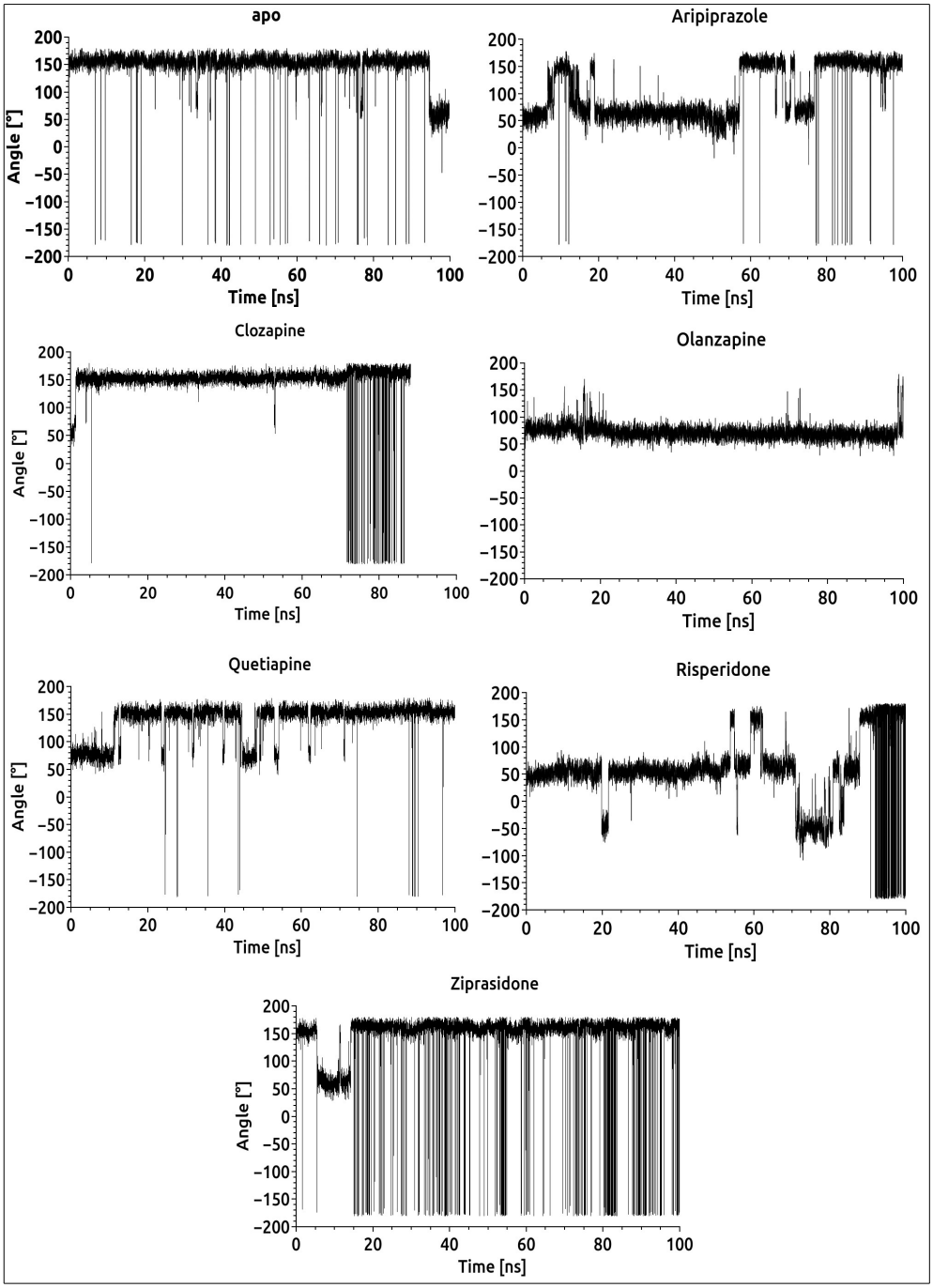


Figure 6.17 : Conformational analysis of critical amino acid residues in ligand binding pocket. Representative positions of amino acid residues which participated in ligand-binding pocket are superimposed and their deviations and displacements from each other are illustrated.



Fugue 6.18 : Dihedral angle analysis (atoms: C-Cα-Cβ-Cγ) of His393 during MD simulation for each complex.

6.4 Conclusion

In Third study we predicted successfully 3D structure of D2R receptor using X-ray crystal structure of inactive D3R with a high amino acid sequence homology/similarity between target and template. Derived model was refined and validated utilizing most widely used homology and validating protocols as described

in Methods section. Ligand-binding pocket of D2R was predicted and optimized by flexible receptor docking of six well-known anti-psychotic drugs. All predicted complexes and one control system (apo form) were submitted individually to 100 ns classic MD simulations. In the light our analysis we report the following results regarding to binding mechanism in D2R:

Ligand-free D2R revealed more flexibility on trans-membrane domains compare to ligand-bound receptors, however this stability difference in backbones was not so significant (conformational change is restricted to cytoplasmic domains of TM5 and TM6).

- Asp114 in the position of TM3 is conclusively conserved in all antagonist-bound D2Rs and it forms hydrogen bond directly with protonated central nitrogen atom at the studied molecules. This residue has established stronger H-bonds with extended antagonists rather compared to class-I ligands.
- Tyr416 and/or Tyr408 in the position of TM7 conclusively play essential role in D2R ligand binding mechanism.
- An aromatic amino acid, Phe390 in TM5 was observed as a conserved residue at the binding pockets of the target and it constructs interactions with the used class-I antagonist in this work.
- In agreement with *in-vitro* data, our elucidation revealed that a hydrophobic residue, Ile184 at the second extra-cellular loop (ECL2) of D2R which connects TM4 and TM5 has a crucial function in ligand binding.

7. MECHANISM OF LIGAND-BINDING IN κ-OPIOID RECEPTOR

7.1 Introduction

G protein-coupled receptors (GPCRs) are the most common family of proteins involved in transmitting signals into cells [182],[183]. These receptors enable the cells to sense external signals (e.g., taste, pain) or to communicate with each other via messenger molecules. They are implicated in a variety of physiological processes and are targeted by ∼40% of current prescription drugs [184]. Despite consistent efforts over the years, the solution of GPCRs structures remains a great challenge: GPCR incorporation into a membrane is a prerequisite for retaining the protein's structural integrity; however, it is hardly achieved experimentally. Additionally, the high flexibility of several loop regions renders their expression arduous. Nevertheless, major progress has been made recently, as several crystal structures were obtained and helped considerably toward understanding of GPCR structure and action [185]-[189]. All of the structures solved so far confirm that GPCRs are integral membrane proteins with seven α-helical membrane- spanning regions. These regions are linked together via three extracellular and three intracellular loops to define a common overall architecture for GPCRs. Opioid (μ, δ, κ, and nociceptin) receptors (ORs) belong to the class A (rhodopsin-like) γ subfamily of GPCRs [190]. Activation of these receptors is associated with a multitude of neuropsychiatric responses (e.g., depression, schizophrenia, analgesia, euphoria) and physiological processes, including memory and learning [191]. The κ-OR subtype represents an excellent model for drug design, since numerous κ-OR−selective agonists/antagonists have been developed as compounds with anti-addictive, antidepressant, and anxiolytic action [192]. Salvinorin A (SalA), which is the active ingredient of the hallucinogenic plant Salvia divinorum, has been found to be a highly selective κ-OR agonist (Figure 7.1a) [193],[194]. Stevens and co-workers have recently reported the crystal structure of human κ-OR in complex with JDTic [195],[196] (a κ-OR antagonist in early stages of clinical trials, Figure 7.1a) at 2.9 Å

resolution [186]. Their findings include information on the structure, molecular recognition and selectivity of κ-OR. The recent availability of high-resolution GPCR structures supports the observation that the receptors are dynamically flexible, and their functions can be modulated by several factors.

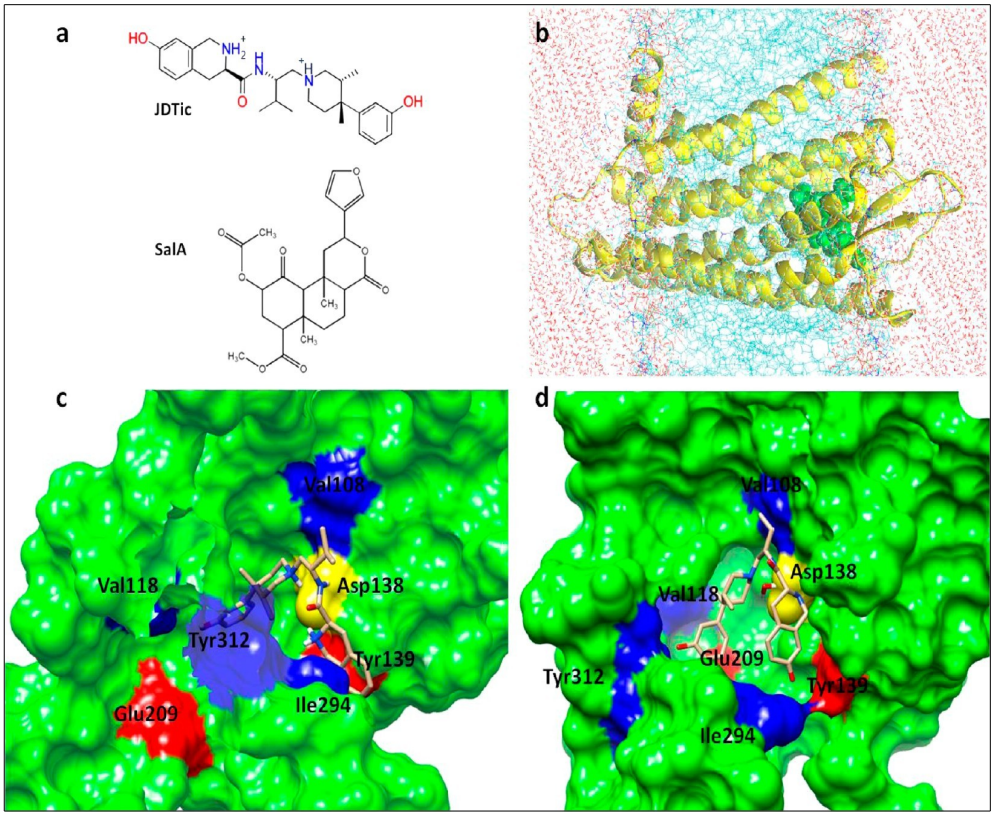


Figure 7.1 : (a) Chemical structures of JDTic and SalA. (b) Antagonist JDTic (green) bound to human κ-OR (yellow); the complex is merged into a DPPC lipid bilayer (blue) surrounded by water molecules (red). JDTic into the binding site of κ-OR, as depicted by (c) the crystal structure, and (d) the representative structure after 100 ns of MD simulation. Residues that are implicated in κ-OR selectivity of JDTic are shown in blue, residues participating in hydrogen bond interactions with JDTic (after the MD calculation) are shown in red, and Asp138 is shown in yellow.

In this consideration, MD appear to be crucial when studying GPCR versatility associated with functioning and ligand recognition. Indeed, for example Shaw and co-workers performed long MD simulations to reveal the pathway and drug binding mechanism in β1 and β2 adrenergic receptors; [197] Heifetz et al. combined homology modeling of orexin receptors with MD to describe the selectivity and binding of several antagonists; [198] Provasi et al. used the prototypic β2 adrenergic

receptor to show that ligands with diverse efficacies induce different GPCR conformations that trigger different biological responses; [199] in two other articles, Provasi et al. proposed the following: (i) activation pathways of the bovine rhodopsin after performing free energy calculations from biased MD [200] and (ii) possible entrance pathways of antagonist naloxone into the binding cavity of δ-OR; [201] Tosh et al. employed in silico fragment screening for adenosine receptor agonists, and they identified several promising derivatives; [202] also, molecular docking calculations have been successfully combined with crystallographic data to describe agonist binding to adenosine receptor; [203] finally, QSAR studies have been used to predict the binding affinity of SalA analogs to κ-OR [204].

Here, we employ a variety of computational approaches to elucidate the mechanism by which JDTic and SalA bind to κ- OR. Our methodology included the following: 1) all-atom, unrestrained MD simulations of JDTic−κ-OR and SalA−κ-OR in explicit water and in lipid bilayers (DPPC), to describe and compare the conformational properties and interactions between the two complexes; 2) MD simulation of apo κ-OR to compare the behavior of the complexes to the unbound receptor. The crystal structure provides information regarding conformations and principal interactions in the κ-OR complex; however, only a static, average description of the system can be offered. Since it has been widely formulated that GPCR structures are rather mobile and alternate between “active” and “inactive” states [182],[205], a thorough approach that describes the evolution of the system is required. Our results reveal the dynamic behavior, structural properties, and the energetic contributions that govern binding. This study is comprehensive description at the molecular level of two drug-bound κ-OR complexes in aqueous and in lipid bilayer media, thus essentially complementing the crystallographic information.

7.2 Methods

7.2.1 Molecular dynamics Simulations

The monomer of κ-OR as obtained from the crystal structure was used for the MD simulations. Initial coordinates for the JDTic complex correspond to the following PDB code: 4DJH. [186] The SalA complex was constructed after removing JDTic and docking SalA into the receptor with DOCK 6. [206] Missing residues

Thr302−Ser303−His304−Ser305−Thr306 have been included to the structure with Modeller 9.10 [51]. After a long minimization with AMBER 11 software package, [207] the structure was evaluated with WHAT_CHECK [208] from WHAT IF Protein Model Check [209]. Crystal water molecules were retained in the structures, and missing hydrogen atoms were added with the tLEaP module of AMBER 11. tLEaP was also used to create the disulfide bond between Cys131 and Cys210. Protonation states and pK a values for histidine residues were predicted with PROPKA [59] under the PDB2PQR (v. 1.8) server [210]. Experimental pK a predictions suggested a diprotonated state for JDTic at pH 7. Asp138 was considered to be negatively charged and deprotonated to interact with positively charged amino groups of JDTic (Figure 7.1a). Atomic partial charges, bond lengths, bond and dihedral angles, force constants, and van der Waals parameters for κ-OR were assigned according to the AMBER ff99SB force field [211]. JDTic and SalA preparation was done as follows: missing hydrogen atoms were added with UCSF Chimera [212]. The ANTECHAMBER module was used to derive the RESP atomic partial charges for each drug, and the general AMBER GAFF force field was employed to obtain the force field parameters [213]. The systems were neutralized in tLEaP with the addition of Cl^- counterions (7 and 5 Cl^- for JDTic and SalA complexes, respectively) and were solvated with approximately 28,000 water molecules. Explicit solvation has been represented by the TIP3P water model [214] in truncated octahedral periodic boundary conditions, with a cutoff distance of 10 Å. Long range electrostatic interactions have been calculated using the particle mesh Ewald (PME) method [181] After minimization, each system was heated over 100 ps under constant volume, with the gradual increase of the temperature from 0 to 310 K. The SHAKE algorithm [215] was applied to constrain bond lengths involving hydrogen atoms to their equilibrium distance, thus enabling the use of 2 fs time step. The Langevin thermostat [216] with a collision frequency of 2.0 ps^{-1} was used to keep an average temperature at 310 K. A restraint of 10 kcal mol^{-1} $Å^{-2}$ was applied to the solute; the restraint was retained for the next 100 ps of constant-pressure equilibration. A last equilibration procedure of 100 ps was realized under constant pressure with the entire system unrestrained. Finally, all-atom, unrestrained MD simulations in the NPT ensemble were continued for 100 ns for each receptor

complex with the PMEMD program under AMBER 11 [207]. The Langevin thermostat, SHAKE, and a 10 Å nonbonded cutoff were applied during the heating, equilibration, and production MD periods. Additionally, a 100 ns MD simulation of apo κ-OR has been performed to compare the behavior of the complexes to the unbound GPCR. Subsequent analysis (RMSD, fluctuations, distances, angles, and HB calculations) was performed on the resulting trajectories with the ptraj module of AMBER. Cutoffs of 3.5 Å for the donor−acceptor distance and of 120° for the donor−hydrogen− acceptor angle have been applied to define HB interactions. Also, a 100 ns MD simulation has been carried out for free JDTic in water. Clustering has been realized with MOIL-View 10.0, [217] based on a hierarchical algorithm. A 1.5 Å RMSD cutoff was introduced to assign 10,000 JDTic conformations (bound to κ-OR) into distinct clusters; for clustering the conformations of unbound JDTic in water, a 2.0 Å RMSD cutoff was applied. Representative conformations (the frame that has the lowest RMSD against the average structure) of JDTic−κ-OR and SalA−κ-OR were used as input structures for simulations in DPPC membranes. Membrane simulations were further continued for another 20 ns with NAMD [126].

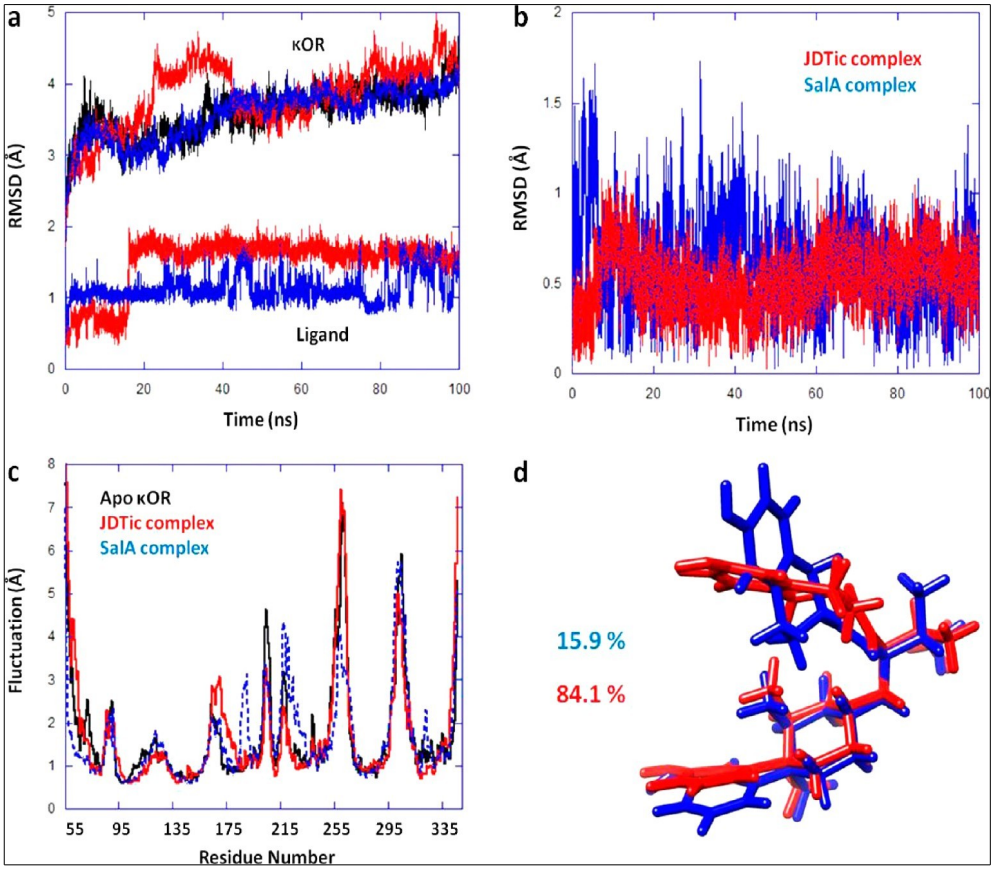


Figure 7.2 : (a) Top: RMSD for Cα atoms of κ-OR residues in JDTic-bound form (red), SalA-bound form (blue), and unbound (apo) form (black). Bottom: RMSD for all atoms of JDTic (red) and SalA (blue) in κ-OR complexes; (b) RMSD for Cα atoms of κ-OR residues participating in hydrogen bonds with JDTic (Asp138, Tyr139, Glu209) and with SalA (Gln115, Leu212, His291); (c) Cα atomic fluctuations of κ-OR residues in its ligand-bound and apo forms; (d) Representative structures of the two dominant JDTic conformations into κ-OR (in water), after clustering analysis. Percentages denote the population of each cluster.

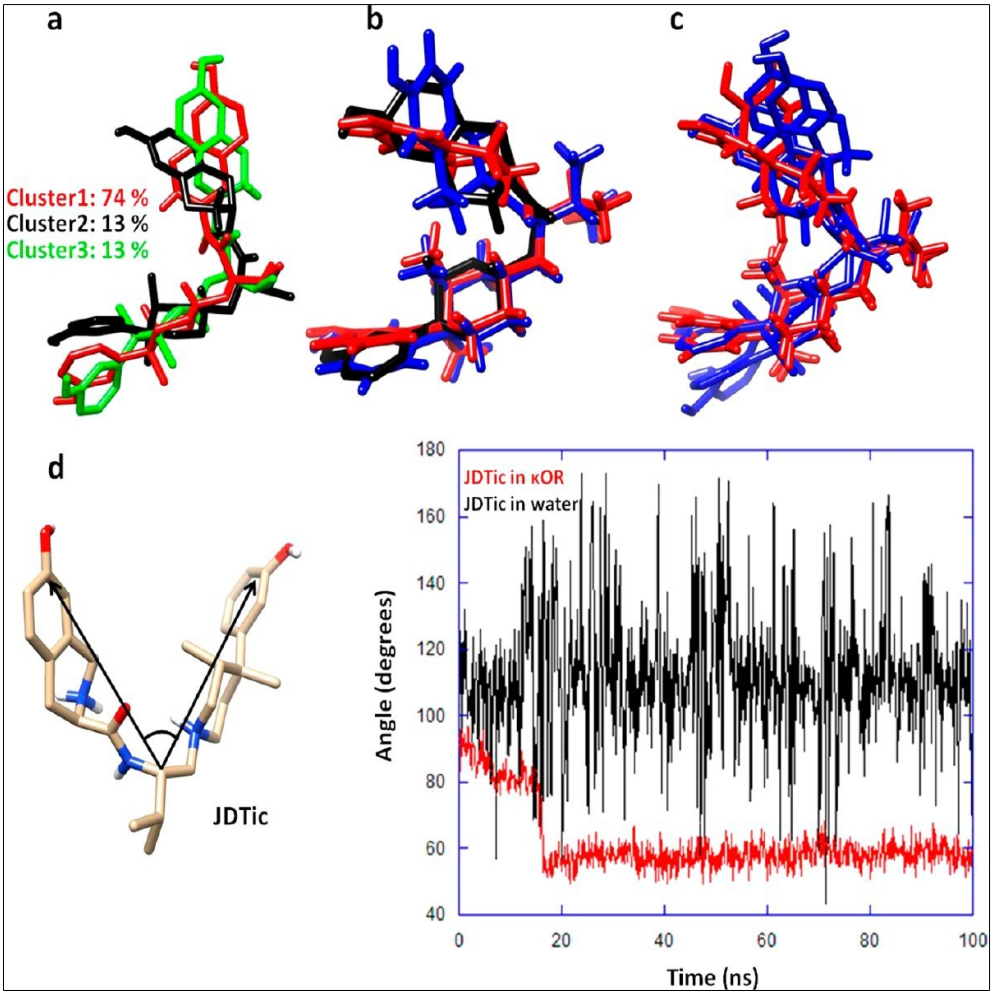


Figure 7.3 : (a) Representative structures of the three dominant JDTic conformations in water, after clustering analysis. Percentages denote the population of each cluster; (b) Comparison of free JDTic (Cluster 2, black) with the JDTic κ-OR−bound structures from Figure 7.2d; (c) Comparison between the three free (blue) and the two bound (red) JDTic structures; (d) Angle variation (left) defines changes in JDTic's shape in water and in κ-OR (right).

7.3 Results and Discussions

In this section, first we investigate the conformational properties of κ-OR upon binding to JDTic and SalA in water and into DPPC lipid bilayer. The MD trajectories were also analyzed to identify hydrogen bond (HB) interactions between the receptor and the ligands.

7.3.1 MD simulations in water

7.3.1.1 Conformational properties of holo and apo κ-OR forms

MD simulations for the JDTic−κ-OR complex and the apo form of the receptor in water were initiated from their crystal structures, while SalA was docked into the receptor site as described in Methods. The simulations eventually yielded relatively stable trajectories regarding GPCR backbone structural changes: Cα-based RMSD calculations with respect to the crystal structure showed that κ-OR structures fluctuate slightly around average values, which range between 3.5 and 4 Å (Figure 7.2a). A noticeable change for the JDTic−κ-OR complex at 18 ns (Figure 7.2a) may be linked to a structural rearrangement of JDTic inside the receptor. As shown in Figure 7.1c and 7.1d, a conformational change of binding site residues induced a proper modification to the shape of the pocket, thus favoring a more closed "V-shape" structure of JDTic. This repositioning of the antagonist may have been due to a rearrangement in HB interactions that stabilize JDTic in the binding site of κ-OR and will be examined in the following paragraphs. After the aforementioned structural change of JDTic, however, the drug remained practically stable throughout the simulation, contrary to SalA, which appeared stable for the first ∼40 ns but increased its flexibility during the second half of the simulation (Figure 7.2a, bottom). The κ-OR structure in both complexes was stable overall; however, regions of the receptor vary in mobility. Cα atomic fluctuation calculations for each residue revealed that intra- cellular (e.g., Phe169, Arg257−Leu259) and extracellular regions (e.g., Asp216−Trp221, Gly300−Thr306) appeared highly flexible (Figure 7.2c). Except for these regions, however, most κ-OR residues presented low fluctuations (in both complexes and in apo form); importantly, all residues that were mentioned above to be crucial toward binding showed particularly low fluctuation values. Clustering calculations for JDTic in κ-OR revealed that the antagonist exists in two (V-shape) major forms. Figure 7.2d displays the two JDTic representative structures, which differ in the position and orientation of the tetrahydroisoquinoline ring. Superposition of the two structures shows that the rings are perpendicular to each other. Interestingly, clustering calculations on a separate JDTic−water 100 ns trajectory revealed the existence of three forms that differ by at least 2 Å RMSD

from each other and showed that ∼13% of the unbound JDTic is in a bent conformation, similar to the one in Figures 1d and 2d (red). The structure comparison is shown in Figure 7.3a and b. For the remaining 87% of the simulation, it was suggested that free JDTic in water adopts more extended (yet V-shape) forms and is significantly more flexible than when bound to κ- OR (Figure 7.3c and d). Indeed, the (average ± standard deviation) values for the angle that defines the shape of JDTic (Figure 7.3d) are 62.14 ± 10.18° and 112.13 ± 19.58° for the drug in κ-OR and in water, respectively. Especially, after the aforementioned structural change at 18 ns, which resulted in a more “closed” conformation for JDTic inside the receptor, the average values for the angle and its variation further diminish (58.05 ± 3.35°, calculations are based on the last 82 ns of the trajectory). The above features of the unbound JDTic may offer enough suppleness to enter the binding pocket and adjust its positioning properly for optimal binding. Indeed, according to Wu et al. [186], upon insertion of JDTic into κ-OR, the drug adopts a V-shape conformation that is characterized by the proximity of its two amino groups. To study further the effect of ligand binding on the structure of the receptor, we also investigated the conformational changes of the binding site region in the apo form of κ-OR and when bound to JDTic or SalA. We selected four pairs of binding site residues that have been implicated in κ-OR interactions with ligands (Gln115−Glu209, Gln115−His291, Glu209−His291, Asp138−His291) and considered the distances between Cα atoms of each pair as proper descriptors of the size/shape of the binding site (Figure 7.4a).

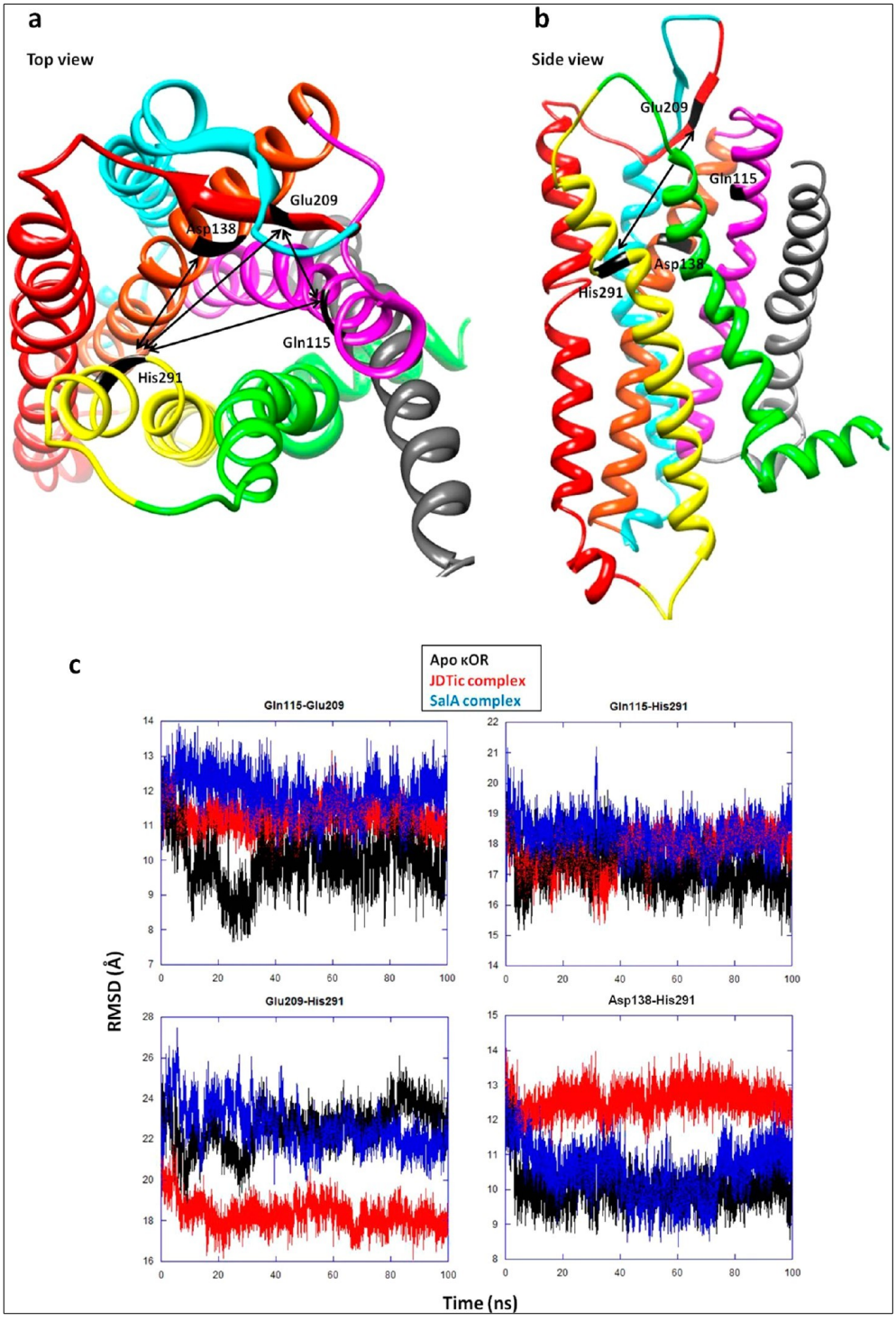


Figure 7.4 : (a) Distances between Cα atoms of selected κ-OR residues (black) that define the shape of the binding site. The seven transmembrane domains are in different colors; (b) Distance between the binding site−covering loop Glu209 (Cα) and His291 (Cα); (c) Distance calculations estimate the size of the binding site in JDTic-bound, SalA-bound, and apo forms of κ-OR.

It was generally suggested that in the apo form of the receptor the binding site is

more confined (Figure 7.4c, black), while upon ligand binding the transmembrane (TM) domains tend to separate more in order to accommodate the substrate (Figure 7.4c, red and blue). Upon binding, JDTic induces greater conformational changes to the binding site than SalA; however, the binding sites of SalA-bound and the apo form of the receptor are more flexible, as shown in Figure 7.4c. The structural change of the binding site region in the presence of JDTic is defined by a Glu209−His291 approach and an Asp138−His291 separation, compared to the apo or SalA-bound forms (Figure 7.4c, bottom). It appears that the region containing Glu209 (Asp204−Phe214) forms a loop that covers the binding site, thus entrapping JDTic into the receptor (Figure 7.4b). The approach of Glu209 and His291 may have facilitated the displacement of the Asp138-containing TM domain (Figure 7.4a, orange) away from His291 to better accommodate JDTic into the receptor.

7.3.1.2 Hydrogen bond interactions

Hydrogen bond analysis on the two κ-OR complexes showed that both ligands are stabilized into the receptor via HBs involving residues Asp138, Glu209, Tyr139 (with JDTic), and Gln115, His291, Leu212 (with SalA). JDTic-related HB interactions are more frequent and involve multiple ligand/receptor sites, compared to SalA interactions (Figure 7.5). Contrary to JDTic, SalA lacks any charged groups or nitrogen atoms; it is therefore expected to display diminished interactions. The HBs between the protonated amines of JDTic (Figure 7.1a) and the side chain of Asp138 totally verified the crystallographic results; [186] moreover, it is noted that the aforementioned structural rearrangement of the binding pocket and the positioning of the drug also facilitated additional HB interactions with Glu209 and Tyr139 (Figure 7.1d). In accordance with the above, the HB between JDTic and Glu209 may be justified by the Glu209−His291 approach (Figure 7.4c), which enabled a proper positioning for the drug to interact with Glu209. Also, it was suggested that a water- mediated HB within JDTic altered the shape of the molecule appropriately to favor additional interactions with the binding site of the receptor (Figure 7.5). Indeed, an intra-JDTic water bridge between the amino groups is formed after ∼18 ns of the simulation, and it coincides with the appearance of the interaction between JDTic and Tyr139 (Figure 7.5), thus well justifying the structural

change of JDTic mentioned above (Figure 7.2a, bottom). Importantly, the water-mediated inter- action within JDTic along with the results of the clustering analysis (Figure 7.3) are also supported by the aforementioned crystallographic study, where the authors denote the significance of a “bent” JDTic structure for its entrance into the binding pocket [186]. The permanent presence of water molecules in the binding site of opioid receptor structures has been also observed in δ-OR complexes, and the role of water in such systems was discussed by Collu et al [218]. RMSD calculations for κ-OR residues that participate in HBs with either JDTic or SalA are reported in Figure 7.2b.

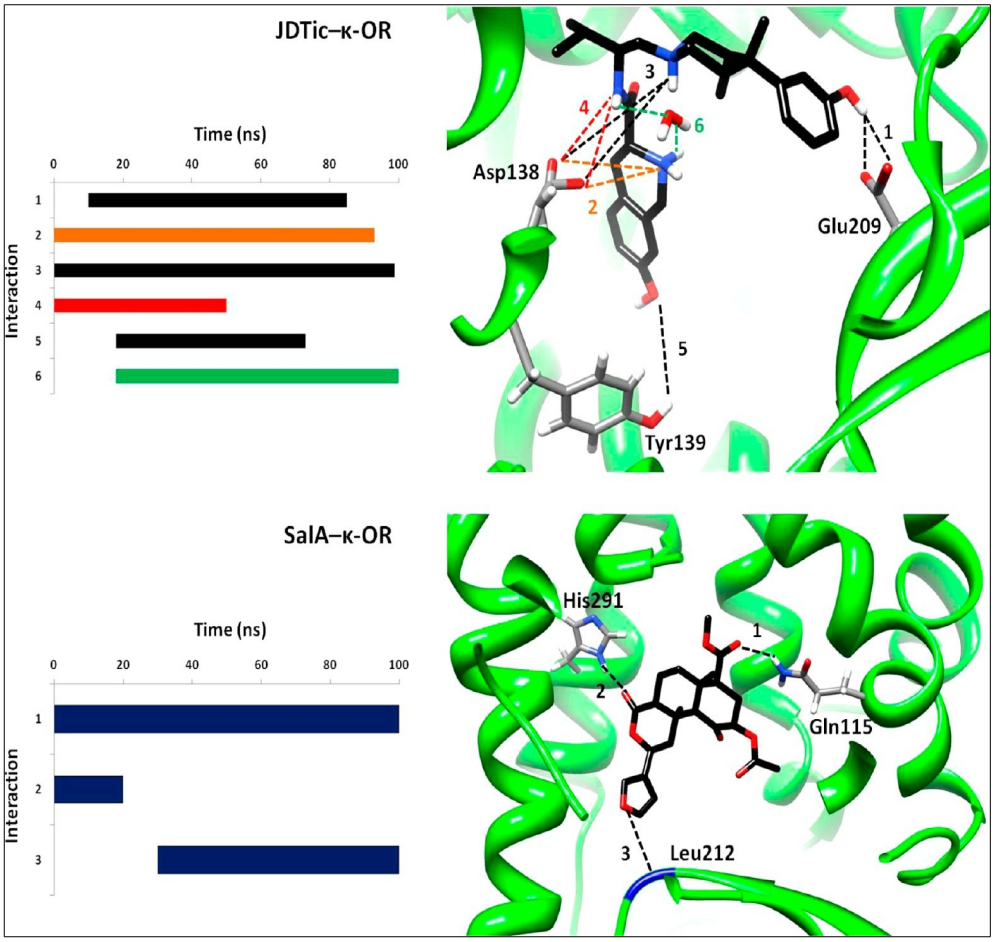


Figure 7.5 : Main hydrogen bond interactions versus time in JDTic−κ-OR and SalA−κ-OR complexes. The numbering on the charts (left) corresponds to the hydrogen bonds shown on the cartoons (right). Chart bars denote the time evolution of HBs and vary in the frequency of HB appearance.

It was observed that residues involved in interactions with SalA are more flexible than residues forming HBs with JDTic. This denotes the capacity of JDTic to

stabilize the structure of the κ-OR binding site more efficiently compared to SalA. More specifically, Glu209 forms an HB (bond 1, Figure 7.5). The water molecule forms an HB bridge between the NH 2+ group of the drug (bond 6, Figure 7.5), and a second one with the backbone carbonyl O of Asp138. Note that this interaction was not observed during the MD calculations; however, the orientation of JDTic toward Asp138 and their proximity indicate that such an HB is possible. Thus, the role of water is further emphasized, as it may facilitate both intra-JDTic and JDTic−receptor interactions. The carboxyl group of Asp138 forms four HBs with JDTic. Two with NH 2+ (bond 2, Figure 7.5, one with the H_{45} bonded to N_{14} (bond 3, Figure 7.5), and the last one with the H_{50} bonded to N_{20} (bond 4, Figure 7.5). This is also true for the contribution of the HB between H_2O and the carboxylate of Asp138. MD calculations showed that these amino acids did not participate in direct HBs with the drug; however, they are considered to be important toward binding, since they are in close proximity to the ligand.

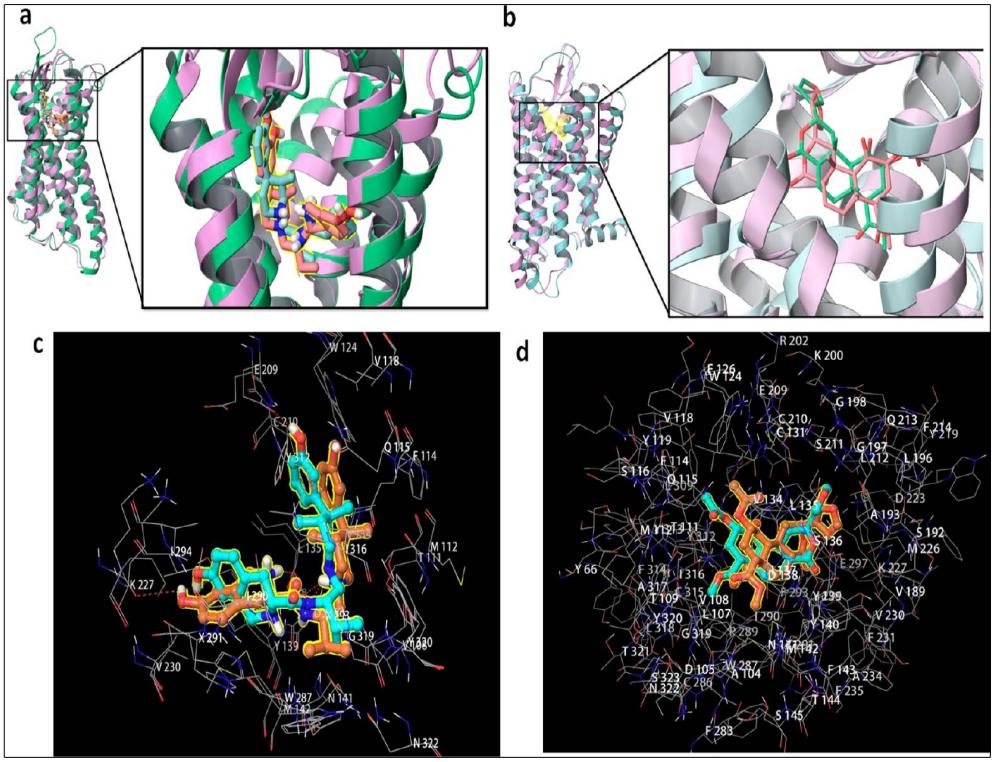


Figure 7.6 : (a) Superimposition of representative structures of receptor−JDTic in water (shown in green ribbons) with receptor−JDTic in lipid bilayer (shown in purple ribbons). RMSD = 2.9 Å; (b) Superimposition of representative structures of receptor−SalA in water (shown in green ribbons) with receptor−SalA in lipid bilayer (shown in purple ribbons). RMSD = 3.2 Å; Superimpositions of ligands (c, JDTic), (d, SalA), and active sites of representative structures.

7.3.2 MD simulations in DPPC lipid bilayer

GPCRs express their functionality in a membrane environment. Therefore, in order to investigate the membrane effect to conformational dynamics of ligands and target, the above systems have been merged into a lipid bilayer (Figures 1b) using the CHARMM-GUI Membrane Builder [219],[220] with the OPM module [221]. Systems' stability throughout the simulations has been verified with all-atom, Cα atoms (Figure 7.7b), HB residues (Figure 7.7c), and ligands (Figure 7.7d) RMSD calculations. While transmembrane (TM) regions were very stable during the simulation (with fluctuations ranging between 0.5 and 1 Å), intracellular and extracellular loops appeared very flexible (up to 3.5 Å, Figure 7.7e).

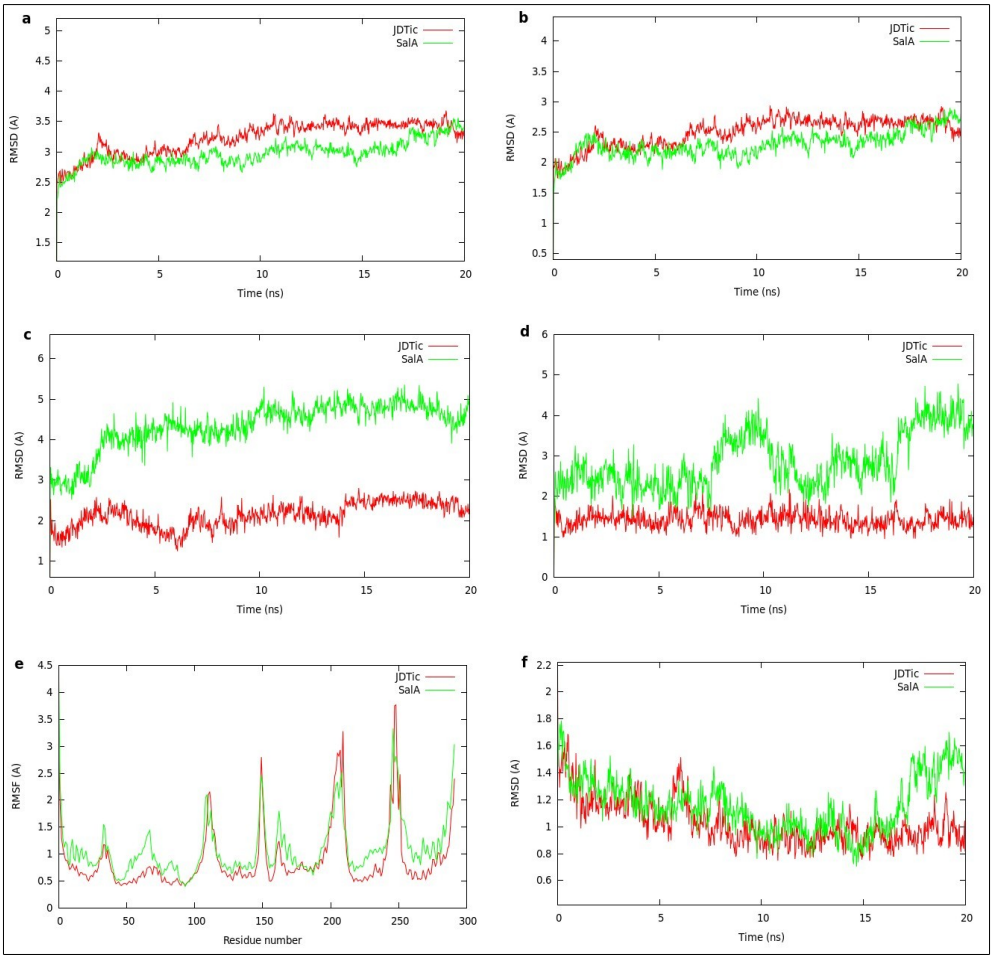


Figure 7.7 : DPPC membrane simulations: (a) All-atom, and (b) Cα RMSD of κOR residues; (c) RMSD of residues that participate in hydrogen bonds with ligands; (d) all-atom RMSD for ligands; (e) Cα RMS Fluctuations for JDTic and SalA complex residues (residue numbering started with 1 in this figure); (f) RMSD of each frame with respect to the average structure.

The RMSD of each frame was screened against the average structure, and the frame with the lowest RMSD was selected as representative structure for the complex (Figure 7.7f). Superimposition of representative structures for the two sets of simulations (in water and in lipid bilayer systems) showed similar conformations for the ligands when bound to κ-OR, either in water or into the bilayer (Figure 7.6). However, a difference was observed between JDTic conformations, where the representative structure in the membrane resembles the least populated cluster in water (Figure 7.2d, blue). Comparison of ligand−receptor interactions between water and lipid environments revealed that the main HBs (observed in water) are conserved upon system insertion into the lipid bilayer.

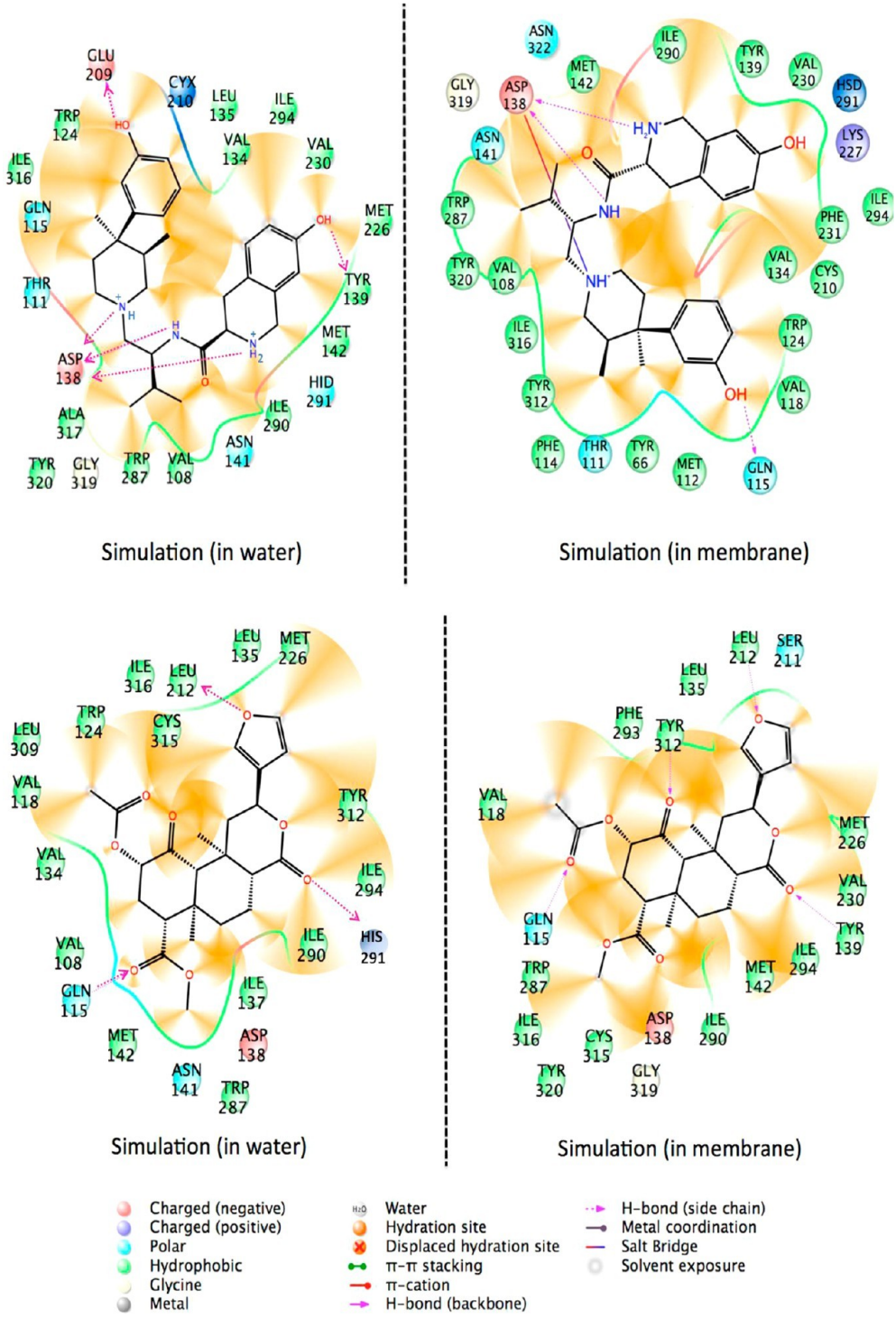


Figure 7.8 : Ligand interaction diagrams of κ-OR−JDTic (top) and of κ-OR−SalA (bottom) in water (left) and in membrane (right).

The reorientation of the tetrahydroisoquinoline ring of JDTic, as expected resulted in abolishment of the HB with Tyr139 (Figure 7.8). On the other hand, two additional

HBs were observed between SalA and κ-OR: interactions with Tyr139 and Tyr312 stabilize further SalA into the binding pocket of the receptor (Figure 7.8). Apart from the amino acids that are involved in HBs with the ligands, the publication by Stevens and co-workers identified κ-OR residues Val108, Val118, Trp287, Ile294, and Tyr312 as particularly important in ligand's selectivity for the receptor, since it was shown that they interact with JDTic uniquely in κ- OR, among other closely related ORs. Our HB analysis did not show any major HBs between these residues and JDTic; however, significant hydrophobic interactions were observed (Figure 7.8). Interestingly, the above residues interact hydro- phobically also with SalA. RMSD values for the five residues suggested that JDTic-bound and apo forms of the receptor undergo similar structural changes, whereas SalA-bound form deviates from this pattern. Such a behavior is anticipated, since agonist−κ-OR complexes are expected to show greater changes than antagonist−κ-OR complexes.

7.4 Conclusion

- Dynamics, interactions, and binding properties of the human κ-opioid receptor (κ-OR) in complexes with antagonist JDTic and agonist Salvinorin A (SalA) have been calculated by means of molecular dynamics approaches. The availability of the JDTic−κ-OR crystal structure enabled us to elucidate the opioid drug binding mechanism and action. The valuable, yet average description offered by the crystal structure conceals important features of such a dynamic system. Here, we explored the dynamic behavior of κ-OR complexes to identify for the first time the properties that govern ligand binding to the receptor. Our analysis led to the following elements regarding the binding mechanism in κ-OR:
- Bound receptor structures (in water and lipid bilayer environments) were significantly stable, except particular extracellular and intracellular regions that appeared expectedly flexible.
- In agreement with the crystal data, HB analysis showed that JDTic is stabilized inside the binding site through multiple HBs that involve mostly Asp138. After 18 ns of the simulation, the binding site of the receptor was eventually rearranged to allow the repositioning of the ligand. This structural

change involved the approach of loops containing Glu209 and His291 and the simultaneous separation of loops containing Asp138 and His291. This resulted in the formation of additional HBs between JDTic and Glu209. Glu209 appears to be crucial toward binding, since it belongs to an extracellular loop that controls the entrance and entrapment of ligands into the binding site of the receptor. SalA also displayed HBs with binding site residues Gln115, His291, and Leu212, but it has more flexibility than JDTic.

- A water molecule mediated an intra-JDTic interaction that induced a “V-shape” to the ligand, with the subsequent formation of an additional HB with Tyr139. The role of water was further emphasized, as it was shown that also forms an HB bridge between JDTic and Asp138.
- JDTic in κ-OR exists in two major “V-shape” forms, which differ in the orientation of the tetrahydroisoquinoline ring, while the drug in water alternates between similar structures and more extended conformations. This feature may offer enough flexibility to the drug in order to enter the binding site and adjust properly for optimal binding.
- MD calculations in membrane complexes showed similar behavior with the systems in water. Moreover, SalA was further stabilized via hydrogen bonds with Tyr139/312, while the Tyr139 interaction was not observed in the representative structure of the JDTic complex.

8. SUGGESTIONS FOR FUTURE WORK

In order to discover novel inhibitors against studied receptors in a less time consuming manner, structure-based virtual screening of large ligand database will be performed for D2R, CCR5 and κ-OR receptors using different docking protocols.

In the thesis, we reported a common pharmacophore model by employing approximately 50 approved D2R inhibitors using 3D-QSAR approach.

This model will be used for fast screening of large ligand database by examining their fitness factor. In order to find novel and high potent anti D2R inhibitors, de-novo drug design approaches will be employed on marketed anti-psychotic drugs, structurally modified via substitution of more than 3000 fragments.

ICL3 of D2R can be remodeled using de-novo loop modeling protocols. The effect of this loop on active side can be better investigated.

Regarding CCR5, a complex of CCR5 with HIV protein can be subjected to long and accelerated MD simulations in order to investigate the inhibition mechanism of CCR5 against HIV in the presence of gp120. In order to prevent gp120 and CCR5 coupling, new peptides will be designed and their potential will be tested using *in-silico* approaches.

REFERENCES

[1] **Audet, M. and Bouvier, M.** (2012) Restructuring G-Protein- Coupled Receptor Activation. *Cell. 151*, 14–2.

[2] **Rasmussen, S.G.F., Choi, H.-J., Fung, J.J., Pardon, E., Casarosa, P., Chae, P.S. et al.** (2011) Structure of a nanobody-stabilized active state of the β(2) adrenoceptor. *Nature*, *469*, 175–80.

[3] **Dror, R.O., Arlow, D.H., Maragakis, P., Mildorf, T.J., Pan, A.C., Xu, H.F. et al.** (2011) Activation mechanism of the beta(2)-adrenergic receptor. *Proceedings of the National Academy of Sciences of the United States of America*, *108*, 18684–9.

[4] **Rosenbaum, D.M., Zhang, C., Lyons, J.A., Holl, R., Aragao, D., Arlow, D.H. et al.** (2011) Structure and function of an irreversible agonist-β(2) adrenoceptor complex. *Nature*, *469*, 236–40.

[5] **Xu, F., Wu, H., Katritch, V., Han, G.W., Jacobson, K.A., Gao, Z.-G. et al.** (2011) Structure of an agonist-bound human A2A adenosine receptor. *Science*, *332*, 322–7.

[6] **Constantinos Potamitis, Zervou, M., Katsiaras, V., Zoumpoulakis, P., Durdagi, S., Papadopoulos, M.G. et al.** (2009) Antihypertensive drug valsartan in solution and at the AT1 receptor: Conformational analysis, dynamic NMR spectroscopy, in silico docking, and molecular dynamics simulations. *Journal of Chemical Information and Modeling*, *49*, 726–39.

[7] **Durdagi, S., Papadopoulos, M.G., Papahatjis, D.P. and Mavromoustakos, T.** (2007) Combined 3D QSAR and molecular docking studies to reveal novel cannabinoid ligands with optimum binding activity. *Bioorganic and Medicinal Chemistry Letters*, *17*, 6754–63.

[8] **Durdagi, S., Reis, H., Papadopoulos, M.G. and Mavromoustakos, T.** (2008) Comparative molecular dynamics simulations of the potent synthetic classical cannabinoid ligand AMG3 in solution and at binding site of the CB1 and CB2 receptors. *Bioorganic and Medicinal Chemistry, 16*, 7377–87.

[9] **Zervou, M., Cournia, Z., Potamitis, C., Patargias, G., Durdagi, S., Grdadolnik, S.G. et al.** (2014) Insights into the molecular basis of action of the AT1 antagonist losartan using a combined NMR spectroscopy and computational approach. *Biochimica et Biophysica Acta - Biomembranes, 1838*, 1031–46.

[10] **Mavromoustakos, T., Agelis, G. and Durdagi, S.** (2013) AT1 antagonists: a patent review (2008 - 2012). *Expert Opinion on Therapeutic Patents*, *23*,

1483–94.

[11] **Li, Y.Y., Hou, T.J. and Goddard, W.A.** (2010) Computational modeling of structure-function of g protein-coupled receptors with applications for drug design. *Current Medicinal Chemistry*, *17*, 1167–80.

[12] **Bruno, A., Costantino, G., de Fabritiis, G., Pastor, M. and Selent, J.** (2012) Membrane-sensitive conformational states of helix 8 in the metabotropic Glu2 receptor, a class C GPCR. *PLoS ONE*, 7.

[13] **Tuccinardi, T., Ferrarini, P.L., Manera, C., Ortore, G., Saccomanni, G. and Martinelli, A.** (2006) Cannabinoid CB2/CB1 selectivity. Receptor modeling and automated docking analysis. *Journal of Medicinal Chemistry*, *49*, 984–94.

[14] **Park, J.H., Scheerer, P., Hofmann, K.P., Choe, H.-W. and Ernst, O.P.** (2008) Crystal structure of the ligand-free G-protein-coupled receptor opsin. *Nature*, *454*, 183–7.

[15] **Azzi, M., Charest, P.G., Angers, S., Rousseau, G., Kohout, T., Bouvier, M. et al.** (2003) Beta-arrestin-mediated activation of MAPK by inverse agonists reveals distinct active conformations for G protein-coupled receptors. *Proceedings of the National Academy of Sciences of the United States of America*, 100, 11406–11.

[16] **Jójárt, B., Kiss, R., Viskolcz, B. and Keseru, G.M.** (2008) Activation mechanism of the human histamine H4 receptor--an explicit membrane molecular dynamics simulation study. *Journal of Chemical Information and Modeling*, *48*, 1199–210.

[17] **Bortolato, A., Mobarec, J.C., Provasi, D. and Filizola, M.** (2009) Progress in elucidating the structural and dynamic character of G Protein-Coupled Receptor oligomers for use in drug discovery. *Current Pharmaceutical Design*, *15*, 4017–25.

[18] **Vanni, S. and Rothlisberger, U.** (2012) A Closer Look into G Protein Coupled Receptor Activation: X-Ray Crystallography and Long-Scale Molecular Dynamics Simulations. *Curr. Med. Chem*. 1135–45.

[19] **Kontoyianni, M. and Liu, Z.** (2012) Structure-Based Design in the GPCR Target Space. *Curr. Med. Chem*. 544–56.

[20] **Filmore, D.** (2004) It's a GPCR world. *Modern Drug Discovery, 7*, 24–7.

[21] **Alder, B. J. and Wainwright, T. E. J**. (1957) Phase Transition for a Hard Sphere System *Chem. Phys*. *27*, 1208.

[22] **Alder, B. J. and Wainwright, T. E. J.** (1959) Studies in molecular dynamics. I. General method. *Chem. Phys*. *31*, 459.

[23] **Stillinger, F. H. and Rahman, A. J.** (1974) Improved Simulation of Liquid Water by Molecular Dynamics, *Chem. Phys. 60*, 1545.

[24] **McCammon, J. A., Gelin, B. R., and Karplus, M**. (1977), Dynamics of folded proteins, *Nature*, 267, 585

[25] **D. McQuarrie, Statistical Mechanics** (1976), New York, Harper & Row,

[26] **D. Chandler, Introduction to Modern Statistical Mechanics** (1987), New York, Oxford University Press.

[27] **Sherman, W., Beard, H. S., & Farid, R.** (2006). Use of an induced fit receptor structure in virtual screening. *Chemical Biology and Drug Design, 67*, 83-4.

[28] **Ramachandran, G. N., & Sasisekharan, V**. (1968). Conformation of polypeptides and proteins. *Advances in Protein Chemistry*, *23*, 283–438.

[29] **Römpler, H., Stäubert, C., Thor, D., Schulz, A., Hofreiter, M. and Schöneberg, T.** (2007) G protein-coupled time travel: evolutionary aspects of GPCR research. *Molecular Interventions*, *7*, 17–25.

[30] **Congreve, M. and Marshall, F.** (2010) The impact of GPCR structures on pharmacology and structure-based drug design. Br. *J. Pharmacol.* 986–96.

[31] **Overington, J.P., Al-Lazikani, B. and Hopkins, A.L.** (2006) How many drug targets are there? *Nat Rev Drug Discov*, *5*, 993–6.

[32] **Kobilka, B.K. and Deupi, X.** (2007) Conformational complexity of G-protein-coupled receptors. *Trends Pharmacol. Sci*. 397–406.

[33] **Rosenbaum, D.M., Rasmussen, S.G.F. and Kobilka, B.K.** (2009) The structure and function of G-protein-coupled receptors. *Nature*, *459*, 356–63.

[34] **Lagerström, M.C. and Schiöth, H.B.** (2008) Structural diversity of G protein-coupled receptors and significance for drug discovery. *Nature Reviews Drug Discovery*, *7*, 339–57.

[35] **Rasmussen, S.G.F., DeVree, B.T., Zou, Y., Kruse, A.C., Chung, K.Y., Kobilka, T.S. et al.** (2011) Crystal structure of the β2 adrenergic receptor–Gs protein complex. *Nature*. 549–55.

[36] **Lebon, G., Warne, T., Edwards, P.C., Bennett, K., Langmead, C.J., Leslie, A.G.W. et al.** (2011) Agonist-bound adenosine A2A receptor structures reveal common features of GPCR activation. *Nature*, *474*, 521–5.

[37] **Kruse, A.C., Ring, A.M., Manglik, A., Hu, J., Hu, K., Eitel, K. et al.** (2013) Activation and allosteric modulation of a muscarinic acetylcholine receptor. *Nature*, *504*, 101–6.

[38] **Scheerer, P., Park, J.H., Hildebrand, P.W., Kim, Y.J., Krauss, N., Choe, H.-W. et al.** (2008) Crystal structure of opsin in its G-protein-interacting conformation. *Nature*, *455*, 497–502.

[39] **Jackson, D.M. and Westlind-Danielsson, A.** (1994) Dopamine receptors: molecular biology, biochemistry and behavioural aspects. *Pharmacology & Therapeutics*, *64*, 291–370.

[40] **Missale, C., Nash, S.R., Robinson, S.W., Jaber, M. and Caron, M.G.** (1998) Dopamine receptors: from structure to function. *Physiological Reviews*, *78*, 189–225.

[41] **Seeman, P., Lee, T., Chau-Wong, M. and Wong, K.** (1976) Antipsychotic drug doses and neuroleptic/dopamine receptors. *Nature*, *261*, 717–9.

[42] **Creese, I., Burt, D.R. and Snyder, S.H.** (1996) Dopamine receptor binding predicts clinical and pharmacological potencies of antischizophrenic drugs. *The Journal of Neuropsychiatry and Clinical Neurosciences*, *8*, 223–6.

[43] **Greengard, P.** (2001) The neurobiology of dopamine signaling. *Bioscience Reports*, 247–69.

[44] **Oerther, S. and Ahlenius, S.** (2000) Atypical antipsychotics and dopamine D(1) receptor agonism: an in vivo experimental study using core temperature measurements in the rat. *The Journal of Pharmacology and Experimental Therapeutics*, *292*, 731–6.

[45] **Kulagowski JJ, Broughton HB, Curtis NR, Mawer IM, Ridgill MP, Baker R, Emms F, Freedman SB, Marwood R, Patel S, Patel S, Ragan CI, Leeson PD**. (1996) 3-[[4-(4-Chlorophenyl)piperazin-1-yl]- methyl]-1H-pyrrolo[2,3-b]pyridine: An Antagonist with High Affinity and Selectivity for the Human Dopamine D 4 Receptor. *J Med Chem*, *39*, 1941–1942.

[46] **Rauser, L., Savage, J.E., Meltzer, H.Y. and Roth, B.L.** (2001) Inverse agonist actions of typical and atypical antipsychotic drugs at the human 5-hydroxytryptamine(2C) receptor. *The Journal of Pharmacology and Experimental Therapeutics*, *299*, 83–9.

[47] **Chien, E.Y.T., Liu, W., Zhao, Q., Katritch, V., Han, G.W., Hanson, M.A. et al.** (2010) Structure of the human dopamine D3 receptor in complex with a D2/D3 selective antagonist. *Science*, *330*, 1091–5.

[48] **Kong, Y. and Karplus, M.** (2007) The Signaling Pathway of Rhodopsin. *Structure*, *15*, 611–23.

[49] **EMBL, SIB Swiss Institute of Bioinformatics and Protein Information Resource (PIR).** (2013) UniProt. *Nucleic Acids Research*, *41*, D43–7.

[50] **Altschul, S.F., Madden, T.L., Schäffer, A.A., Zhang, J., Zhang, Z., Miller, W. et al.** (1997) Gapped BLAST and PSI-BLAST: A new generation of protein database search programs. *Nucleic Acids Res*. 3389–402.

[51] **Sali, A. and Blundell, T.L.** (1993) Comparative protein modelling by satisfaction of spatial restraints. *Journal of Molecular Biology*, *234*, 779–815.

[52] **Thompson, J.D., Higgins, D.G. and Gibson, T.J.** (1994) CLUSTAL W: improving the sensitivity of progressive multiple sequence alignment through sequence weighting, position-specific gap penalties and weight matrix choice. *Nucleic Acids Research*, *22*, 4673–80.

[53] **Jacobson, M.P., Pincus, D.L., Rapp, C.S., Day, T.J.F., Honig, B., Shaw, D.E. et al.** (2004) A Hierarchical Approach to All-Atom Protein Loop Prediction. *Proteins: Structure, Function and Genetics*, *55*, 351–67.

[54] **Mandell DJ, Coutsias EA, Kortemme T**. (2009) Sub-angstrom accuracy in protein loop reconstruction by robotics-inspired conformational sampling.

Nat Methods, *6*, 551-552.

[55] **Kim, D.E., Chivian, D. and Baker, D.** (2004) Protein structure prediction and analysis using the Robetta server. *Nucleic Acids Research*, *32*, W526–31.

[56] **Laskowski, R.A., Rullmannn, J.A., MacArthur, M.W., Kaptein, R. and Thornton, J.M.** (1996) AQUA and PROCHECK-NMR: programs for checking the quality of protein structures solved by NMR. *Journal of Biomolecular NMR*, *8*, 477–86.

[57] **Madhavi Sastry, G., Adzhigirey, M., Day, T., Annabhimoju, R. and Sherman, W.** (2013) Protein and ligand preparation: Parameters, protocols, and influence on virtual screening enrichments. *Journal of Computer-Aided Molecular Design*, *27*, 221–34.

[58] **Jorgensen, W.L. and Tirado-Rives, J.** (1988) The OPLS Potential Functions for Proteins. Energy Minimizations for Crystals of Cyclic Peptides and Crambin. *Journal of the American Chemical Society*, *110*, 1657–66.

[59] **Li, H., Robertson, A.D. and Jensen, J.H.** (2005) Very fast empirical prediction and rationalization of protein pK a values. *Proteins: Structure, Function and Genetics*, *61*, 704–21.

[60] **Go, N., Noguti, T. and Nishikawa, T.** (1983) Dynamics of a small globular protein in terms of low-frequency vibrational modes. *Proceedings of the National Academy of Sciences of the United States of America*, *80*, 3696–700.

[61] **Brooks, B., Brooks, B., Karplus, M. and Karplus, M.** (1983) Harmonic dynamics of proteins: normal modes and fluctuations in bovine pancreatic trypsin inhibitor. *Proc Natl Acad Sci U S A*, *80*, 6571–5.

[62] **Hinsen, K., Petrescu, A.J., Dellerue, S., Bellissent-Funel, M.C. and Kneller, G.R.** (2000) Harmonicity in slow protein dynamics. *Chemical Physics*, *261*, 25–37.

[63] **Grant, B.J., Rodrigues, A.P.C., ElSawy, K.M., McCammon, J.A. and Caves, L.S.D.** (2006) Bio3d: an R package for the comparative analysis of protein structures. *Bioinformatics (Oxford, England)*, *22*, 2695–6.

[64] **Irwin, J.J. and Shoichet, B.K.** (2005) ZINC - A free database of commercially available compounds for virtual screening. *Journal of Chemical Information and Modeling*, *45*, 177–82.

[65] **Chen, I.J. and Foloppe, N.** (2010) Drug-like bioactive structures and conformational coverage with the ligprep/confgen suite: Comparison to programs MOE and catalyst. *Journal of Chemical Information and Modeling*, *50*, 822–39.

[66] **Tubert-Brohman, I., Sherman, W., Repasky, M. and Beuming, T.** (2013) Improved docking of polypeptides with glide. *Journal of Chemical Information and Modeling*, *53*, 1689–99.

[67] **Kaminski, G.A., Friesner, R.A., Tirado-Rives, J. and Jorgensen, W.L.** (2001) Evaluation and reparametrization of the OPLS-AA force field for

proteins via comparison with accurate quantum chemical calculations on peptides. *Journal of Physical Chemistry B*, *105*, 6474–87.

[68] **Sherman, W., Day, T., Jacobson, M.P., Friesner, R.A. and Farid, R.** (2006) Novel procedure for modeling ligand/receptor induced fit effects. *Journal of Medicinal Chemistry*, *49*, 534–53.

[69] **Wang, R., Lai, L. and Wang, S.** (2002) Further development and validation of empirical scoring functions for structure-based binding affinity prediction. *Journal of Computer-Aided Molecular Design*, *16*, 11–26.

[70] **Friesner, R.A., Banks, J.L., Murphy, R.B., Halgren, T.A., Klicic, J.J., Mainz, D.T. et al.** (2004) Glide: A New Approach for Rapid, Accurate Docking and Scoring. 1. Method and Assessment of Docking Accuracy. *Journal of Medicinal Chemistry*, *47*, 1739–49.

[71] **Friesner, R.A., Murphy, R.B., Repasky, M.P., Frye, L.L., Greenwood, J.R., Halgren, T.A. et al.** (2006) Extra precision glide: Docking and scoring incorporating a model of hydrophobic enclosure for protein-ligand complexes. *Journal of Medicinal Chemistry*, *49*, 6177–96.

[72] **Dixon, S.L., Smondyrev, A.M., Knoll, E.H., Rao, S.N., Shaw, D.E. and Friesner, R.A.** (2006) PHASE: A new engine for pharmacophore perception, 3D QSAR model development, and 3D database screening: 1. Methodology and preliminary results. *Journal of Computer-Aided Molecular Design*, *20*, 647–71.

[73] **Hanson, M.A., Cherezov, V., Griffith, M.T., Roth, C.B., Jaakola, V.P., Chien, E.Y.T. et al.** (2008) A specific cholesterol binding site is established by the 2.8 angstrom structure of the human beta(2)-adrenergic receptor. *Structure*, *16*, 897–905

[74] **Fu, W., Shen, J., Luo, X., Zhu, W., Cheng, J., Yu, K. et al.** (2007) Dopamine D1 receptor agonist and D2 receptor antagonist effects of the natural product (-)-stepholidine: molecular modeling and dynamics simulations. *Biophysical Journal*, *93*, 1431–41.

[75] **Del Carmine, R., Molinari, P., Sbraccia, M., Ambrosio, C. and Costa, T.** (2004) “Induced-fit” mechanism for catecholamine binding to the beta2-adrenergic receptor. *Molecular Pharmacology*, 66, 356–63.

[76] **Liapakis, G., Chan, W.C., Papadokostaki, M. and Javitch, J.A.** (2004) Synergistic contributions of the functional groups of epinephrine to its affinity and efficacy at the beta2 adrenergic receptor. *Molecular Pharmacology*, *65*, 1181–90.

[77] **Malo, M., Brive, L., Luthman, K. and Svensson, P.** (2012) Investigation of D 2 Receptor-Agonist Interactions Using a Combination of Pharmacophore and Receptor Homology Modeling. *ChemMedChem*, *7*, 471–82.

[78] **McRobb, F.M., Capuano, B., Crosby, I.T., Chalmers, D.K. and Yuriev, E.** (2010) Homology modeling and docking evaluation of aminergic g protein-coupled receptors. *Journal of Chemical Information and Modeling*, *50*, 626–37.

[79] **Shi, L. and Javitch, J.A.** (2002) The binding site of aminergic G protein-coupled receptors: the transmembrane segments and second extracellular loop. *Annual Review of Pharmacology and Toxicology*, *42*, 437–67.

[80] **Reyaz-Ahmed, A. and Zhang, Y.-Q.Z.Y.-Q.** (2007) Protein Secondary Structure Prediction Using Genetic Neural Support Vector Machines. *2007 IEEE 7th International Symposium on BioInformatics and BioEngineering*,.

[81] **Kalani, M.Y.S., Vaidehi, N., Hall, S.E., Trabanino, R.J., Freddolino, P.L., Kalani, M.A. et al.** (2004) The predicted 3D structure of the human D2 dopamine receptor and the binding site and binding affinities for agonists and antagonists. *Proceedings of the National Academy of Sciences of the United States of America*, *101*, 3815–20.

[82] **Homan, E.J., Wikstrom, H. V and Grol, C.J.** (1999) Molecular modeling of the dopamine D2 and serotonin 5-HT1A receptor binding modes of the enantiomers of 5-OMe-BPAT. *Bioorg Med Chem*, *7*, 1805–20.

[83] **Javitch, J.A., Fu, D., Chen, J. and Karlin, A.** (1995) Mapping the binding-site crevice of the dopamine D2 receptor by the substituted-cysteine accessibility method. *Neuron*, *14*, 825–31.

[84] **Wang, C.D., Gallaher, T.K. and Shih, J.C.** (1993) Site-directed mutagenesis of the serotonin 5-hydroxytrypamine2 receptor: identification of amino acids necessary for ligand binding and receptor activation. *Molecular Pharmacology*, *43*, 931–40.

[85] **Shi, L. and Javitch, J.A.** (2004) The second extracellular loop of the dopamine D2 receptor lines the binding-site crevice. *Proceedings of the National Academy of Sciences of the United States of America*, *101*, 440–5.

[86] **Shi, L., Simpson, M.M., Ballesteros, J.A. and Javitch, J.A.** (2001) The first transmembrane segment of the dopamine D2 receptor: Accessibility in the binding-site crevice and position in the transmembrane bundle. *Biochemistry*, *40*, 12339–48.

[87] **Guo, W., Shi, L. and Javitch, J.A.** (2003) The fourth transmembrane segment forms the interface of the dopamine D2 receptor homodimer. *Journal of Biological Chemistry*, *278*, 4385–8.

[88] **Javitch, J.A., Ballesteros, J.A., Chen, J., Chiappa, V. and Simpson, M.M.** (1999) Electrostatic and aromatic microdomains within the binding-site crevice of the D2 receptor: Contributions of the second membrane-spanning segment. *Biochemistry*, *38*, 7961–8.

[89] **Fu D, Ballesteros J a, Weinstein H, Chen J, Javitch** J a. (1996) Residues in the seventh membrane-spanning segment of the dopamine D2 receptor accessible in the binding-site crevice. *Biochemistry*, *35*, 11278–11285.

[90] **Javitch, J.A., Fu, D. and Chen, J.** (1995) Residues in the fifth membrane-spanning segment of the dopamine D2 receptor exposed in the binding-site crevice. *Biochemistry*, *34*, 16433–9.

[91] **Javitch, J.A., Ballesteros, J.A., Weinstein, H. and Chen, J.** (1998) A cluster of

aromatic residues in the sixth membrane-spanning segment of the dopamine D2 receptor is accessible in the binding-site crevice. *Biochemistry*, *37*, 998–1006.

[92] **Mansour, A., Meng, F., Meador-Woodruff, J.H., Taylor, L.P., Civelli, O. and Akil, H.** (1992) Site-directed mutagenesis of the human dopamine D2 receptor. *European Journal of Pharmacology*, *227*, 205–14.

[93] **Cox, B.A., Henningsen, R.A., Spanoyannis, A., Neve, R.L. and Neve, K.A.** (1992) Contributions of conserved serine residues to the interactions of ligands with dopamine D2 receptors. *Journal of Neurochemistry*, 59, 627–35.

[94] **Cho, W., Taylor, L.P., Mansour, A. and Akil, H.** (1995) Hydrophobic residues of the D2 dopamine receptor are important for binding and signal transduction. *Journal of Neurochemistry*, *65*, 2105–15.

[95] **Coley, C., Woodward, R., Johansson, A.M., Strange, P.G. and Naylor, L.H.** (2000) Effect of multiple serine/alanine mutations in the transmembrane spanning region V of the D2 dopamine receptor on ligand binding. *Journal of Neurochemistry*, *74*, 358–66.

[96] **Pease, J.E. and Horuk, R.** (2009) Chemokine receptor antagonists: Part 1. *Expert Opinion on Therapeutic Patents*, *19*, 39–58.

[97] **Pease, J.E. and Horuk, R.** (2009) Chemokine receptor antagonists: part 2. *Expert Opinion on Therapeutic Patents*, *19*, 199–221.

[98] **Qin, K., Dong, C., Wu, G. and Lambert, N.A.** (2011) Inactive-state preassembly of Gq-coupled receptors and Gq heterotrimers. *Nat. Chem. Biol*, 740–7.

[99] **Murphy, P.M.** (2002) International Union of Pharmacology. Update on chemokine receptor nomenclature. *Pharmacological Reviews*, *54*, 227–9.

[100] **Gerard, C. and Rollins, B.J.** (2001) Chemokines and disease. *Nature Immunology*, *2*, 108–15.

[101] **Lazennec, G. and Richmond, A.** (2010) Chemokines and chemokine receptors: new insights into cancer-related inflammation. *Trends Mol. Med*, 133–44.

[102] **Viola, A. and Luster, A.D.** (2008) Chemokines and their receptors: drug targets in immunity and inflammation. *Annual Review of Pharmacology and Toxicology*, *48*, 171–97.

[103] **de Voux, A., Chan, M.C., Folefoc, A.T., Madziva, M.T. and Flanagan, C.A.** (2013) Constitutively Active CCR5 Chemokine Receptors Differ in Mediating HIV Envelope-dependent Fusion. *PLoS ONE*, 8.

[104] **Kondru, R., Zhang, J., Ji, C., Mirzadegan, T., Rotstein, D., Sankuratri, S. et al.** (2008) Molecular interactions of CCR5 with major classes of small-molecule anti-HIV CCR5 antagonists. *Molecular Pharmacology*, *73*, 789–800.

[105] **Baba, M., Nishimura, O., Kanzaki, N., Okamoto, M., Sawada, H., Iizawa, Y. et al.** (1999) A small-molecule, nonpeptide CCR5 antagonist with highly potent and selective anti-HIV-1 activity. *Proceedings of the National*

Academy of Sciences of the United States of America, *96*, 5698–703.

[106] **Barré-Sinoussi, F., Chermann, J.C., Rey, F., Nugeyre, M.T., Chamaret, S., Gruest, J. et al.** (1983) Isolation of a T-lymphotropic retrovirus from a patient at risk for acquired immune deficiency syndrome (AIDS). *Science (New York, NY)*, *220*, 868–71.

[107] **Murakami, M. and Kouyama, T.** (2008) Crystal structure of squid rhodopsin. *Nature*, *453*, 363–7.

[108] **Wu, B., Chien, E.Y.T., Mol, C.D., Fenalti, G., Liu, W., Katritch, V. et al.** (2010) Structures of the CXCR4 chemokine GPCR with small-molecule and cyclic peptide antagonists. *Science (New York, NY)*, *330*, 1066–71.

[109] **Cherezov, V., Rosenbaum, D.M., Hanson, M.A., Rasmussen, S.G.F., Thian, F.S., Kobilka, T.S. et al.** (2007) High-resolution crystal structure of an engineered human beta2-adrenergic G protein-coupled receptor. *Science*, *318*, 1258–65.

[110] **Rasmussen, S.G.F., Choi, H.-J., Rosenbaum, D.M., Kobilka, T.S., Thian, F.S., Edwards, P.C. et al**. (2007) Crystal structure of the human beta2 adrenergic G-protein-coupled receptor. *Nature*, *450*, 383–7.

[111] **Choe, H.-W., Kim, Y.J., Park, J.H., Morizumi, T., Pai, E.F., Krauss, N. et al.** (2011) Crystal structure of metarhodopsin II. *Nature*, *471*, 651–5.

[112] **Tan, Q., Zhu, Y., Li, J., Chen, Z., Han, G.W., Kufareva, I. et al**. (2013) Structure of the CCR5 chemokine receptor-HIV entry inhibitor maraviroc complex. *Science*, *341*, 1387–90.

[113] **Weissman, D., Rabin, R.L., Arthos, J., Rubbert, A., Dybul, M., Swofford, R. et al**. (1997) Macrophage-tropic HIV and SIV envelope proteins induce a signal through the CCR5 chemokine receptor. *Nature*, *389*, 981–5.

[114] **Alkhatib, G., Combadiere, C., Broder, C.C., Feng, Y., Kennedy, P.E., Murphy, P.M. et al**. (1996) CC CKR5: a RANTES, MIP-1alpha, MIP-1beta receptor as a fusion cofactor for macrophage-tropic HIV-1. *Science*, *272*, 1955–8.

[115] **Gao, P., Zhou, X.-Y., Yashiro-Ohtani, Y., Yang, Y.-F., Sugimoto, N., Ono, S. et al.** (2003) The unique target specificity of a nonpeptide chemokine receptor antagonist: selective blockade of two Th1 chemokine receptors CCR5 and CXCR3. *Journal of Leukocyte Biology*, *73*, 273–80.

[116] **Napier, K.B., Wang, Z.X., Peiper, S.C. and Trent, J.O.** (2007) CCR5 interactions with the variable 3 loop of gp120. *Journal of Molecular Modeling*, *13*, 29–41.

[117] **Kothandan, G., Gadhe, C.G. and Cho, S.J**. (2012) Structural insights from binding poses of CCR2 and CCR5 with clinically important antagonists: A combined in silico study. *PLoS* ONE, **7**.

[118] **Gadhe, C.G., Kothandan, G. and Cho, S.J.** (2013) Computational modeling of human coreceptor CCR5 antagonist as a HIV-1 entry inhibitor: using an integrated homology modeling, docking, and membrane molecular

dynamics simulation analysis approach. *Journal of Biomolecular Structure & Dynamics*, *31*, 1251–76.

[119] **Kondru, R., Zhang, J., Ji, C., Mirzadegan, T., Rotstein, D., Sankuratri, S. et al**. (2008) Molecular interactions of CCR5 with major classes of small-molecule anti-HIV CCR5 antagonists. *Molecular Pharmacology*, *73*, 789–800.

[120] **Tamamis, P. and Floudas, C.A**. (2014) Molecular recognition of CCR5 by an HIV-1 gp120 V3 loop. *PLoS ONE*, 9.

[121] **Eswar, N., Webb, B., Marti-Renom, M.A., Madhusudhan, M.S., Eramian, D., Shen, M.-Y. et al**. (2007) Comparative protein structure modeling using MODELLER. *Curr Protoc Protein Sci*, 0209.

[122] **Madhavi Sastry, G., Adzhigirey, M., Day, T., Annabhimoju, R. and Sherman, W.** (2013) Protein and ligand preparation: Parameters, protocols, and influence on virtual screening enrichments. *Journal of Computer-Aided Molecular Design*, *27*, 221–34.

[123] **Lomize, M.A., Lomize, A.L., Pogozheva, I.D. and Mosberg, H.I.** (2006) OPM: Orientations of proteins in membranes database. *Bioinformatics*, *22*, 623–5.

[124] **Humphrey, W., Dalke, A. and Schulten, K.** (1996) VMD-Visual Molecular Dynamics. *Journal of Molecular Graphics*, *14*, 33–8.

[125] **Jorgensen, W.L., Chandrasekhar, J., Madura, J.D., Impey, R.W. and Klein, M.L.** (1983) Comparison of simple potential functions for simulating liquid water. *J. Chem*. Phys, 926.

[126] **Nelson, M.T., Humphrey, W., Gursoy, A., Dalke, A., Kale, L. V., Skeel, R.D. et al.** (1996) NAMD: a Parallel, Object-Oriented Molecular Dynamics Program. Int. J. High Perform. *Comput. Appl*, 251–68.

[127] **Huang, J. and Mackerell, A.D.** (2013) CHARMM36 all-atom additive protein force field: Validation based on comparison to NMR data. *Journal of Computational Chemistry*, *34*, 2135–45.

[128] **Vanommeslaeghe, K. and MacKerell, A.D.** (2012) Automation of the CHARMM general force field (CGenFF) I: Bond perception and atom typing. *Journal of Chemical Information and Modeling*, *52*, 3144–54.

[129] **Pearson, K.** (1901) LIII. On lines and planes of closest fit to systems of points in space. *The London, Edinburgh, and Dublin Philosophical Magazine and Journal of Science*, *2*, 559–72.

[130] **Hotelling, H.** (1933) Analysis of a complex of statistical variables into principal components. J. Educ. *Psychol*, 417–41.

[131] **Ichiye, T. and Karplus, M.** (1991) Collective motions in proteins: a covariance analysis of atomic fluctuations in molecular dynamics and normal mode simulations. *Proteins*, *11*, 205–17.

[132] **García, A.** (1992) Large-amplitude nonlinear motions in proteins. *Phys. Rev. Lett*, 2696–9.

[133] **Rother, K.** (2005) Introduction to PyMOL. *Methods In Molecular Biology Clifton Nj*, *635*, 0–32.

[134] **R Development Core Team, R**. (2011) R: A Language and Environment for Statistical Computing. R *Found. Stat. Comput*, 409.

[135] **The Mendeley Support Team.** (2011) Import citations into your digital library using the Mendeley, *Mendeley Deskt*, 1–16.

[136] **Zou, Y., Weis, W.I. and Kobilka, B.K.** (2012) N-Terminal T4 Lysozyme Fusion Facilitates Crystallization of a G Protein Coupled Receptor. *PLoS ONE*, 7.

[137] **Jaakola, V.-P., Griffith, M.T., Hanson, M.A., Cherezov, V., Chien, E.Y.T., Lane, J.R. et al.** (2008) The 2.6 angstrom crystal structure of a human A2A adenosine receptor bound to an antagonist. *Science*, *322*, 1211–7.

[138] **Wu, B., Chien, E.Y.T., Mol, C.D., Fenalti, G., Liu, W., Katritch, V. et al.** (2010) Structures of the CXCR4 chemokine GPCR with small-molecule and cyclic peptide antagonists. *Science*, *330*, 1066–71.

[139] **Shimamura, T., Shiroishi, M., Weyand, S., Tsujimoto, H., Winter, G., Katritch, V. et al.** (2011) Structure of the human histamine H1 receptor complex with doxepin. *Nature*, *475*, 65–70.

[140] **Kruse, a C., Hu, J., Pan, a C., Arlow, D.H., Rosenbaum, D.M., Rosemond, E. et al.** (2012) Structure and dynamics of the M3 muscarinic acetylcholine receptor. *Nature*, *482*, 552–6.

[141] **Haga, K., Kruse, a C., Asada, H., Yurugi-Kobayashi, T., Shiroishi, M., Zhang, C. et al.** (2012) Structure of the human M2 muscarinic acetylcholine receptor bound to an antagonist. *Nature*, *482*, 547–51.

[142] **Hansen, K.B. and Bra, H.** (2009) G Protein-Coupled Receptors in Drug Discovery. *Receptor*, *552*, 253–68.

[143] **Chun, E., Thompson, A.A., Liu, W., Roth, C.B., Griffith, M.T., Katritch, V. et al.** (2012) Fusion partner toolchest for the stabilization and crystallization of G protein-coupled receptors. *Structure*, *20*, 967–76.

[144] **Dragic, T., Trkola, A., Thompson, D.A., Cormier, E.G., Kajumo, F.A., Maxwell, E. et al.** (2000) A binding pocket for a small molecule inhibitor of HIV-1 entry within the transmembrane helices of CCR5. *Proc Natl Acad Sci U S A*, *97*, 5639–44.

[145] **Castonguay, L.A., Weng, Y., Adolfsen, W., Di Salvo, J., Kilburn, R., Caldwell, C.G. et al.** (2003) Binding of 2-aryl-4-(piperidin-1-yl)butanamines and 1,3,4-trisubstituted pyrrolidines to human CCR5: A molecular modeling-guided mutagenesis study of the binding pocket. *Biochemistry*, *42*, 1544–50.

[146] **Tsamis, F., Gavrilov, S., Kajumo, F., Seibert, C., Kuhmann, S., Ketas, T. et al.** (2003) Analysis of the mechanism by which the small-molecule CCR5 antagonists SCH-351125 and SCH-350581 inhibit human immunodeficiency virus type 1 entry. *Journal of Virology*, *77*, 5201–8.

[147] **Govaerts, C., Bondue, A., Springael, J.Y., Olivella, M., Deupi, X., Le Poul, E. et al.** (2003) Activation of CCR5 by chemokines involves an aromatic cluster between transmembrane helices 2 and 3. *Journal of Biological Chemistry*, *278*, 1892–903.

[148] **Nishikawa, M., Takashima, K., Nishi, T., Furuta, R.A., Kanzaki, N., Yamamoto, Y. et al.** (2005) Analysis of binding sites for the new small-molecule CCR5 antagonist TAK-220 on human CCR5. *Antimicrobial Agents and Chemotherapy*, *49*, 4708–15.

[149] **Imamura, S., Ichikawa, T., Nishikawa, Y., Kanzaki, N., Takashima, K., Niwa, S. et al.** (2006) Discovery of a piperidine-4-carboxamide CCR5 antagonist (TAK-220) with highly potent anti-HIV-1 activity. *Journal of Medicinal Chemistry*, *49*, 2784–93.

[150] **Maeda, K., Das, D., Ogata-Aoki, H., Nakata, H., Miyakawa, T., Tojo, Y. et al.** (2006) Structural and molecular interactions of CCR5 inhibitors with CCR5. *Journal of Biological Chemistry*, *281*, 12688–98.

[151] **Kondru, R., Zhang, J., Ji, C., Mirzadegan, T., Rotstein, D., Sankuratri, S. et al.** (2008) Molecular interactions of CCR5 with major classes of small-molecule anti-HIV CCR5 antagonists. *Molecular Pharmacology*, *73*, 789–800.

[152] **Wang, T. and Duan, Y.** (2008) Binding modes of CCR5-targetting HIV entry inhibitors: Partial and full antagonists. *Journal of Molecular Graphics and Modelling*, *26*, 1287–95.

[153] **Garcia-Perez, J., Rueda, P., Alcami, J., Rognan, D., Arenzana-Seisdedos, F., Lagane, B. et al.** (2011) Allosteric model of maraviroc binding to CC Chemokine Receptor 5 (CCR5). *Journal of Biological Chemistry*, *286*, 33409–21.

[154] **Watson, C., Jenkinson, S., Kazmierski, W. and Kenakin, T.** (2005) The CCR5 receptor-based mechanism of action of 873140, a potent allosteric noncompetitive HIV entry inhibitor. *Molecular Pharmacology*, *67*, 1268–82.

[155] **Rucker, J., Samson, M., Doranz, B.J., Libert, F., Berson, J.F., Yi, Y. et al.** (1996) Regions in β-chemokine receptors CCR5 and CCR2b that determine HIV-1 cofactor specificity. *Cell*, *87*, 437–46.

[156] **Chee, M.J.S., Mörl, K., Lindner, D., Merten, N., Zamponi, G.W., Light, P.E. et al.** (2008) The third intracellular loop stabilizes the inactive state of the neuropeptide Y1 receptor. *Journal of Biological Chemistry*, *283*, 33337–46.

[157] **Amadei, A., Linssen, A.B.M. and Berendsen, H.J.C.** (1993) Essential dynamics of proteins. *Proteins: Structure, Function and Genetics*, *17*, 412–25.

[158] **Shenkin, P.S. and Mcdonald, D.Q.** (1994) Cluster Analysis of Molecular Conformations. *Journal of Computational Chemistry*, *15*, 899–916.

[159] **Hess, B.** (2002) Convergence of sampling in protein simulations. *Physical Review E - Statistical, Nonlinear, and Soft Matter Physics*, 65.

[160] **Hess, B.** (2000) Similarities between principal components of protein dynamics and random diffusion. *Physical Review E - Statistical Physics, Plasmas, Fluids, and Related Interdisciplinary Topics*, *62*, 8438–48.

[161] **King, N., Hittinger, C.T. and Carroll, S.B.** (2003) Evolution of key cell signaling and adhesion protein families predates animal origins. *Science*, *301*, 361–3.

[162] **Venkatakrishnan, A.J., Deupi, X., Lebon, G., Tate, C.G., Schertler, G.F. and Babu, M.M.** (2013) Molecular signatures of G-protein-coupled receptors. *Nature*, *494*, 185–94.

[163] **Hollenstein, K., De Graaf, C., Bortolato, A., Wang, M.W., Marshall, F.H. and Stevens, R.C.** (2014) Insights into the structure of class B GPCRs. Trends Pharmacol. *Sci*, 12–22.

[164] **Palczewski, K.** (2000) Crystal Structure of Rhodopsin: A G Protein-Coupled Receptor. *Science*, 739–45.

[165] **Contreras, F., Fouillioux, C., Bolívar, A., Simonovis, N., Hernández-Hernández, R., Armas-Hernandez, M.J. et al.** (2002) Dopamine, hypertension and obesity. *Journal of Human Hypertension*, *16 Suppl* 1, S13–7.

[166] **Schultz, W.** (2007) Multiple dopamine functions at different time courses. *Annual Review of Neuroscience*, *30*, 259–88.

[167] **Kienast, T. and Heinz, A.** (2006) Dopamine and the diseased brain. *CNS & Neurological Disorders Drug Targets*, *5*, 109–31.

[168] **Fuxe, K., Manger, P., Genedani, S. and Agnati, L.** (2006) The nigrostriatal DA pathway and Parkinson's disease. *Journal of Neural Transmission Supplementum*, 71–83.

[169] **Maas, J.W., Bowden, C.L., Miller, A.L., Javors, M.A., Funderburg, L.G., Berman, N. et al.** (1997) Schizophrenia, psychosis, and cerebral spinal fluid homovanillic acid concentrations. *Schizophrenia Bulletin*, *23*, 147–54.

[170] **Paul, M.L., Graybiel, A.M., David, J.C. and Robertson, H.A.** (1992) D1-like and D2-like dopamine receptors synergistically activate rotation and c-fos expression in the dopamine-depleted striatum in a rat model of Parkinson's disease. *The Journal of Neuroscience : The Official Journal of the Society for Neuroscience*, *12*, 3729–42.

[171] **Wettschureck, N. and Offermanns, S.** (2005) Mammalian G proteins and their cell type specific functions. *Physiological Reviews*, *85*, 1159–204.

[172] **Platania, C. B. M., Salomone, S., Leggio, G. M., Drago, F., & Bucolo, C**. (2012). Homology modeling of dopamine D2 and D3 receptors: molecular dynamics refinement and docking evaluation. *PloS One*, *7*, e44316.

[173] **Laskowski, R.A., MacArthur, M.W., Moss, D.S. and Thornton, J.M.** (1993) PROCHECK: a program to check the stereochemical quality of protein structures. *J. Appl. Crystallogr*, 283–91.

[174] **Wiederstein, M. and Sippl, M.J.** (2007) ProSA-web: Interactive web service for the

recognition of errors in three-dimensional structures of proteins. *Nucleic Acids Research*, 35.

[175] **Zhang, L. and Skolnick, J.** (1998) What should the Z-score of native protein structures be? *Protein Science : A Publication of the Protein Society*, *7*, 1201–7.

[176] **Farid, R., Day, T., Friesner, R.A. and Pearlstein, R.A.** (2006) New insights about HERG blockade obtained from protein modeling, potential energy mapping, and docking studies. *Bioorganic and Medicinal Chemistry*, *14*, 3160–73.

[177] **Lomize, M. A., Lomize, A. L., Pogozheva, I. D. & Mosberg, H. I.** (2006) OPM: Orientations of proteins in membranes database. *Bioinformatics 22*, 623–625.

[178] **Zeng, F., Soldner, A. & Scho, T.** Conserved Extracellular Cysteine Pair in the M 3 Muscarinic Acetylcholine Receptor Is Essential for Proper Receptor Cell Surface Localization but Not for G Protein Coupling. *J. Neurochem. 72*, 2404–2414 (1999).

[179] **Miyamoto, S. and Kollman, P.A.** (1992) SETTLE: an analytical version of the SHAKE and RATTLE algorithm for rigid water models. *Journal of Computational Chemistry*, *13*, 952–62.

[180] **Bussi, G. and Parrinello, M.** (2007) Accurate sampling using Langevin dynamics. *Physical Review E - Statistical, Nonlinear, and Soft Matter Physics*, 75.

[181] **Darden, T., York, D. and Pedersen, L.** (1993) Particle mesh Ewald: An N log(N) method for Ewald sums in large systems. *The Journal of Chemical Physics*, *98*, 10089.

[182] **Kolb, P.; Klebe, G**. (2011) The golden age of GPCR structural biology: any impact on drug design? *Angew. Chem., Int. Ed. Engl*, *50*, 11573−11575.

[183] **Stevens, R.C., Cherezov, V., Katritch, V., Abagyan, R., Kuhn, P., Rosen, H. et al.** (2013) The GPCR Network: a large-scale collaboration to determine human GPCR structure and function. *Nature Reviews Drug Discovery*, *12*, 25–34.

[184] **Hausch, F. and Holsboer, F.** (2012) The seven pillars of molecular pharmacology: Gpcr research honored with nobel prize for chemistry. *Angewandte Chemie - International Edition*, *51*, 12172–5.

[185] **Cherezov, V., Rosenbaum, D.M., Hanson, M.A., Rasmussen, S.G.F., Thian, F.S., Kobilka, T.S. et al.** (2007) High Resolution crystal structure of an engineered human beta2-adrenergic G protein-coupled receptor. *Science*, *318*, 1258–65.

[186] **Wu, H., Wacker, D., Mileni, M., Katritch, V., Han, G.W., Vardy, E. et al.** (2012) Structure of the human kappa-opioid receptor in complex with JDTic. *Nature*, *485*, 327–U69.

[187] **Manglik, A., Kruse, A.C., Kobilka, T.S., Thian, F.S., Mathiesen, J.M., Sunahara, R.K. et al.** (2012) Crystal structure of the μ-opioid receptor bound to

a morphinan antagonist. *Nature*, 321–6.

[188] **Hollenstein, K., Kean, J., Bortolato, A., Cheng, R.K., Dore, A.S., Jazayeri, A. et al.** (2013) Structure of class B GPCR corticotropin-releasing factor receptor 1. *Nature*, *499*, 438–43.

[189] **Hanson, M.A., Roth, C.B., Jo, E., Griffith, M.T., Scott, F.L., Reinhart, G. et al.** (2012) Crystal Structure of a Lipid G Protein-Coupled Receptor. *Science*, 851–5.

[190] **Fredriksson, R., Lagerström, M.C., Lundin, L.-G. and Schiöth, H.B.** (2003) The G-protein-coupled receptors in the human genome form five main families. Phylogenetic analysis, paralogon groups, and fingerprints. *Molecular Pharmacology*, *63*, 1256–72.

[191] **Waldhoer, M., Bartlett, S.E. and Whistler, J.L.** (2004) Opioid receptors. *Annu Rev Biochem*, *73*, 953–90.

[192] **Carlezon Jr., W.A., Béguin, C., Knoll, A.T. and Cohen, B.M.** (2009) Kappa-opioid ligands in the study and treatment of mood disorders. *Pharmacology & Therapeutics*, *123*, 334–43.

[193] **Roth, B.L., Baner, K., Westkaemper, R., Siebert, D., Rice, K.C., Steinberg, S. et al.** (2002) Salvinorin A: a potent naturally occurring nonnitrogenous kappa opioid selective agonist. *Proceedings of the National Academy of Sciences of the United States of America*, *99*, 11934–9.

[194] **Yan, F., Bikbulatov, R. V, Mocanu, V., Dicheva, N., Parker, C.E., Wetsel, W.C. et al.** (2009) Structure-based design, synthesis, and biochemical and pharmacological characterization of novel salvinorin A analogues as active state probes of the kappa-opioid receptor. *Biochemistry*, *48*, 6898–908.

[195] **Carroll, I., Thomas, J.B., Dykstra, L.A., Granger, A.L., Allen, R.M., Howard, J.L. et al.** (2004) Pharmacological properties of JDTic: a novel kappa-opioid receptor antagonist. *European Journal of Pharmacology*, *501*, 111–9.

[196] **Thomas, J.B., Atkinson, R.N., Rothman, R.B., Fix, S.E., Mascarella, S.W., Vinson, N.A. et al.** (2001) Identification of the first trans-(3R,4R)-dimethyl-4-(3-hydroxyphenyl)piperidine derivative to possess highly potent and selective opioid kappa receptor antagonist activity. *Journal of Medicinal Chemistry*, *44*, 2687–90.

[197] **Dror, R.O., Pan, A.C., Arlow, D.H., Borhani, D.W., Maragakis, P., Shan, Y. et al.** (2011) Pathway and mechanism of drug binding to G-protein-coupled receptors. *Proceedings of the National Academy of Sciences*, *108*, 13118–23.

[198] **Heifetz, A., Morris, G.B., Biggin, P.C., Barker, O., Fryatt, T., Bentley, J. et al.** (2012) Study of Human Orexin-1 and-2 G-Protein-Coupled Receptors with Novel and Published Antagonists by Modeling, Molecular Dynamics Simulations, and Site-Directed Mutagenesis. *Biochemistry*, *51*, 3178–97.

[199] **Provasi, D., Artacho, M.C., Negri, A., Mobarec, J.C. and Filizola, M.** (2011) Ligand-Induced modulation of the Free-Energy landscape of G protein-coupled receptors explored by adaptive biasing techniques. *PLoS Computational Biology*, 7.

[200] **Provasi, D. and Filizola, M.** (2010) Putative active states of a prototypic g-protein-coupled receptor from biased molecular dynamics. *Biophysical Journal*, *98*, 2347–55.

[201] **Provasi, D., Bortolato, A. and Filizola, M.** (2009) Exploring molecular mechanisms of ligand recognition by opioid receptors with metadynamics. *Biochemistry*, *48*, 10020–9.

[202] **Tosh, D.K., Phan, K., Gao, Z.G., Gakh, A.A., Xu, F., Deflorian, F. et al.** (2012) Optimization of adenosine 5′-carboxamide derivatives as adenosine receptor agonists using structure-based ligand design and fragment screening. *Journal of Medicinal Chemistry*, *55*, 4297–308.

[203] **Deflorian, F., Kumar, T.S., Phan, K., Gao, Z.-G., Xu, F., Wu, H. et al.** (2012) Evaluation of molecular modeling of agonist binding in light of the crystallographic structure of an agonist-bound A2A adenosine receptor. *Journal of Medicinal Chemistry*, *55*, 538–52.

[204] **McGovern, D.L., Mosier, P.D., Roth, B.L. and Westkaemper, R.B.** (2010) CoMFA analyses of C-2 position Salvinorin A analogs at the kappa-opioid receptor provides insights into epimer selectivity. *Journal of Molecular Graphics and Modelling*, *28*, 612–25.

[205] **Perez, D.M. and Karnik, S.S.** (2005) Multiple signaling states of G-protein-coupled receptors. *Pharmacological Reviews*, *57*, 147–61.

[206] **Graves, A.P., Shivakumar, D.M., Boyce, S.E., Jacobson, M.P., Case, D.A. and Shoichet, B.K.** (2008) Rescoring Docking Hit Lists for Model Cavity Sites: Predictions and Experimental Testing. *Journal of Molecular Biology*, *377*, 914–34.

[207] **Case, D.A., Cheatham, T.E., Darden, T., Gohlke, H., Luo, R., Merz, K.M. et al.** (2005) The Amber biomolecular simulation programs. *J. Comput. Chem*, 1668–88.

[208] **Hooft, R.W., Vriend, G., Sander, C. and Abola, E.E.** (1996) Errors in protein structures. *Nature*, 272.

[209] **Vriend, G.** (1990) WHAT IF: a molecular modeling and drug design program. *Journal of Molecular Graphics*, *8*, 52–6, 29.

[210] **Dolinsky, T.J., Nielsen, J.E., McCammon, J.A. and Baker, N.A.** (2004) PDB2PQR: An automated pipeline for the setup of Poisson-Boltzmann electrostatics calculations. *Nucleic Acids Research*, *32*.

[211] **Hornak, V., Abel, R., Okur, A., Strockbine, B., Roitberg, A. and Simmerling, C.** (2006) Comparison of multiple amber force fields and development of improved protein backbone parameters. *Proteins Struct. Funct. Genet*, 712–25.

[212] **Pettersen, E.F., Goddard, T.D., Huang, C.C., Couch, G.S., Greenblatt, D.M.,**

Meng, E.C. et al. (2004) UCSF Chimera--a visualization system for exploratory research and analysis. *Journal of Computational Chemistry*, *25*, 1605–12.

[213] **Wang, J., Wolf, R.M., Caldwell, J.W., Kollman, P.A. and Case, D.A.** (2004) Development and testing of a general AmCrystal Structure of a Lipid G Protein-Coupled Receptor.ber force field. *Journal of Computational Chemistry*, *25*, 1157–74.

[214] **Jorgensen, W.L., Chandrasekhar, J., Madura, J.D., Impey, R.W. and Klein, M.L.** (1983) Comparison of simple potential functions for simulating liquid water. *J. Chem. Phys*, 926.

[215] **Ryckaert, J.-P., Ciccotti, G. and Berendsen, H.J..** (1977) Numerical integration of the cartesian equations of motion of a system with constraints: molecular dynamics of n-alkanes. *Journal of Computational Physics*, *23*, 327–41.

[216] **Lzaguirre, J.A., Catarello, D.P., Wozniak, J.M. and Skeel, R.D.** (2001) Langevin stabilization of molecular dynamics. *Journal of Chemical Physics*, *114*, 2090–8.

[217] **Simmerling, C.; Elber, R.; Zhang, J.** (1995) Moil-view-A program for visualization of structure and dynamics of biomolecules and STO-A program for computing stochastic paths. The Jerusalem Symposia on Quantum Chemistry and Biochemistry, Modelling of Biomolecular Structures and Mechanisms, Pullman, A., Jortner, J., Eds.; Springer: *Jerusalem, Israel*, 241−265.

[218] **Collu, F., Ceccarelli, M. and Ruggerone, P**. (2012) Exploring Binding Properties of Agonists Interacting with a ??-Opioid Receptor. *PLoS ONE*, 7.

[219] **Jo, S., Kim, T., Iyer, V.G. and Im, W.** (2008) CHARMM-GUI: A web-based graphical user interface for CHARMM. *Journal of Computational Chemistry*, *29*, 1859–65.

[220] **Jo, S., Lim, J.B., Klauda, J.B. and Im, W**. (2009) CHARMM-GUI membrane builder for mixed bilayers and its application to yeast membranes. *Biophysical Journal*, *97*, 50–8.

[221] **Lomize, M.A., Lomize, A.L., Pogozheva, I.D. and Mosberg, H.I.** (2006) OPM: Orientations of proteins in membranes database. *Bioinformatics*, *22*, 623–5.

CURRICULUM VITAE



Name Surname: Ramin EKHTEIARI SALMAS

Place and Date of Birth: IRAN/URMIA – 11/05/1980

Address: Turkey/Istanbul, Maslak, ITU.

E-Mail: ekhteiarisalmas@itu.edu.tr

B.Sc.: URMIA UNIVERSITY

M.Sc. : ARDABIL UNIVERSITY

PROFESSIONAL EXPERIENCE AND REWARDS:

- Structural Variation of PARP-1 over Inhibitory Treatment, Holo State Definitional from Apo Form : Approaching MD and Docking Simulation, **Ramin Ekhteiari Salmas**, Ayhan Unlu, Mine Yurtsever, Sergei Y Noskov, Serdar Durdagi Turkey, International BAU-Drug Design Congress 2014. (Best presentation award)

PUBLICATIONS, PRESENTATIONS AND PATENTS ON THE THESIS:

- Micro-second Molecular Dynamics Simulations of Dopamine D2 Receptor (D2R) Elucidates Its Inhibition Mechanism, **Ramin Ekhteiari Salmas**, Mine Yurtsever, Serdar Durdagi. Submitted to *Journal of Enzyme Inhibition and Medicinal Chemistry*. 2014.

- Investigation of Inhibition Mechanism of Chemokine Receptor CCR5 by Micro-second Molecular Dynamics Simulations, **Ramin Ekhteiari Salmas**, Mine Yurtsever, Serdar Durdagi, Submitted to *Scientific Reports*. 2014.

- Discovering of Novel Carbonic Anhydrase Type IX (CA IX) Inhibitors by Ligand-based Virtual Screening Approach, **Ramin Ekhteiari Salmas**, Mine Yurtsever, Serdar Durdagi. Submitted to *Journal of Enzyme Inhibition and Medicinal Chemistry*, 2014.

- Protein Engineering Studies of Active and Inactive States of Human Dopamine D2 Receptor (D2R) and Investigation of Drug/Modeled Receptor Interactions, **Ramin Ekhteiari Salmas**, Mine Yurtsever, Matthias Stein,

Serdar Durdagi. *Molecular Diversity*. 2015. DOI 10.1007/s11030-015-9569-3

- Elucidation of Conformational States, Dynamics and Mechanism of Binding in Human κ-opioid Receptor Complexes, Georgios Leonis, Aggelos Avramopoulos, **Ramin Ekhteiari Salmas**, Serdar Durdagi, Mine Yurtsever, Manthos G. Papadopoulos. *J. Chem. Inf. Model*., 2014, *54* (8), pp 2294–2308.

OTHER PUBLICATIONS, PRESENTATIONS AND PATENTS:

- Mutated Form (G52E) of Inactive Diphtheria Toxin CRM197: Molecular Dynamics Simulations Clearly Display Effect of this Mutation to NAD Binding, **Ramin Ekhteiari Salmas**, Mert Mestanoglu, Ayhan Unlu, Mine Yurtsever, Serdar Durdagi. Submitted to *Scientific Reports*, 2014.

- Virtual Screening of a Large Ligand Database for Discovery of Candidates of Novel PARP-1 Inhibitors, **Ramin Ekhteiari Salmas**, Mert Mestanoglu, Ayhan Unlu, Mine Yurtsever, Serdar Durdagi. Submitted to *journal of molecular graphics and modelling*, 2014.

- Kinetic and in silico studies of hydroxy-based inhibitors of carbonic anhydrase isoforms I and II, **Ramin Ekhteiari Salmas**, Mert Mestanoglu, Serdar Durdagi, Murat Sentürk, A. Afşin Kaya, Elif Çelenk Kaya. Accepted at *Journal of Enzyme Inhibition and Medicinal Chemistry*, 2014.

- In-Silico investigation of PARP-1 catalytic domains in holo and apo states and drug design studies for high affinity PARP-1 inhibitors, **Ramin Ekhteiari Salmas**, Ayhan Unlu, Mine Yurtsever, Sergei Y Noskov, Serdar Durdagi. Accepted at *Journal of Enzyme Inhibition and Medicinal Chemistry*, 2014.

- Carbonic Anhydrase Inhibitory Properties of Novel Benzylsulfamides Using Molecular Modelling and Experimental Studies, Süleyman Göksu, Ali Naderi, Yusuf Akbaba, Pınar Kalın, Akın Akıncıoğlu, İlhami Gülçin, Serdar Durdagi, **Ramin Ekhteiari Salmas**. *Bioorganic Chemistry*, 2014, Pages 75–82.

- Silver−Sodium Ion Exchange Dynamics in LTA Zeolite Membranes, **Ramin Ekhteiari Salmas**, Barış Demir, Erol Yıldırım, Ahmet Sirkecioğlu, Mine Yurtsever and M. Göktuğ Ahunbay. *J. Phys. Chem. C* 2013, 117, 1663−1671.

- Kolera Toksininin Üç Boyutlu Yapısının, Etkileşim Bölgelerinin ve Etki Mekanizmasının Moleküler Dinamik Yöntemlerle İncelenmesi, **Ramin Ekhteiari Salmas**, Ayhan Unlu, Mine Yurtsever, Sergei Y Noskov, Serdar Durdagi.26. Ulusal Biyofizik Kongresi kongre, Tokat, Turkey, 2014.

- In Silico Studies on K-RAS-PDEδ Interaction Inhibition to Design Novel Anti-Cancer Drugs, Modeling of Biomolecular Systems Interactions, Dynamics, and Allostery: Bridging Experiments and Computations **Ramin Ekhteiari Salmas**, Mert Mestanoglu, Mine Yurtsever, Serdar Durdagi,

ISTANBUL, TURKEY, 2014.

- Surface Functionalization of Graphene Analogs and Its Effects On The Exfoliation Behaviour and Interactions With Small Molecules: A MD Study, Berkay sutay, **Ramin Ekhteiari Salmas**, Mine Yurtsever, ECOSS-30 - 30th European Conference on Surface Science. Turkey, Antalya, 2014,

- Mechanistic investigation of PARP-1 bound with a novel inhibitor through in-silico methods, **Ramin Ekhteiari Salmas**, Ayhan Unlu, Mine Yurtsever, Sergei Y Noskov, Serdar Durdagi XI. Chemical Physics Congress, Turkey, Istanbul, 2014.

- Dopamin D2 reseptör antagonisti antipsikotik ilaçlar için in siliko çalışmalar, **Ramin Ekhteiari Salmas**, Mine Yurtsever, Matthias Stein, Serdar Durdagi 12th National Neuroscience Congress, Bahçeşehir University, Beşiktaş, İstanbul, Turkey 2014.

- In silico study of approved antipsychotic drugs as D2R antagonists: Homology modeling and docking approach, **Ramin Ekhteiari Salmas**, Mine Yurtsever, Matthias Stein, Serdar Durdagi Turkey, International BAU-Drug Design Congress 2014.

- Structural Variation of PARP-1 over Inhibitory Treatment, Holo State Definitional from Apo Form : Approaching MD and Docking Simulation, **Ramin Ekhteiari Salmas**, Ayhan Unlu, Mine Yurtsever, Sergei Y Noskov, Serdar Durdagi Turkey, International BAU-Drug Design Congress 2014. (Best presentation award)

- Molecular Simulation of Zn+, Cu2+, NH4+, Ion-Exchange on Clinoptilolites, **Ramin Ekhteiari Salmas**, Barış Demir, Erol Yıldırım, Ahmet Sirkecioğlu, Mine Yurtsever and M. Göktuğ Ahunbay International Zeolite Conference, France, 2013.

- Antibacterial Activity of Polymer/Zeolite Nanocomposite Materials:A MD Study, **Ramin Ekhteiari Salmas**, Barış Demir, Erol Yıldırım, Ahmet Sirkecioğlu, Mine Yurtsever and M. Göktuğ AhunbayTurkey, BAU-Drug Design Symposium, 2013.

- Monte Carlo Simulations of HCN Adsorption in LTA zeolites, Barış Demir **Ramin Ekhteiari Salmas**, Mine Yurtsever and M. Göktuğ Ahunbay International Conference on Innovations in Chemical Engineering and MedicalSciences, Dubai,UAE, 2012

- LTA Zeolitlerde Na-Ag İyon Değişimi Dinamiği, **Ramin Ekhteiari Salmas**, Barış Demir, Erol Yıldırım, Ahmet Sirkecioğlu, Mine Yurtsever and M. Göktuğ Ahunbay, Turkey, koç university, 2012.

- Diffusion of Water in Zeolites Ag-LTA, **Ramin Ekhteiari Salmas**, Barış Demir, Erol Yıldırım, Ahmet Sirkecioğlu, Mine Yurtsever and M. Göktuğ

Ahunbay Chemical Physics Congress XTOBB University of Economics and Technology Ankara, Turkey, 2012.

- Na─Ag ion exchange dynamics in LTA zeolites, **Ramin Ekhteiari Salmas**, Barış Demir, Erol Yıldırım, Ahmet Sirkecioğlu, Mine Yurtsever and M. Göktuğ Ahunbay France, 12th International Conference on Inorganic Membranes, 2012.

- Molecular simulation of Na─Ag ion exchange in zeolite A, **Ramin Ekhteiari Salmas**, Barış Demir, Erol Yıldırım, Ahmet Sirkecioğlu, Mine Yurtsever and M. Göktuğ Ahunbay Holland, ICOM, 2011

Oral Presentations

- Microsecond Molecular Dynamics Simulations of Chemokine Receptor CCR5 Clearly Demonstrate the Inhibitory Mechanism, **Ramin Ekhteiari Salmas**, Mine Yurtsever, Serdar Durdagi XI. Chemical Physics Congress, Turkey, Istanbul, 2014.

- Dopamin (D2) Reseptorünün Aktif ve Aktif Olmayan Konformasyonlarının Protein Modelleme Teknikleri ile Geliştirilmesi ve Şizofreni İlaçları İle Olan Etkileşimlerinin Aydınlatılması, **Ramin Ekhteiari Salmas**, Mine Yurtsever, Matthias Stein, Serdar Durdagi, Ulusal Biyofizik Kongresi Turkey, Trabzon, 2013.